SEISMIC PERFORMANCE EVALUATION OF THE SADABAT 1 (V3) VIADUCT

by

Göktürk ÖNEM

B.S. in Civil Engineering, Yıldız Teknik University, 1997

Submitted to the Kandilli Observatory and

Earthquake Research Institute in partial fulfillment of

the requirements for the degree of

Master of Science

in

Earthquake Engineering

Boğaziçi University
2002

ACKNOWLEDGMENTS

I would like to express my deepest gratitude to my supervisor, Prof. Dr. Nuray Aydınoğlu for his wide scope of engineering approach, enormous guidance, encouragement and technical support that he has provided during all steps of this thesis.

Next, I must offer my sincerest thank you to our department head, Prof. Dr. Mustafa Erdik for providing me with the incredible technical opportunity of Earthquake Engineering Department. I would like to express my thanks to Prof. Dr. Özal Yüzügüllü for his valuable suggestions and critics.

I would like to express my special thanks to my parents for their great support, patient and devotion through my educational life.

I am most grateful and greatly indebted to the members of the Department of Earthquake Engineering especially to Ph.D. students, Umut Utku Celep for his support, and valuable discussion throughout the study, Bülent Hakan Akman for his helps.

I would also like to thank Mrs. Nurdan Apaydın, the head engineer of the bridge department of the Area 17 of the General Directorate of Highways, for providing me drawing records of the bridge.

ABSTRACT

Sadabat V3 was designed in the late 1980's as a connector highway bridge in conjunction of Okmeydanı and Hastal on Kınalı-Sakarya motorway route, which is a major component of the transportation system of Istanbul. The bridge shows some typical examples of old seismic design philosophy such as low level of design forces and lack of modern ductile detailing.

Based on the visual inspection, any detrimental effects such as cracking or spalling of cover concrete due to corrosion could not be observed. Generally, it can be say that current condition of the bridge is good.

The bridge is evaluated as a critical bridge because of the location on major traveled route. The bridge is expected to remain functional immediately following a destructive earthquake. Seismic performance of the bridge has been assessed by using nonlinear time history analysis and pushover analysis. At the end of the analysis, deformation demand determined from the analysis has been compared with the predetermined component deformation capacity to obtain whether the bridge provides expected performance.

Analysis shows that elastomeric bearings, particularly located on flexible intermediate piers have insufficient displacement capacities in transverse direction to remain elastic. Displacement ductility of the piers are inadequate due to the poor detailing of the plastic hinge region. Because of the low ductility capacity, the piers are unlikely to tolerate cyclic displacement much exceeding yield in transverse direction. However, it can be concluded that the bridge response is essentially elastic in longitudinal direction.

ÖZET

Sadabat V3 viyadüğü, İstanbul ulaşım sisteminin önemli bir parçası olan Kınalı_Sakarya Otoyolu üzerinde ve Okmeydanı Hastal arasında bağlantı köprüsü olarak inşaa edilmiştir. Köprü, düşük deprem yükleri gözönüne alma ve modern düktil detaylandırmadan yoksun olamak gibi eski dizayn pirensiplerine ait örnekler içermektedir.

Yerinde yapılan incelemeler sonucu, kabuk betonunda çatlama ya da kabuk betonunun dağılması gibi zaralı etkiler görülmemiştir. Genel olarak köprünün iyi durumda olduğu söylenebilir.

Köprü üzerinde bulunduğu ulaşım sisteminin önemi sebebiyle kritik köprülerden biri olarak değerlendirilmiştir. Köprüden beklenen performans yıkıcı deprem hareketinden sonra köprünün işlevini devam ettirebilmesidir. Köprünün performansı doğrusal olmayan dinamik analiz ve statik kapasite analiz metodları kullanılarak incelenmiştir. Umulan performansı sağlayıp sağlamadığı analiz sonucunda elde edilen depremin talep ettiği deformasyonlarla sistem elemanlarının deformasyon kapasiteleri karşılaştırılarak incelenmiştir.

Analiz sonuçları göstermektedir ki, enine yönde deprem etkisi altında esnek ayaklar üzerinde oturan elastomer mesnetlerin deplasman kapasiteleri yeterli değildir. Ayakların deplasman kapasiteleri plastik mafsal bölgelerindeki yetersiz detaylandırma sebebiyle düşüktür. Bu sebeple, ayaklar elastik sınırı aşan periyodik deplasmanlara dayanamayabilir. Bununla birlikte, köprünün boyuna yöndeki davranışı hemen hemen elastik sısnırlar içindedir.

CONTENTS

LIST OF FIGURES

LIST OF TABLES

1. INTRODUCTION

Developments in the seismic design philosophy and understanding of the seismic behavior of structures collected from extensive testing and destructive earthquakes indicate that damage is related to deformation rather than strength. For many decades traditional strength based design formed the basis of seismic design where members are proportioned according to the strength demand derived from elastic models that are mostly based on uncracked section properties.

Even though the capacity design philosophy, emerged in early 70's from New Zealand, intended to compensate the disadvantages of strength based methodology by avoiding brittle modes of failure, the methodology is founded on a single level performance state; life safety. That is, considerably heavy damage beyond repair is accepted in the structure without causing causalities. However, bridges of high level of importance should be designed to withstand earthquakes with minor damage that correspond to essentially elastic performance even though they satisfy current force based core philosophy assuring life safety.

The importance of the bridge is related to many factors such as its role as a unique connector or the high level of traffic it carries. Sadabat (V3) is one of the important bridges in Istanbul that acts as a major component of the Kınalı-Sakarya motorway. The bridge has most of the common features such as lap splices above the foundation level and poor confinement details at the potential plastic hinge regions.

Despite the bridges performed well during the 1999 Kocaeli and Düzce earthquakes due to their structural configuration and proximity to the ruptured fault segments, lessons learned from past earthquakes, such as the 1971 San Fernando CA, 1989 Loma Prieta CA, 1994 Northridge CA and 1995 Kobe Japan, indicate that bridges designed according to past codes may cause loss of life and interruption of traffic. Bearing in mind the expected destructive earthquake in the Sea of Marmara, it became clear that seismic performance of important bridges in Istanbul should be assessed in detail. This study is part of the seismic performance evaluation process being carried out in the Department of Earthquake Engineering.

2. DESCRIPTION OF THE BRIDGE

Sadabat V3 is located at the European side of the Istanbul. The viaduct is one of the six long bridges,which were designed during Kınalı-Sakarya Motorway Project (Including Istanbul Second Bosphorus Crossing.). Sadabat V3 viaduct was constructed in the late 1980. The Viaduct is on the motorway connecting Okmeydanı and Hasdal, and located between 3+938 km and 4+726.8 km. The alignment of the bridge is in a north-south direction.

Sadabat V3 viaduct is fourteen span, 788.8m long bridge with prestressed concrete superstructure. The bridge is composed of two symmetrical system that are completely separated from each other and carrying opposite direction of traffic as shown in Figure 2.4 Horizontal alignment of the bridge is straight but vertically curved. The viaduct crosses deep valley with a slope of % 3.475 at the beginning and % 2.043 at the end as shown in Figure 2.3. The radius of the vertical curve is R=14295.00 km.

Superstructure is consisting of fourteen spans. Length of central and end spans are 58m and 46.4 m respectively. Superstructure was constructed by using incremental launching deck technique, which is widely used in designing long bridges crossing deep valley in European countries, and composed of 28 deck segments, the launching direction is shown in Figure 2.3. Therefore, the deck is continuous and simply supported on the piers by means of reinforced elastomeric bearings.

Each pier has four elastomeric bearing supporting the deck. From pier 9 to13 and abutment at axis 14, PTFE elastomeric sliding bearings were used to reduce thermal and time-dependent forces in longitudinal direction. Sliding mechanisms was provided only in longitudinal direction. In transverse direction, all elastomeric bearing are elastic deformable. At the abutments, lateral guides restrain the movement of the deck in transverse direction so the deck is pinned at the abutments. Deformation ability of the elastomeric bearings is shown in Figure 2.5 in detail.

Superstructure cross section shape is single-spine box girder, 12.65m wide by 5.05 m deep. Dimensions of the section are as shown in Figure 2.6. Along the superstructure, as the sections close to support, soffit and web thickness increase. The section has 34 prestressing tendons of grade 1770. Six of them are in the web as a curved cable. Area of tendons is 16.68 cm^2. Specified concrete compressive strength used in design of the superstructure is 35 Mpa.

As to substructure of the bridge, superstructure is supported by 13 single column bents with varying heights. Pier1 is the shortest column with the height of 8.57 m, the tallest column is pier4 at about 47.63 m. Section type of piers is rectangular hollow section 4.7 m by 3 m. Both longitudinal and transverse reinforcement ratios decrease gradually along the piers. At the bottom cross section of the columns, diameters of reinforcement bars used in designing of the piers are ϕ32, S420 for pier 2 to 10, and ϕ25, S420 for pier 1,11,12 and 13. Piers have specified concrete compressive strength of 25 Mpa. The concrete specified for pier heads has a strength of 40 Mpa. Detailed information about columns are summarized in Table2.1.

Seat-type abutment system was selected in designing of superstructure–abutment connection. Behavior of the deck in longitudinal was controlled by tie back device anchoring the deck with 58 prestressing dywidag bars with diameters of 32 mm back to abutment at axis 0. Yield strength and ultimate strength of the bars are 500 Mpa and 550 Mpa respectively. In case of movement of the deck towards the abutment, to reduce pounding effect, six reinforced elastomeric bearings (60 cm by 50 cm and h = 9.1 cm) were installed as a bumper at the interface between deck and abutment. Under longitudinal seismic response, resistance of the abutment was provided by friction slab, which is 67 m long and 13.35 m wide per superstructure. Thickness of the slab is 50 cm. Abutment-superstructure connection details are shown in Figure 2.6.

Sadabat V3 viaduct crosses deep valley mainly covered rock lying below broad soil deposit. At the mid of the valley, many piers founded on soft soil. Some side piers and abutments are on rock. As can be seen in elevation of the bridge (see Figure 2.3), a river crosses between pier 4 and pier 5. Any information about soil type and parameters couldn't be found. According to soil profile type classification of A.A.S.H.T.O.,1983, soil profile type III was selected in determining of site coefficient in calculation report. In A.A.S.H.T.O. 1996, this soil profile corresponds to soil profile type IV. Soil profile IV is a profile with soft clays or silts greater than 12m in depths. Shear wave velocity is less than 150m/s.

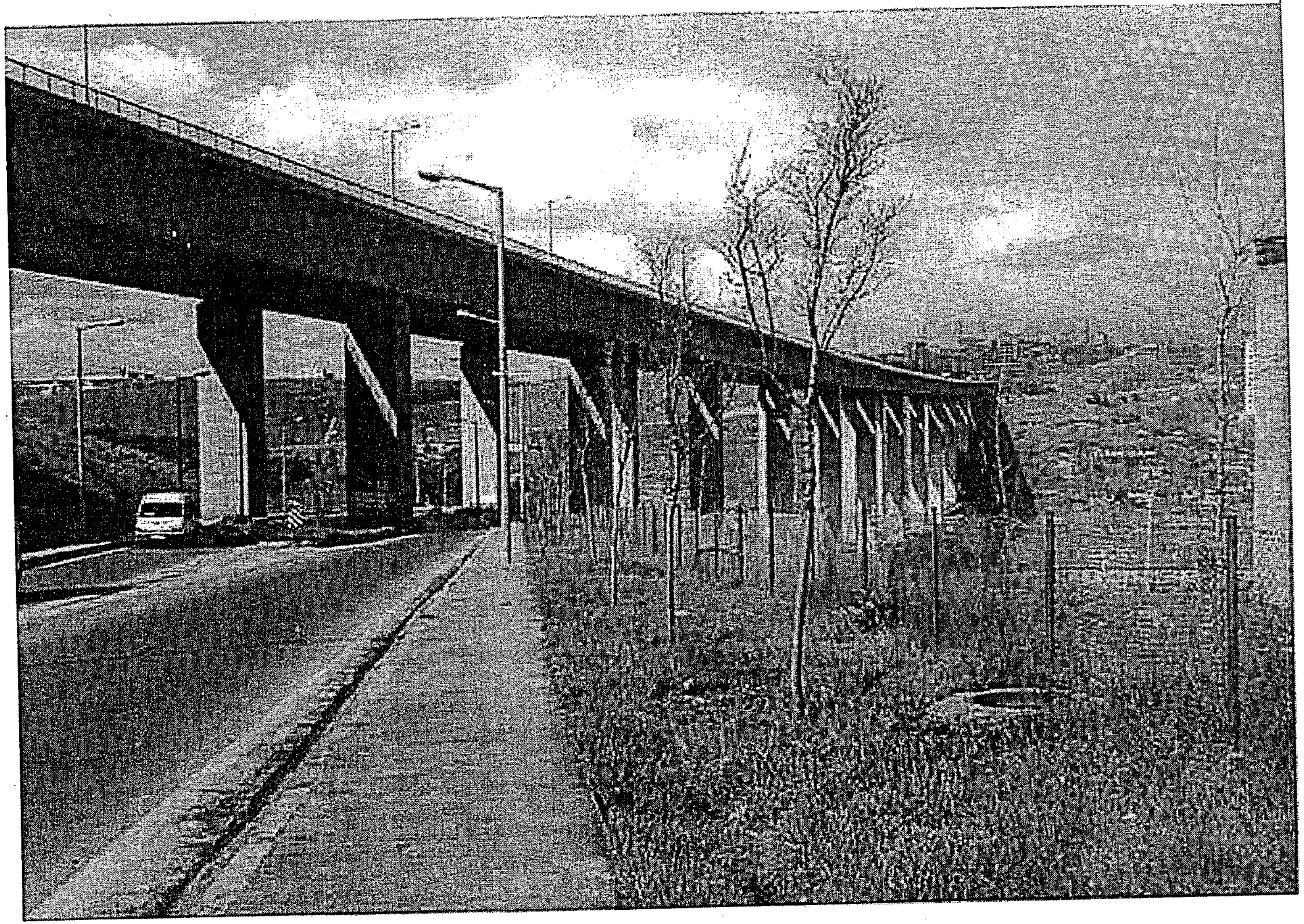

Figure 2.1 General view of the Sadabat V3 Viaduct (from Hasdal End)

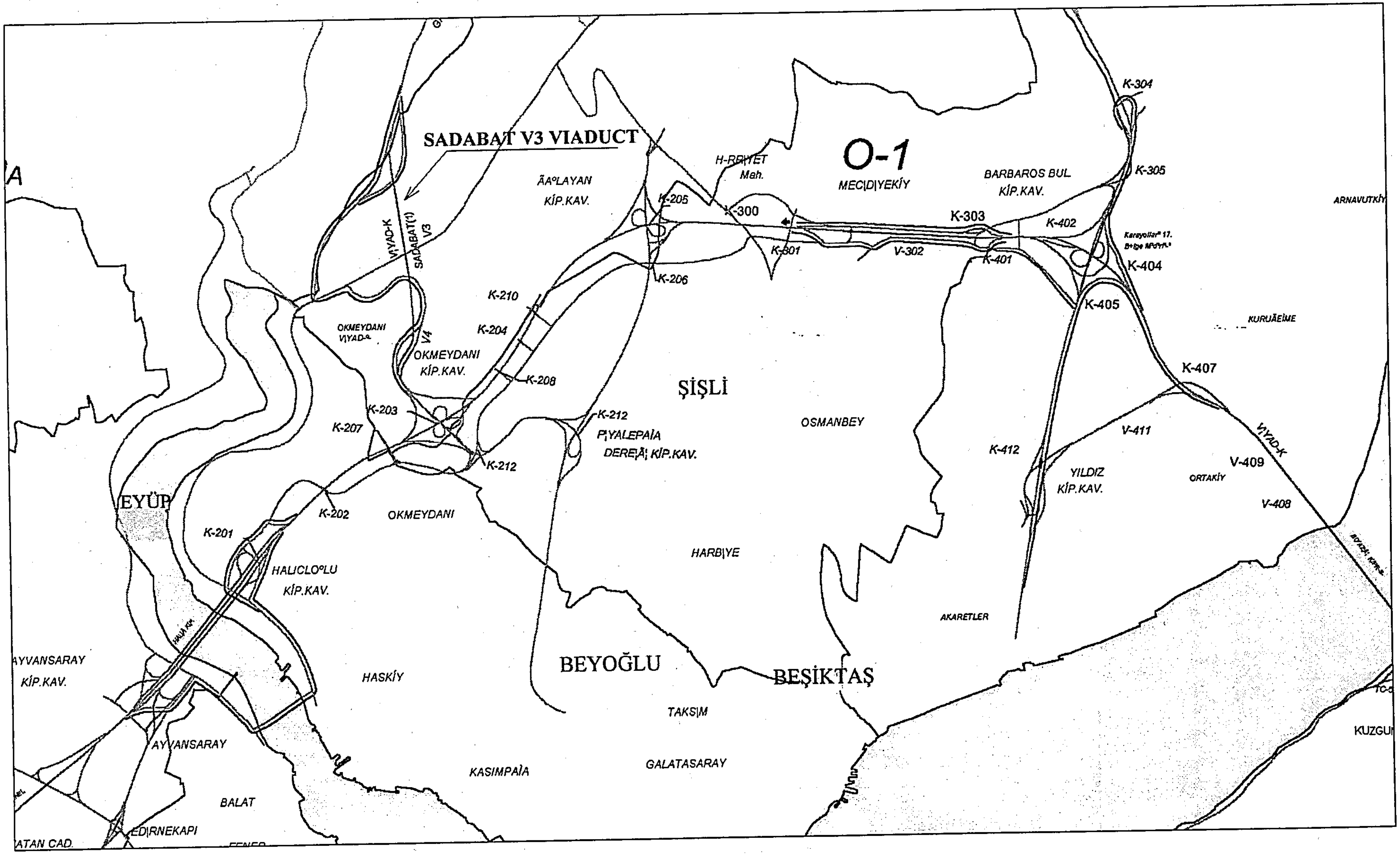

Figure 2.2. Location of the Sadabat V3 viaduct.

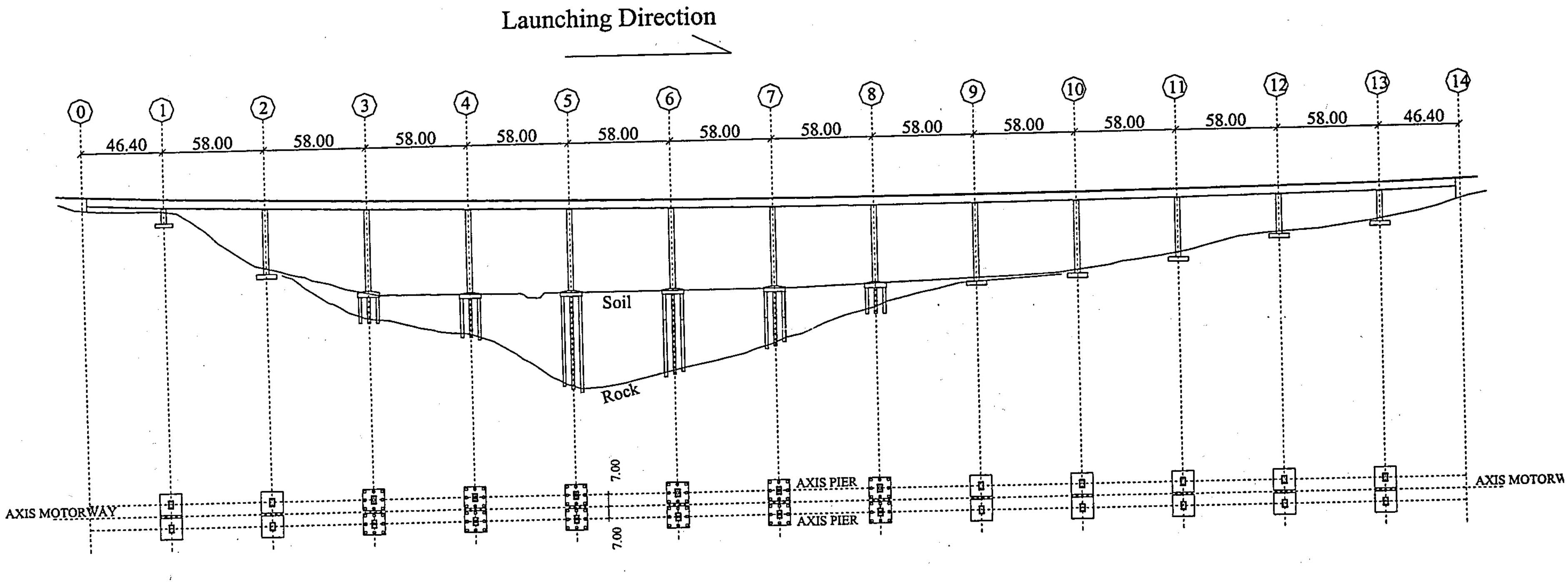

Figure 2.3. Plan and Elevation of The Bridge

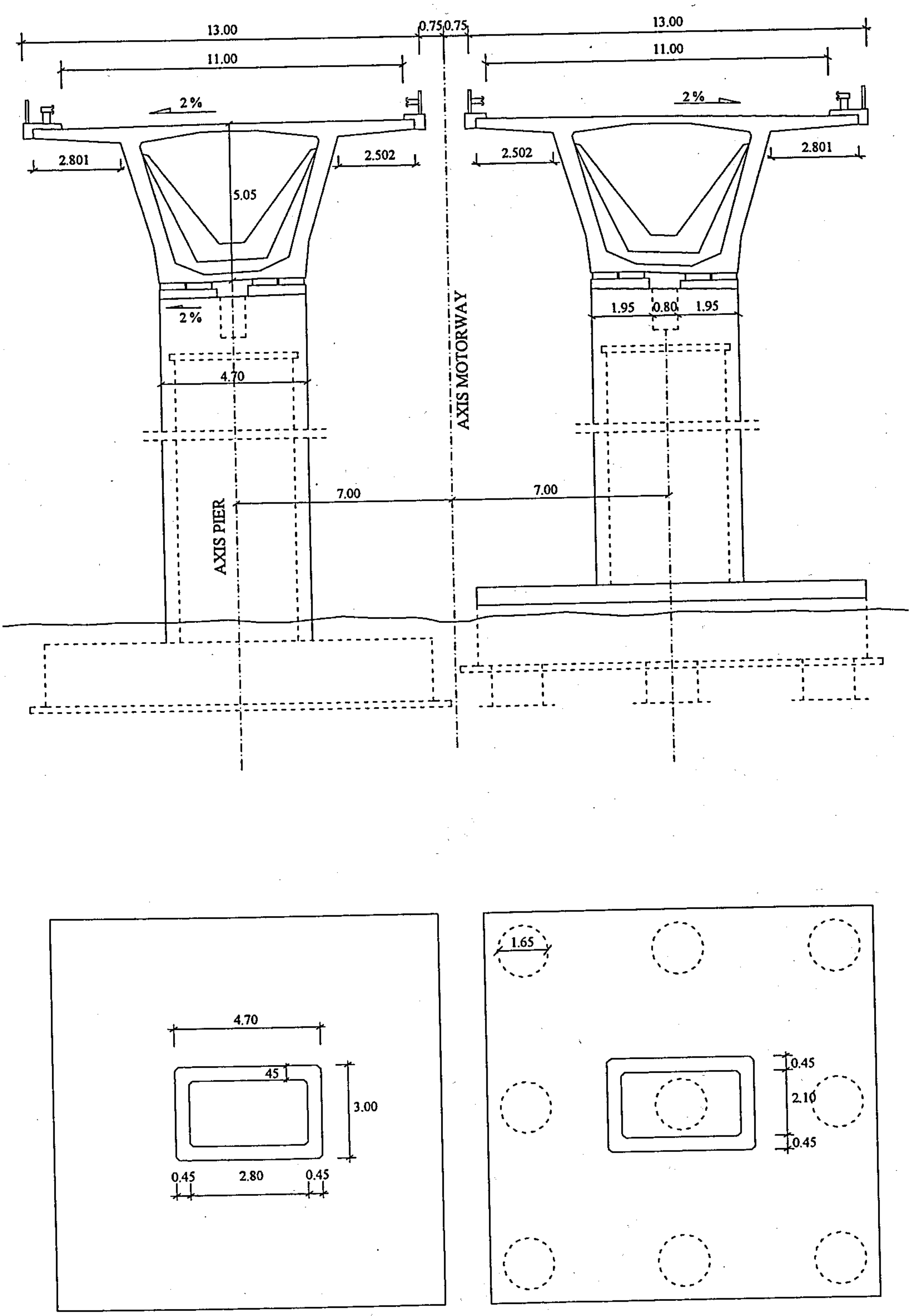

Figure 2.4. Section of the Bridge

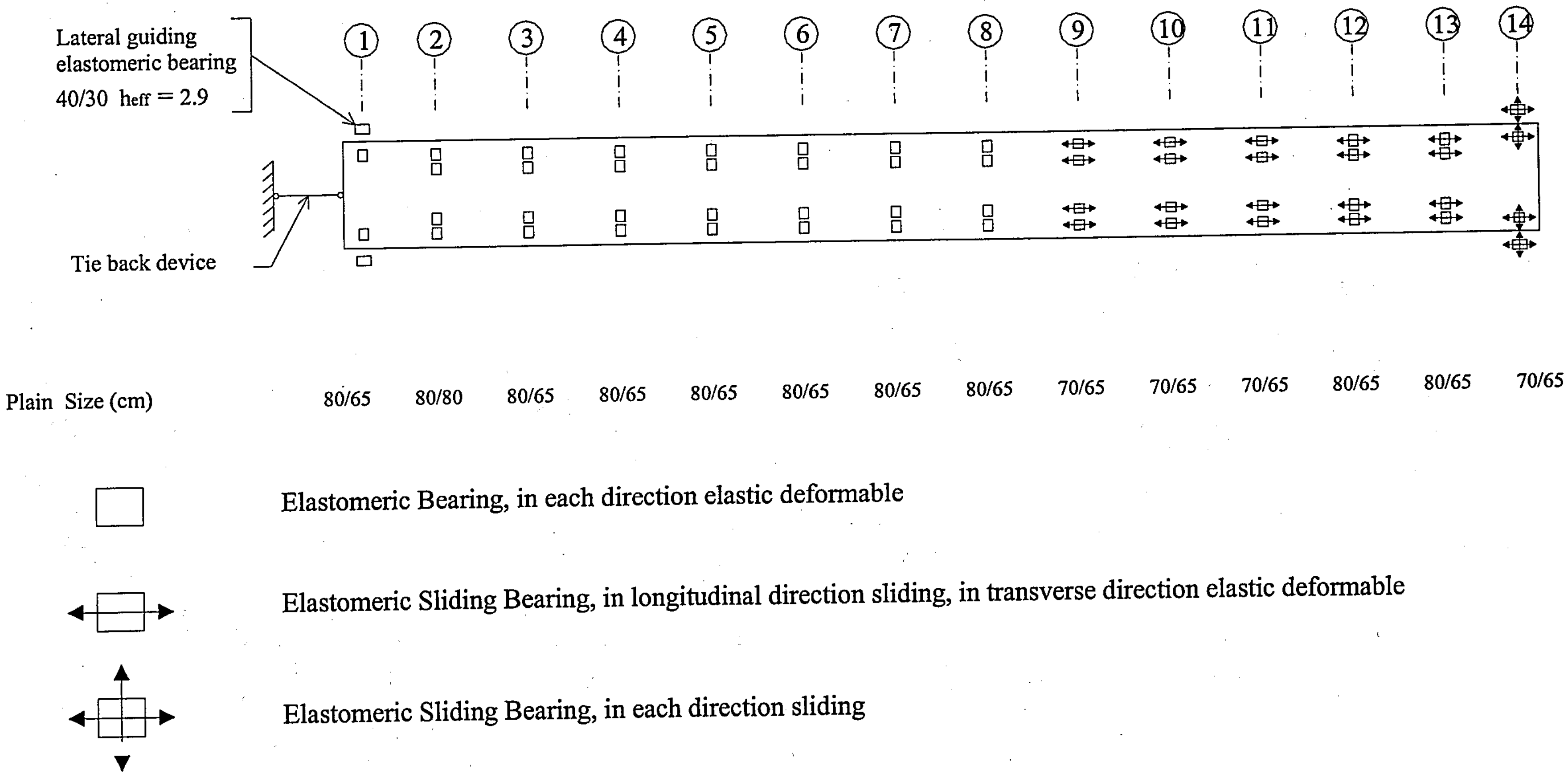

Figure 2.5. Deformation ability of the elastomeric bearings.

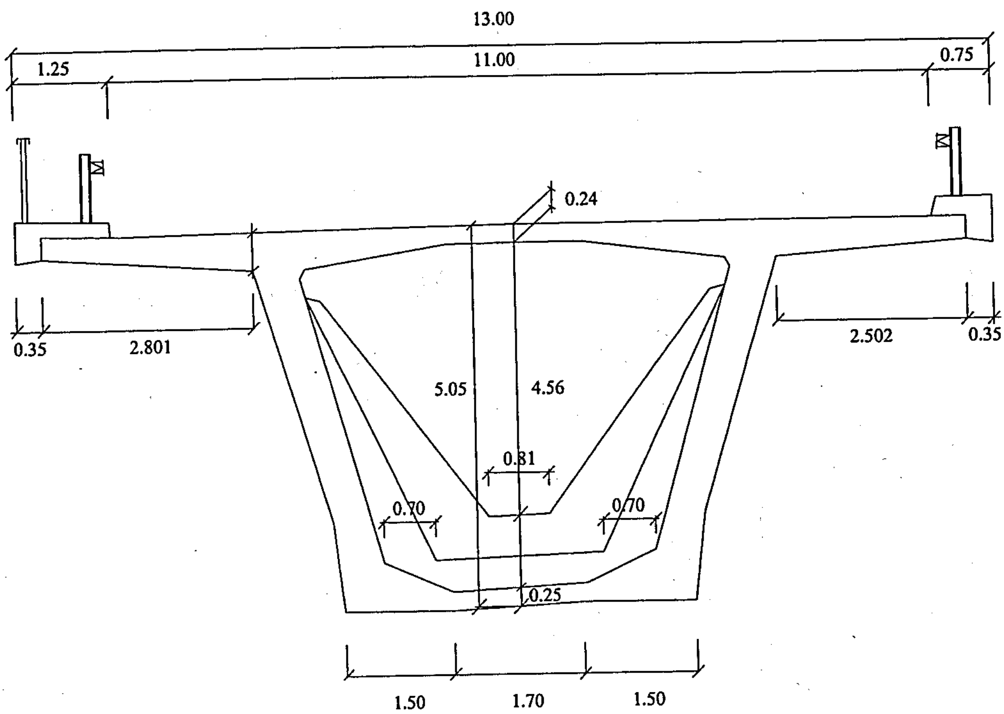

Figure 2.6. Superstructure Cross section

Table 2.1.Information about pier columns

Pier Number	Length of the column (m)	Gross Area (m^2)	Longitudinal Reinforcement ratio ρl (%)	Approximate Axial Force Due to Dead Load	Approximate Dead Load Ratio $P/f_c'*A_g$
1	8.567	6.12	1.15	19802.50	0.129
2	37.452	6.12	1.53	24392.83	0.159
3	46.773	6.12	2.36	25789.50	0.169
4	47.628	6.12	2.36	25789.50	0.169
5	46.618	6.12	2.36	25789.50	0.169
6	45.845	6.12	2.36	25789.50	0.169
7	45.305	6.12	2.36	25562.66	0.167
8	44.002	6.12	2.36	25393.63	0.166
9	44.883	6.12	2.36	25393.63	0.166
10	41.85	6.12	2.31	25064.48	0.164
11	34.202	6.12	1.31	23827.94	0.156
12	22.64	6.12	1.25	22297.82	0.146
13	17.512	6.12	1.25	21274.78	0.139

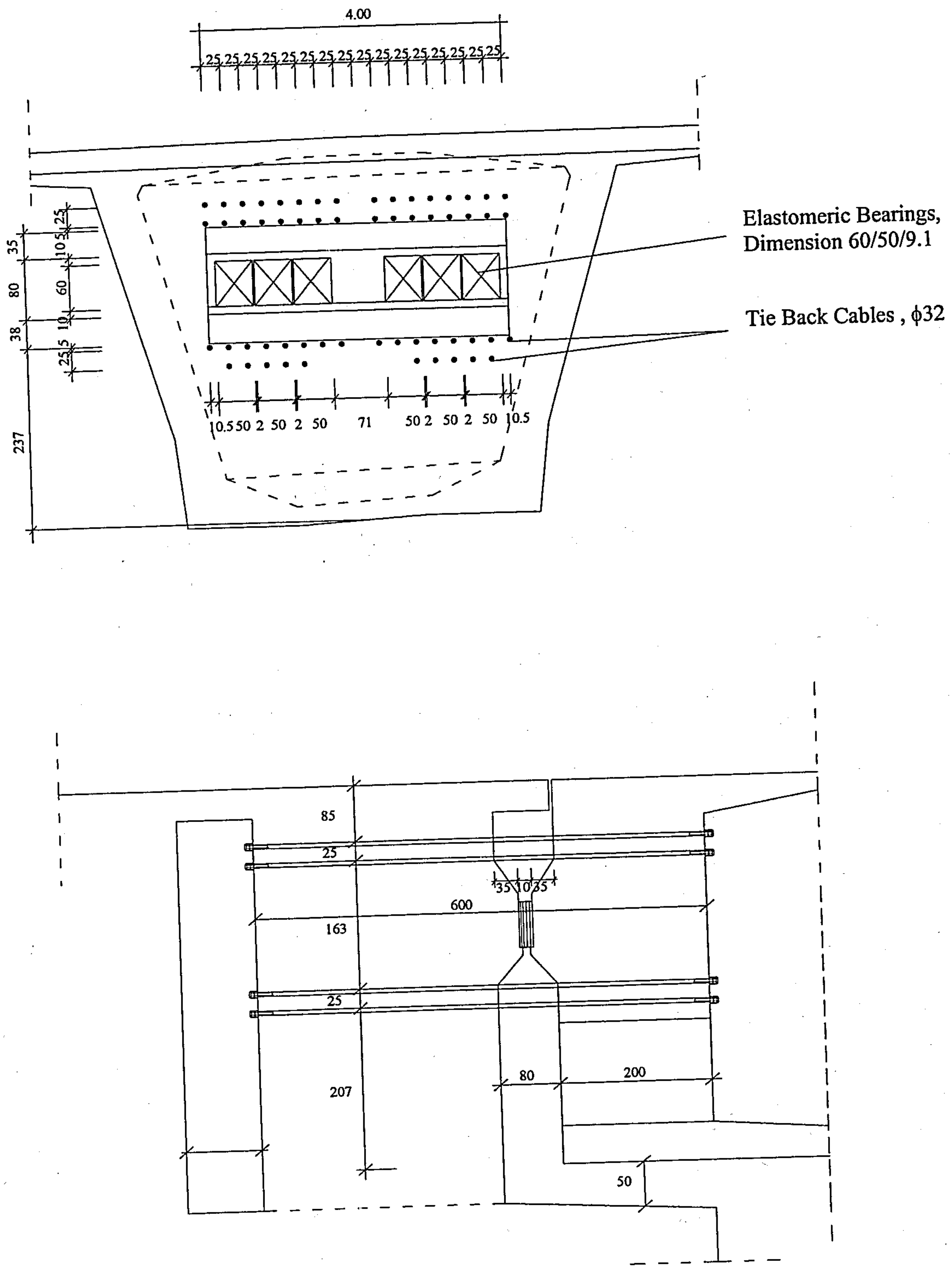

Figure 2.6. Detail of Tie Back device and Bumper System

3. SITE INVESTIGATION

Sadabat V3 Viaduct was visited in winter. During survey of the bridge, ground water table was approximately at surface near intermediate piers.

At the base of the columns, any significant corrosion such as cracking or spalling cover concrete could not be observed.

At the abutments, elastomeric pads between deck and shear key was installed to reduce pounding effect in transverse direction, but required dimensions for the stability of the elastomeric pads as noted in construction drawings was not provided well. Therefore, these pads lost their function.

As mentioned in previous section, sliding elastomeric bearings were used at pier 9 to13 and abutment at axis 14. PTFE bearings are used as a sliding support to allow superstructure movement in case of thermal and earthquake induced forces. Therefore, friction coefficient should be within intended limits. Regular inspection and service are required to protect sliding mechanism. As a result of observation at abutment, PTFE sliding bearings surface had rusted.

As a result of the site investigation, it can be said that the viaduct is generally in a good condition.

4.MODELING OF THE BRIDGE

4.1. Modeling objectives

The purpose of the mathematical modeling of any system is to quantify the response of the structure under earthquake loading based on the specified geometric and material properties. It is generally more preferable to create a simple model to capture meaningful seismic demand, rather than complex model. The seismic assessment of an existing bridge is typically aimed at a quantification of available capacities. The main objective of the mathematical model of Sadabat V3 viaduct is representation of available component capacities. Particularly, in the assessment of existing bridges, it is possible to quantification of capacities of subsystems based on known dimensions and probable material characteristics. In the model of the bridge, force deformation behavior of subsystems, such as piers and tie back device were developed. Other components, such as superstructure and elastomeric bearings intended to remain elastic, are modeled by elements, which have linear elastic behavior. As a final stage, deformation, force and displacement demands estimated by analysis of three-dimensional mathematical model of the viaduct were compared with the capacities of the components.

For the analysis of the bridge, sap2000 v7.40 Nonlinear Dynamic Analysis Program was used. The coordinate system used in the capacity and demand analysis is shown in Figure 4.1. The X and Y axes are referred to as the global longitudinal and transverse directions, respectively.

The model doesn't include soil structure interaction effect. Abutments were assumed to be infinitely rigid. Ground motion was assumed to be uniform for the supports, so asynchronous motion effect was neglected.

4.2. Superstructure

For the earthquake analysis of the bridges, it is common to use three-dimensional beam-column element (line element) to represent the behavior of the superstructure. The properties of the superstructure beam-column elements are selected to represent the properties of the box girder.

The geometry and connectivity of the elements and nodes of the model are shown in Figure 4.1. For each span, the box girder was discretized using 14 elements. Around support, due to the variation in cross section dimensions of the box girder, element length were selected properly to reflect accurate mass distribution and stiffness. Masses, assigned to the nodes, were determined from tributary element length by the analysis program. Only translation masses were assigned to the nodes of the superstructure. Contribution of rotational masses to the seismic response of the bridge was neglected and it was proved by mathematical model with superstructure that was modeled with shell elements. The nodes lie on the geometric center of the superstructure. At the supports (piers), connection of the node, lying on the geometric center of the box girder, to the elements representing elastomeric bearings was provided by massless and infinitely rigid beam–column elements. These nodes were assumed to behave rigid body under seismic loads.

Superstructure of the Sadabat V3 viaduct was expected to remain elastic. Therefore, the superstructure was modeled by linear elastic beam–column elements. The flexural stiffness of the box girder is based on gross section moment of inertia (I_{gross}). Gross-section area (A_{gross}) was used to model axial stiffness. Cross section properties of the superstructure are summarized in Table 4.1.

Table.4.1 Superstructure cross section properties

	Area, Agross(m^2)	Moment of Inertia, Iyy(m^4)	Moment of Inertia, Izz(m^4)	Torsion Constant, Jo (m^4)
Section 1	11.038	38.401	97.98	53.38
Section 2	14.609	48.876	108.8	70.5
Section 3	19.339	60.23	118.26	83.06

4.3. Elastomeric Bearings

Superstructure of the bridge was supported on the piers by means of rectangular reinforced elastomeric bearings pads. Reinforced elastomeric bearing is a kind of isolation system widely used in designing of long bridge. Besides having sufficient vertical load capacity, it provides horizontal flexibility and energy dissipation.

Four bearing pads support the girder on the top of every pier. Behavior of the bearings was intended to remain elastic. Therefore, elastomeric bearings were modeled by elastic spring elements. Lateral stiffness of the bearings was calculated based on the following equation. Shear modulus of the rubber was assumed 1.0 Mpa. Vertical stiffness of the bearings was assumed to be infinitely rigid.

$$k_b = \frac{G * A}{h_{eff}}$$

G = Shear modulus of rubber

A = Plan area of pad

h_{eff} = Effective rubber thickness.

4.4. Sliding Bearing

Sliding bearing was used as sliding support on the top of pier9 to13 and abutment at axis 14. Siding mechanism was provided only in longitudinal direction except for the bearing at the abutment. For the bearings at the abutment, sliding mechanism was provided in each horizontal direction. Elastomeric bearing was used as a centering device in conjunction with PTFE (one above the other). Therefore, response of the sliding bearings in low slip rate is governed by PTFE, depending on friction coefficient. In case of transverse movement during ground motion, behavior of the sliding bearing at the top of pier9 to 13 depends on elastomeric bearing. Friction coefficient at the bearing surface is about 0.02 and 0.03 for very low slip rate. In case of earthquake-induced movement, variation of friction coefficient increases with sliding velocity.

The so-called isolator 2, which is employed in sap2000 as a nonlinear link element, was used to model sliding bearings. Isolator 2 is used to model friction-pendulum isolator. The slipping surface of the bearings is flat, so pendulum behavior can be neglected to define zero radius and corresponding shear force due to pendulum behavior is zero. The friction forces are directly proportional to compressive axial force in the element. The element cannot carry tension force. The friction model is based on the research about base isolation analysis conducted by Nagarajaiah, Reinhorn and Constantinou. The frictional force – deformation relationship are given by

$$f_f = -P * \mu * z$$

P = Axial force

μ = Friction coefficient

z = Internal hysteretic variable

$$\mu = fast - (fast - slow) * e^{-rate*d}$$

fast = Maximum mobilized coefficient of friction

slow = Minimum mobilized coefficient of friction

rate = Parameter that controls the variation of the coefficient with the velocity of sliding

4.5. Piers

In the mathematical model of the bridge, every pier was represented by two non-linear spring elements in each horizontal direction as a subsystem. All of the dynamic response characteristics such as mass, stiffness were lumped to the non-linear spring elements. Force – deformation behavior of the piers, called pushover curve, was performed in strong and weak direction. Nonlinear behavior parameters, which are secant stiffness to the yielding point, post-yield stiffness and yield strength, of the pushover curves were assigned to non-linear spring elements according to bilinear approximation of the curves. The masses of the piers computed according to generalized single degree of freedom approach, which characterizes distributed mass along the length of the pier, was lumped to the non-linear spring elements. Generalized mass at pier top is expressed based on the linear deformation model in Figure 4.2 and the following equation.

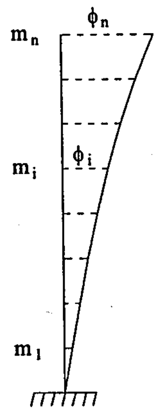

Figure 4.2. Definition of distributed mass and corresponding modal displacement

$$m^* = \sum_{i=1}^{n} m_i * \phi_i$$

4.6 Abutments and Tie Back Devices

Significant force is transmitted through the superstructure to the abutment by means of tie back device and bumper located at the interface between the abutment and the superstructure. When the superstructure moves away from the abutment, response of the system primarily depends on tie back device anchoring the deck with 58 cables with diameters of 32 mm to the abutment. In opposite direction six reinforced elastomeric bearings, reducing the pounding effect, transmit the forces to the abutment. To resist and provide sufficient stiffness, abutment at axis 0 has been designed with friction slab conservatively, so abutment was assumed infinitely rigid in the analysis.

This type of link system between deck and abutment makes the structure more flexible and reduces the forces transmitted to the abutment due to inelastic behavior of the cables. Non-linear spring element was used to model tie back device to observe inelastic behavior in cables for time history analysis. For response spectrum analysis, initial elastic stiffness is assigned to the spring element to reflect elastic behavior. Rigidity of the tie back was calculated according to total axial stiffness of the cables. To model bumper, compression only element was used with zero gap. Axial stiffness of the bumper and tie back device was calculated in accordance with the following equations.

$$k_{tieback} = E * A / L$$

E = 2e+5 kN/m^2

A = Total area of cables (58 (number of cables) *16.68 cm^2)

L = Length of the cable (6m)

$$k_{bumper} = \frac{6 * G * S^2 * A * k}{(6 * G * S^2 + k) * h}$$

G = Shear modulus

S = Shape factor

A = Area

k = Rubber bulk modulus

h = Total rubber height

4.7. Structural Model Used In The Analysis

Model#1 : Pier columns are represented by linear spring elements. Stiffness of the spring were determined based on the effective stiffness. Effective stiffness is assumed to secant stiffness to the yielding point determined from the pushover curve of the piers. Elastomeric bearings and tieback devices are also represented by linear spring element. This model will be used for response spectrum and pushover analyses.

Model#2 : The model is used for nonlinear time history analysis. Pier columns and tieback device are represented by nonlinear spring element defining its nonlinear hysteretic behavior. For PTFE elastomeric bearings located on the pier9 to pier13 and abutment at the axis14, nonlinear spring elements defining velocity dependent force deformation behavior are used.

In both mathematical models, superstructure behavior is represented by linear elastic frame element

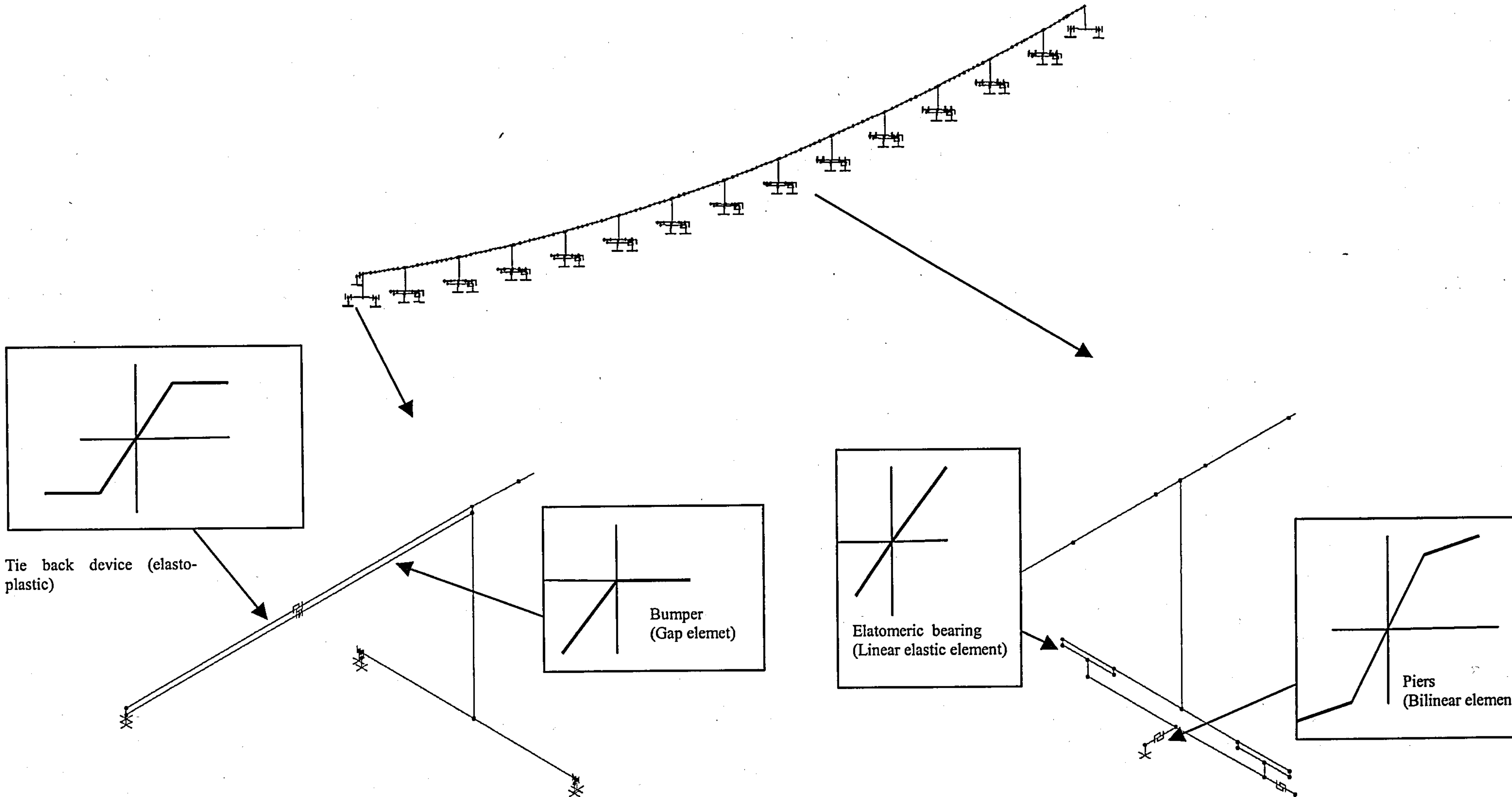

Figure 4.1. Model of Sadabat V3 viaduct

5. CAPACITY ESTIMATION

5.1. General

Estimation of strength, stiffness and deformability of structural elements are necessary to develop models for estimating structural demands and for evaluating the adequacy of the structure to sustain these demands. Realistic global behavior of the bridge depends on the nonlinear deformation characteristics of the components, which are directly related to the material properties. Therefore it is required to include nonlinear behavior of the material. In the assessment of the member capacity, widely used and accepted concrete and steel model have been used to reflect material nonlinearities. Characteristic material strengths belonging to concrete and steel are determined from as-built construction drawings and calculation report of the bridge.

All components, which are probable to exhibit nonlinear behavior, have been evaluated and idealized mathematically to represent nonlinear force-deformation relations using in the analyses. Therefore, this chapter primarily focuses on the pier columns, elastomeric bearings, superstructure and tieback devices.

5.2. Pushover Analysis of The Piers

Inelastic static (pushover) analysis was performed to determine lateral force and deformation capacities of the piers based on distributed flexibility approach in both longitudinal and transverse direction. Only flexural mode of inelastic deformation was considered in carrying out pushover analysis. It was assumed that lap splices and column reinforcement anchorages do not fail.

Local displacement capacity of a pier column is based on its rotation capacity, which is based on its curvature capacity. Curvature capacity can be determined by moment curvature analysis of the section.

5.2.1. Moment Curvature Analyses

Column moment curvature relations at the discrete section along the piers were obtained using xSECTION. The reinforced concrete section analysis program xSECTION is designed to predict strength and ductility of a reinforced concrete cross section subjected to axial load and incremental bending moment. The program includes various stress strain behavior for concrete and steel.

Transverse reinforcement details of the piers as shown in Figure 5.1 shows that amount of transverse reinforcement used in pier cross sections are insufficient to confine the compressed concrete within the core region. Therefore, for stress-strain relation of the concrete, unconfined concrete model was used in the moment curvature analysis. Mander's unconfined concrete model was used in the section analysis. The steel material model used for the analysis is based on Kent & Park's steel model considering strain hardening. Concrete and steel models used in the moment-curvature analysis are illustrated in Figure 5.2.

Moment-curvature analysis was performed for discrete sections or slices to take into consideration flexural behavior along the piers. Generally, column flexural behavior is conducted by the inelastic flexural deformation of the plastic hinge region. However, for tall piers, it should be considered variation of longitudinal reinforcement ratio and variation of axial forces acting at the discrete sections along the length, which affect the flexural strength and curvature ductility capacity. As an example, location of slices and corresponding moment curvature relations in longitudinal direction for pier11 are shown in Figure 5.3. and Figure 5.4, respectively. Slices were placed more closely than those at the other region of the column to represent plasticity at plastic hinge region.

5.2.2. Pushover Analysis Procedure

Pushover analysis was performed to determine lateral force and deformation capacities of the piers in both longitudinal and transverse direction. Pushover analysis was carried out under monotonically increasing load applied at the top of pier, tracing inelastic flexural deformation at slices mentioned above. At each load step, moment acting at the slices and corresponding curvature was integrated to find the top displacement based on virtual work method. Displacement at any load step can be expressed by the equation below. Analysis will stop when moment at the base reaches ultimate moment or moment corresponding to ultimate curvature of bottom cross section.

$$\delta u^i = \int_0^{Hc} M^i(x)\phi^i(x)dx$$

δu^i = displacement at any load step

Hc = Height of Column

$M^i(x)$ = Moment acting through the length of the column

$\phi^i(x)$ = Curvature distribution along the length

As a result of the pushover analysis, nonlinear properties, which are initial stiffness, post-yield stiffness and yield base shear, were defined based on bilinear approximation of the pushover curve.

There is only one potential plastic hinge location for single column bent system. Therefore ductility capacity of the pier depends on available plastic rotation capacity within the plastic hinge region. It is also well known that distribution and amount of transverse reinforcement enhance ductility of the section, and affects the ductility capacity of the member. Based on the relation between plastic rotation capacity and member ductility, bilinear force-deformation relations of the piers were presented by following steps and in Figure 5.5.

- Make a bilinear idealization of the moment-curvature analysis for the cross section at the base to determine theoretical yield curvature.

- Under incremental load applied at the top of column, when the critical section reaches its yield curvature (φ_y), double integration of the curvature distribution along the column results in the column top yield displacement (u_y). Yield displacement and corresponding yield force (P_y) are determined from the following equation:

$$\varphi_y(x) = \int_0^L \kappa_y(x)d(x), \qquad u_y(x) = \int_0^L \varphi_y(x)d(x)$$

$$P_y = M_{yi} / L$$

- Using the same way, as a result of the double integration, ultimate top displacement (u_u) is determined when the critical section reaches its ultimate curvature (φ_u). Plastic displacement (u_p) and plastic rotation (φ_p) is obtained.

$$\varphi_u(x) = \int_0^L \kappa_u(x)d(x), \qquad u_u(x) = \int_0^L \varphi_u(x)d(x)$$

$$P_u = M_u / L$$

$$\varphi_p = \varphi_p(L) = \varphi_u(L) - \varphi_y(L)$$

$$u_p = u_p(L) = u_u(L) - u_y(L)$$

- Compare pushover curve and bilinear approximation of the force deformation relations of the piers.

Example pushover and its bilinear idealization for pier11 are shown in Figure 5.6. As a result of the bilinear approximation of the piers, yield and ultimate displacements and corresponding ductility capacity of the piers for both transverse and longitudinal direction are summarized in Table 5.1

5.3. Shear Strength of The Piers

Behavior of the piers not only depends on the flexural behavior of the plastic hinge region but also depending on the details of the column, other actions such as shear failure, poor confinement and inadequate anchorage of the longitudinal reinforcement. Particularly for the columns constructed before development of modern ductile detailing, shear failure because of the inadequate confinement can be observed. Therefore, it is necessary to inhibit shear failure by ensuring that shear strength exceeds the shear corresponding to the maximum flexural strength.

The evaluation of shear capacity of bridge columns is an active area of research. The shear force capacity of a column depends on the contribution of the concrete, the transverse and longitudinal reinforcement, and on the axial force resisted by the column. The maximum shear force component resisted by the concrete depends on the amount of inelastic flexural deformation because of shear-flexure interaction and degradation of the concrete in the plastic hinge region.

The formulation by Priestley (Priestley et al., 1996) has been used to estimate the shear strength of the pier columns. The proposed method by Priestley provides significantly improved correlation with experimental results. The column shear strength is given as;

$$V_n = V_c + V_p + V_s$$

Vc is the concrete component of shear strength, Vp is the contribution of the axial load in the column and Vs is the contribution of the transverse reinforcement. The concrete contribution of the column is given as:

$$V_c = k * \sqrt{fc'} * A_e$$

k= factor to account for member ductility. For this analysis, the factor is related to curvature ductility

$$= \begin{cases} 0.29 & \text{for} \quad \mu \le 3 \\ 0.43 - 0.048\mu & \text{for} \quad 3 < \mu \le 7 \\ 0.15 - 7.3*10^{-3}\mu & \text{for} \quad 7 < \mu \le 15 \\ 0.042 & \text{for} \quad \mu > 13 \end{cases} \text{ for uniaxial ductilty}$$

μ = Curvature ductility.

fc' = Compressive strength of concrete.

A_e = Effective shear area ($0.8*A_{gross}$).

V_c = Concrete component of shear strength

Axial load contribution to the shear strength is explained in Figure 5.7 and given as:

$$V_p = \frac{D-c}{2*a} * P$$

D = Overall section depth.

c = Depth of the flexural compression zone

a = L for single bending, L/2 for double bending.

L = Height of the column

P = Axial load in member.

V_p = Contribution of axial load

The contribution of the transverse reinforcement is given as:

$$V_s = \frac{A_s * f_{yh} * D'}{s} * \cot(\phi)$$

D' = Distance between transverse reinforcement.

f_{yh} = Yield stress of transverse reinforcement.

ϕ = Angle of inclined cracking.

A_s = Area of transverse reinforcement.

S = Spacing of transverse reinforcement layer.

V_s = Contribution of steel reinforcement

Angle of inclined cracking was assumed 45°, Shear strength of the piers has been determined from the equations including displacement ductility level of the piers. Shear strength estimation was made for only pier1 and pier13. Because, these piers will probably attract more shear forces as compared to the flexible piers. In addition, considering transverse reinforcement details of the flexible piers better than short piers, short pier are more susceptible to fail in the case of large shear force demand. Comparison of shear strength and flexural strength of the pier1 and pier13 in both directions are illustrated in Figure 5.8 and Figure5.9.

5.4. Elastomeric Bearings

Lateral displacement capacity of a laminated rubber bearing depends on the maximum shear strain of the rubber. Maximum shear strain resisted by the elastomeric pad prior to failure was assumed 150% according to Caltrans Seismic Design Criteria. Effective rubber heights of the elastomeric bearings are equal to 8cm. Consequently, displacement capacity of the bearings are equal to 12cm for all elastomeric bearings.

5.5. Superstructure Flexural Capacity

Bridges, which are crossing deep valley with continuous deck, which is simply supported on tall piers, are displacement sensitive structures in transverse direction, like Sadabat V3 viaduct. Therefore, it is required special consideration for seismic loads.

Behavior of the viaduct under transverse seismic effect may result in large displacement demand at the mid of the deck because of its flexibility. In addition, the design of superstructures, which are simply supported on the piers, is generally governed by vertical and time dependent forces. Therefore, flexural capacity of the deck may be insufficient to resist unexpected forces due to an earthquake excitation in transverse direction.

As a result of the consideration above, flexural capacity of the superstructure in horizontal plane was evaluated to assure elastic response of continuous deck. Moment-curvature analysis was performed to determine flexural capacity.

5.5.1. Moment curvature Analysis

The reinforced concrete section analysis program XTRACT, coded by *Imbsen Sofware Systems,* was used to evaluate cross section behavior of the deck. The program provides various material models for concrete, steel and prestressing steel. The cross section was discretized by using mesh generation to provide realistic estimation. Fiber models of the cross sections at mid span and at the support are shown in Figure 5.10.

Mander's unconfined concrete model was used to represent stress strain behavior of the concrete as stated in section 5.2.1. Characteristic compressive strength of the concrete is 35 Mpa. For the prestressing steel model, typical tensile stress strain behavior of strand (Grade 1770) was used in the analysis. Prestressing steel model used in the moment curvature analysis is shown in Figure 5.11.

Current stress and corresponding strain distribution due to the moment acting at the cross sections under dead load was evaluated before monotonic moment loading in transverse direction. Analysis was performed for both earthquake direction at the mid and at the support of the span.

Moment capacity was determined from the moment-curvature curve, based on the assumption that moment capacity is equal to the moment, reported at concrete strain of 0.002 or at prestressing steel stress of 0.0076, whichever occurs first. Moment capacity at the mid and at the support are summarized in Table 5.2, according to the sign conventions in Figure

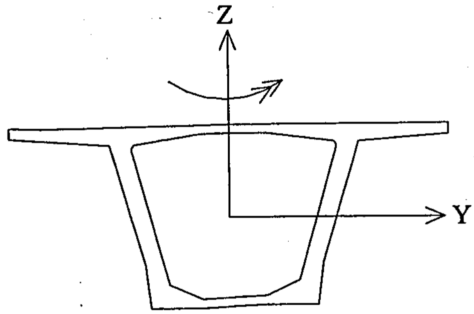

5.12.

Positive Bending

Figure 5.12 Sign Convention for Superstructure Forces

Table 5.2. Superstructure flexural capacity in horizontal plane

Middle	Support
(+) Bending Moment Capacity(kNm)	(-) Bending Moment Capacity(kNm)
303900	293700
306300	282000

5.6 Axial Force Capacity of Tie Back device

Nonlinear force displacement relation of the tieback device directly depends on the stress strain behavior of the cables anchoring the deck to the abutment. Stress strain behavior of the cable shown in Figure 5.13 was used to determine axial force capacity of the tie-back device. Because it is difficult to model nonlinear hysteretic behavior of the steel considering strain hardening portion, dashed curve was used to represent inelastic behavior of the tie-back device. Initial elastic stiffness and yield force of the tie-back was calculated according to the following equation. Based on the this assumption, assumed hysteretic rule as shown in Figure 5.14.

$$K = \frac{E * A}{L}$$

E = Elastisite modulus of the steel

A = Total area of cables

L = Length of the cables

$$F_y = f_{sy} * A$$

F_y = Yield strength of the tie-back device

F_{sy} = Yield stress of the cable

$K = (2E+8 \text{ kN/m}^2 * 4.66E\text{-}2 \text{ m}^2) / 6 \text{ m} = 1.533.333 \text{ kN/m}$

$F_y = 500.000 \text{ kN/m}^2 * 4.66E\text{-}2 \text{ m}^2 = 23.300 \text{ kN}$

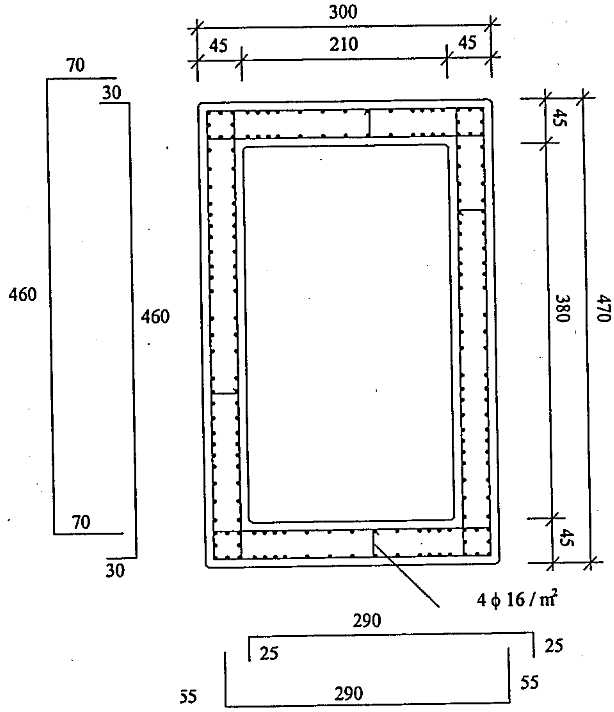

Figure 5.1. Typical transverse reinforcement detail.

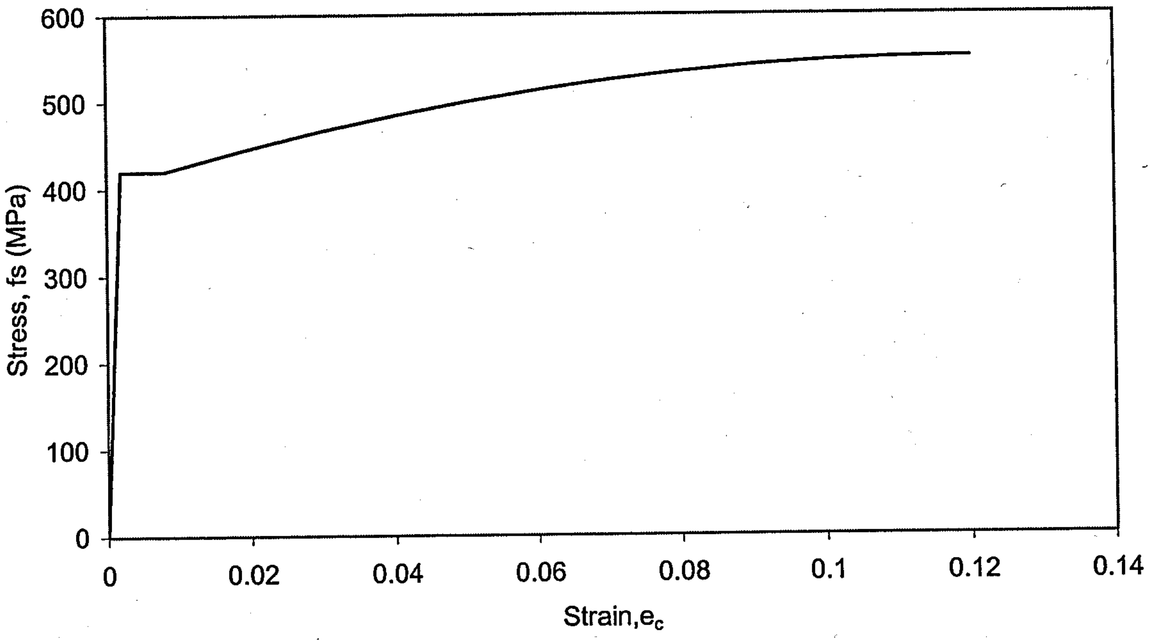

(a)

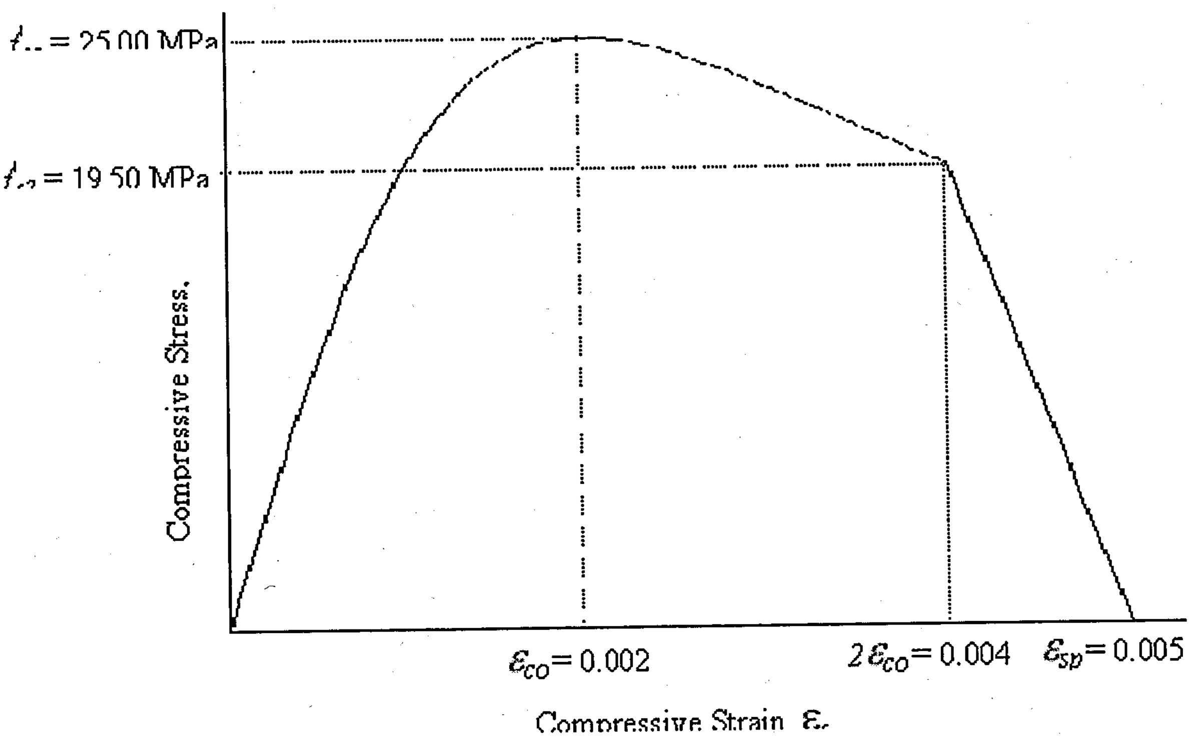

(b)

Figure 5.2. Material models for steel (a) and concrete (b)

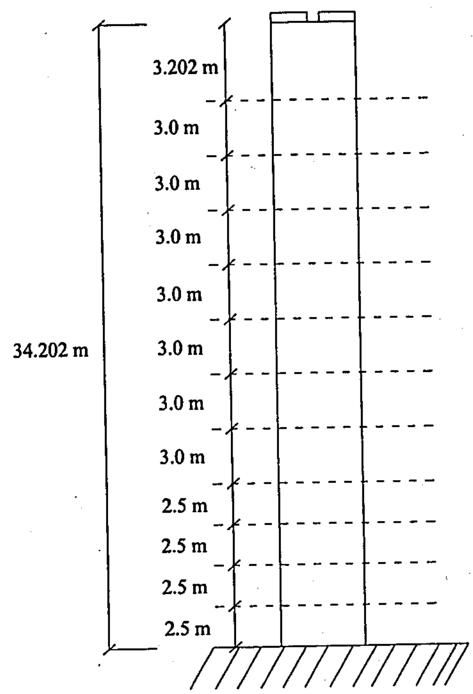

Figure 5.3. Location of the sections considered in moment-curvature analysis for Pier11

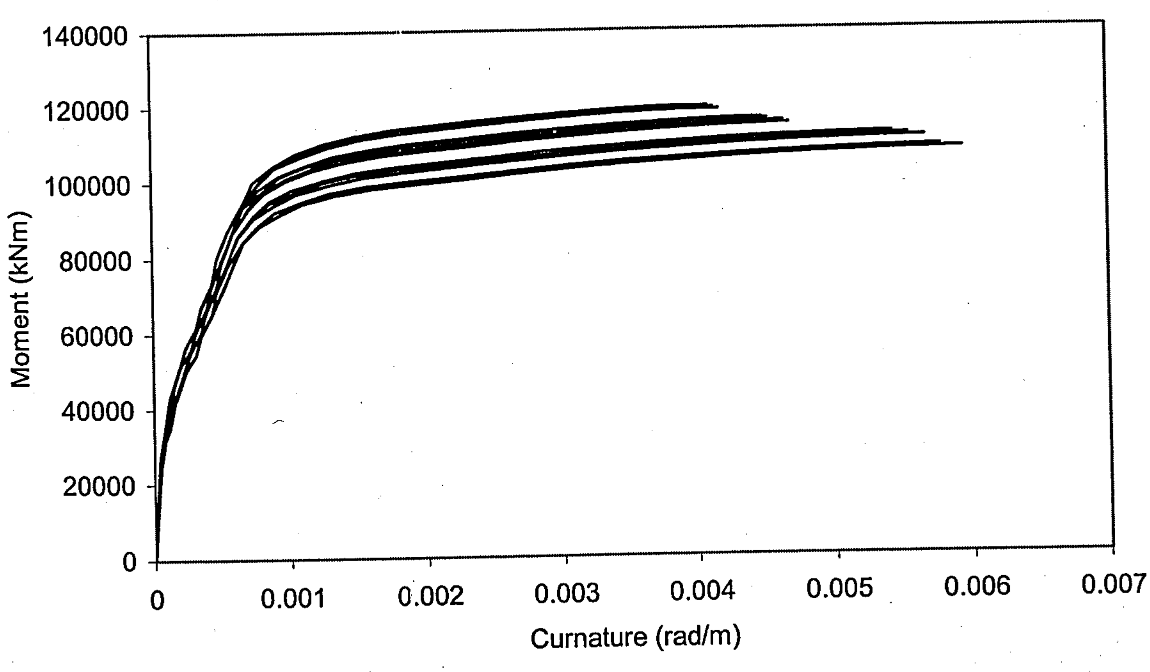

Figure 5.4. Moment curvature relations of the slices for Pier11

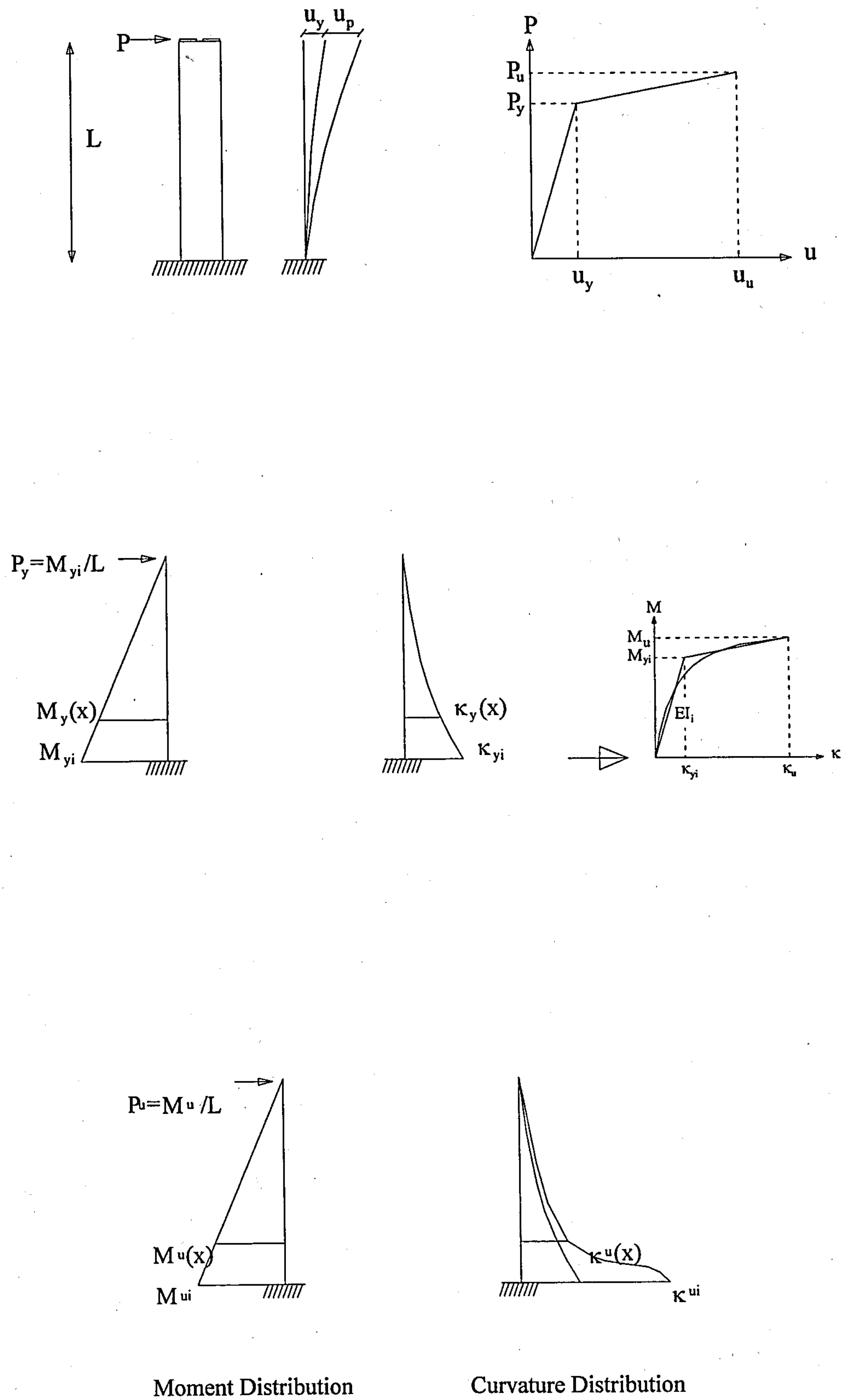

Figure 5.5. Bilinear idealization procedure for the piers

Table 5.1.Displacements and corresponding ductility capacity of the piers for both direction.

	In Transverse Earthquake Direction		
	Δ_{yield}(m)	$\Delta_{ultimate}$(m)	$\mu_{Capacity}=\Delta_{ultimate}/\Delta_{yield}$
Pier 1	0.011	0.042	3.82
Pier 2	0.28	0.601	2.15
Pier 3	0.513	0.823	1.60
Pier 4	0.532	0.862	1.62
Pier 5	0.51	0.823	1.61
Pier 6	0.493	0.793	1.61
Pier 7	0.48	0.765	1.59
Pier 8	0.522	0.821	1.57
Pier 9	0.543	0.857	1.58
Pier 10	0.461	0.71	1.54
Pier 11	0.172	0.488	2.84
Pier 12	0.086	0.244	2.84
Pier 13	0.053	0.157	2.96

	In Transverse Earthquake Direction		
	Δ_{yield}(m)	$\Delta_{ultimate}$(m)	$\mu_{Capacity}=\Delta_{ultimate}/\Delta_{yield}$
Pier 1	0.018	0.063	3.47
Pier 2	0.399	1.219	3.05
Pier 3	0.725	1.891	2.61
Pier 4	0.752	1.973	2.62
Pier 5	0.720	1.877	2.61
Pier 6	0.696	1.808	2.60
Pier 7	0.738	1.763	2.39
Pier 8	0.768	2.065	2.69
Pier 9	0.800	2.201	2.75
Pier 10	0.662	1.592	2.40
Pier 11	0.344	1.061	3.08
Pier 12	0.155	0.495	3.20
Pier 13	0.091	0.321	3.53

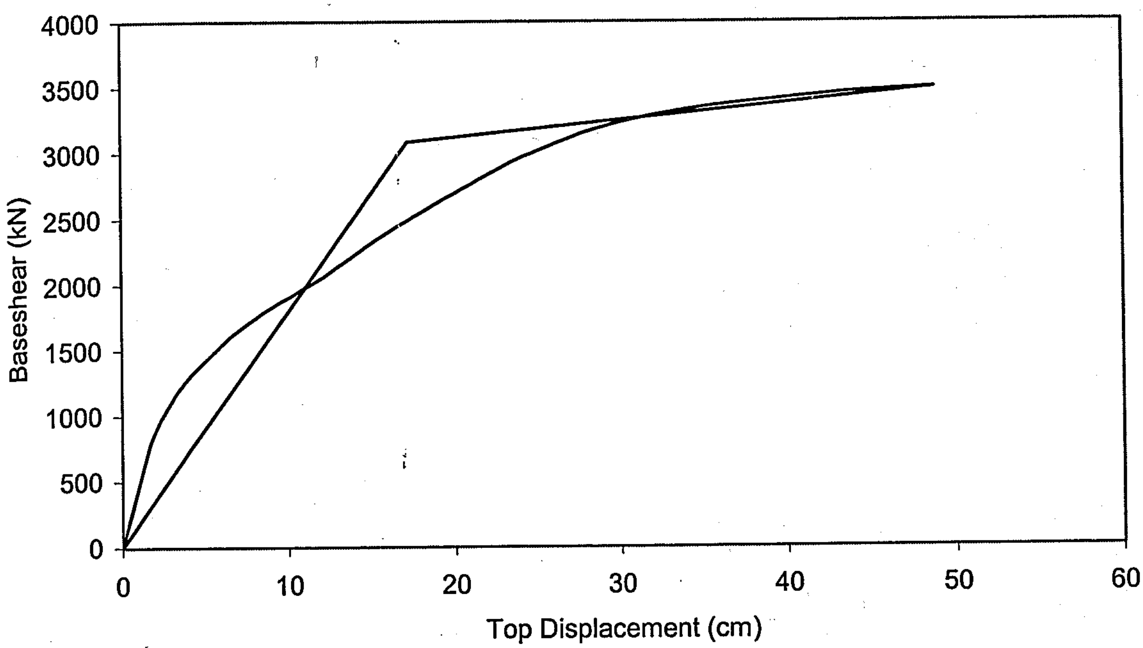

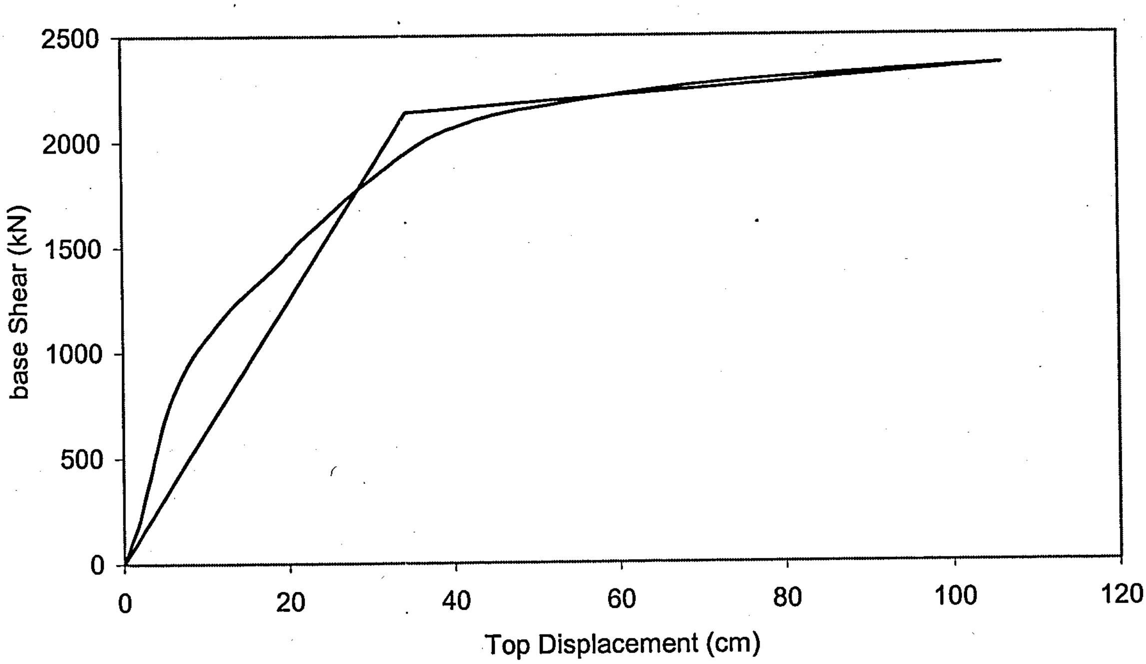

Figure 5.6. Pushover curve and bilinear representation in transverse and longitudinal direction for Pier11

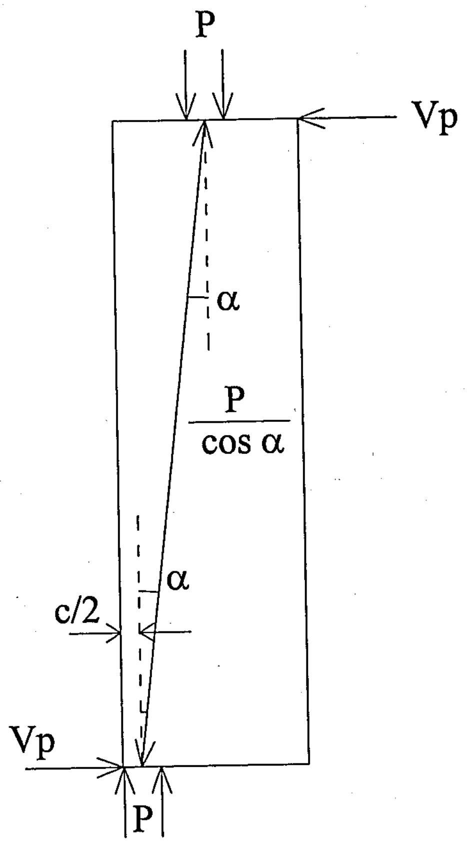

Figure 5.7. Contribution of axial force to column shear strength

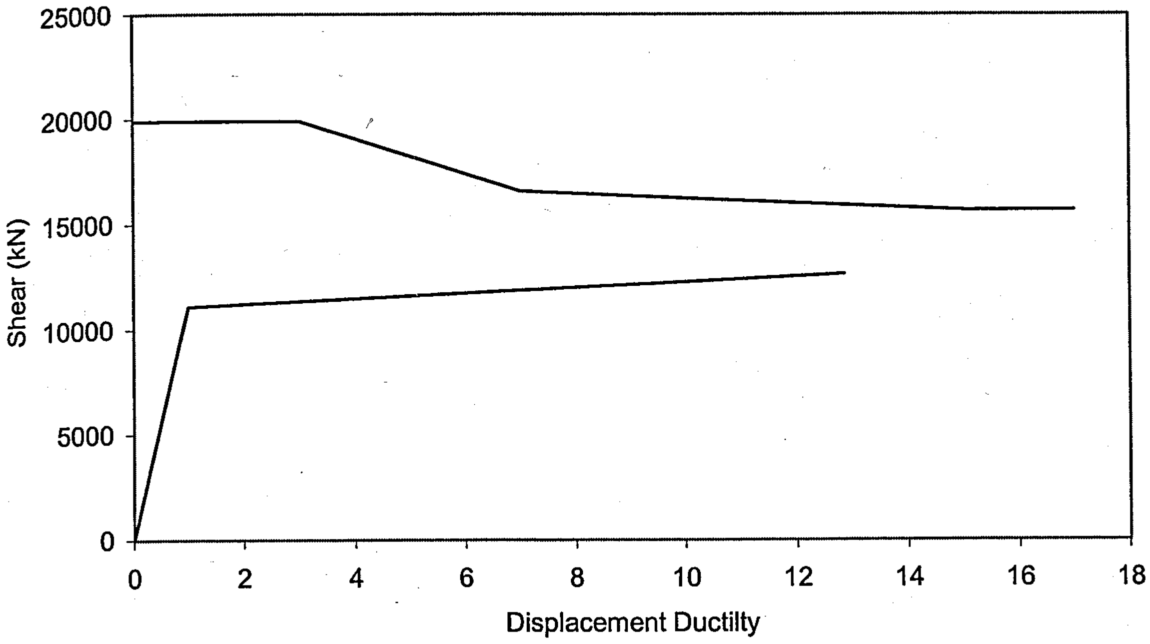

(a)

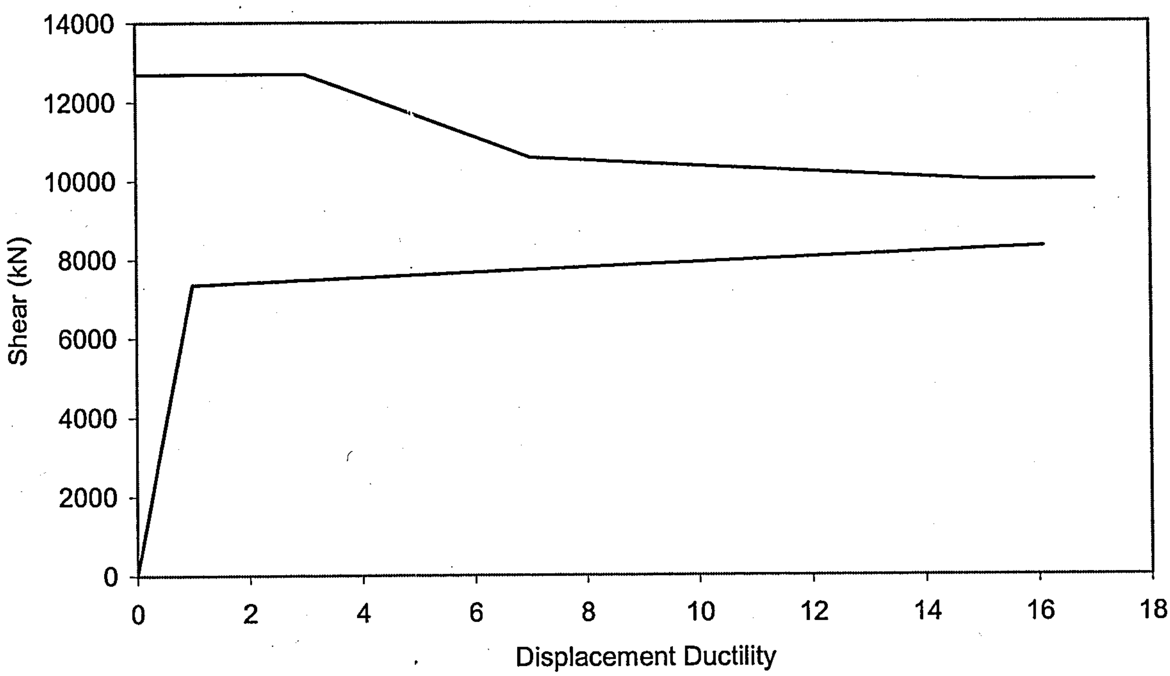

(b)

Figure 5.8. Shear strength degradation based on displacement ductility for Pier1 (a) in each direction, (a) transverse, (b)longitudinal.

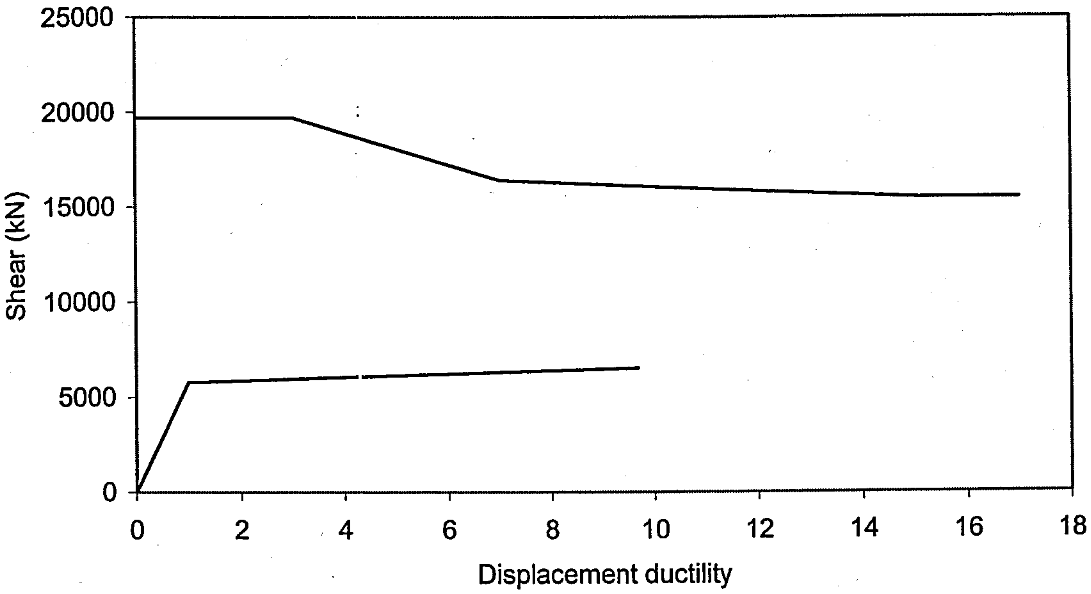

(a)

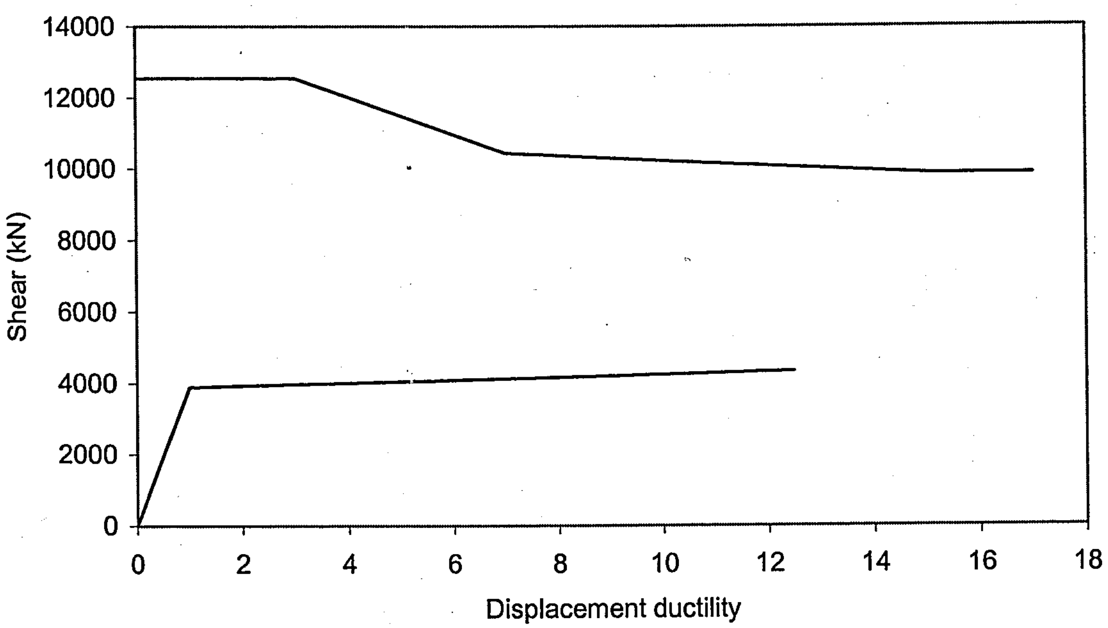

(b)

Figure 5.9. Shear strength degradation based on displacement ductility for Pier1 (a) in each direction, (a) transverse, (b)longitudinal.

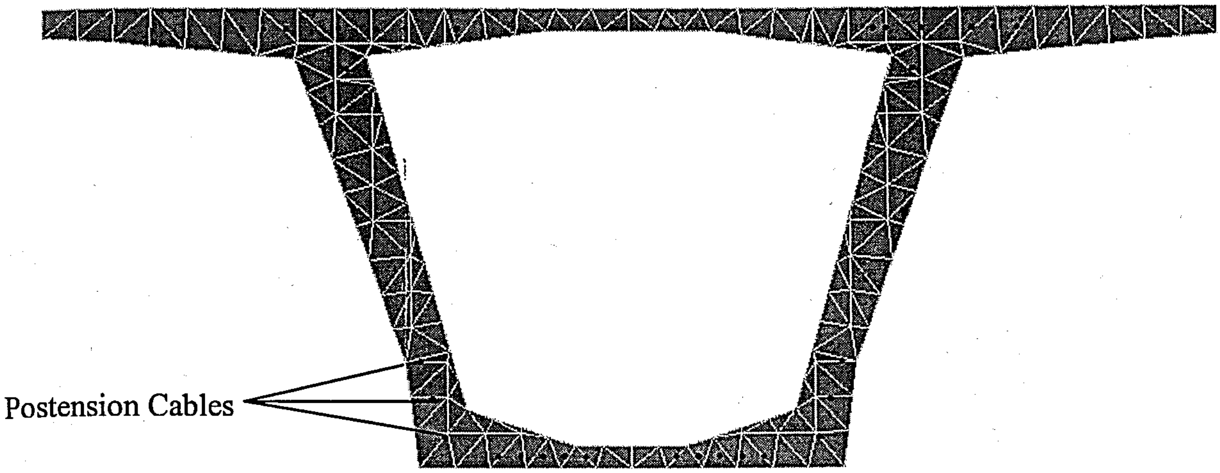

(a)

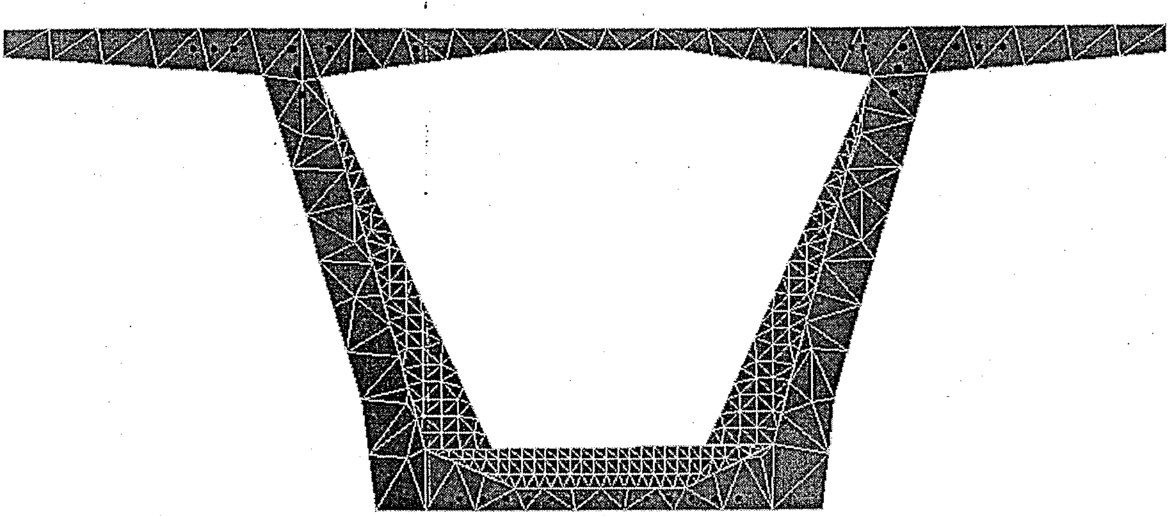

(b)

Figure 5.10. Superstructure cross section discretization for the section at mid span (a) and above the piers (b)

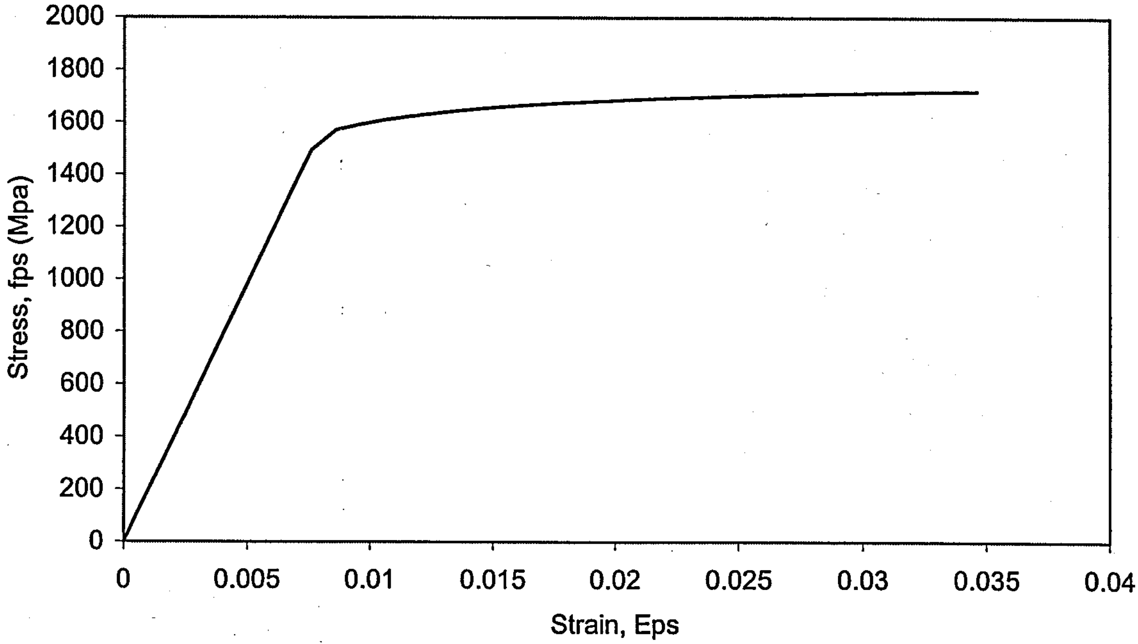

Figure 5.11. Prestressing steel model

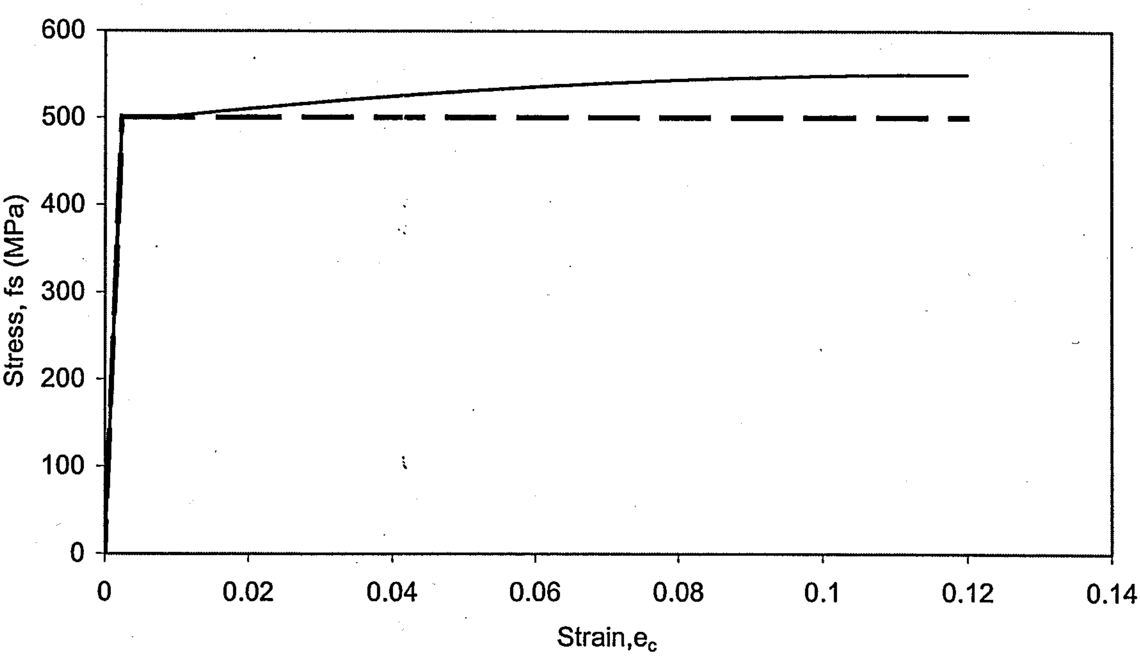

Figure 5.13. Realistic and assumed steel model for tie back cables

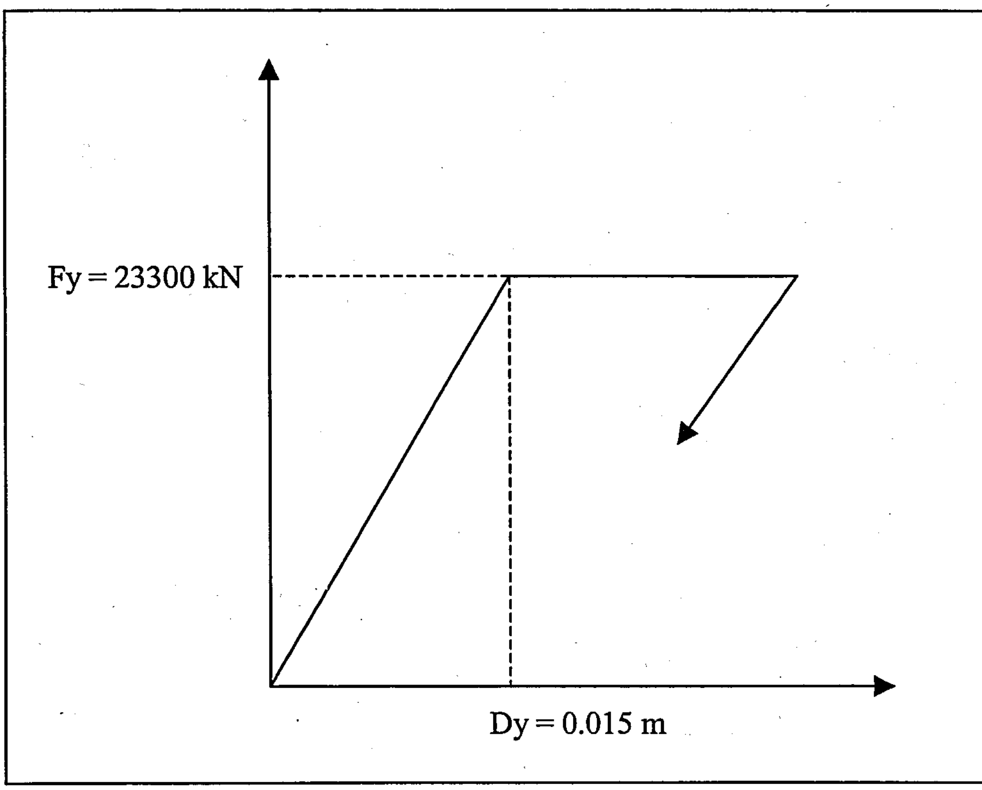

Figure 5.14. Assumed Hysteretic Rule for Tie Back device

6. PERFORMANCE EVALUATION

6.1. Evaluation Approach

Seismic performance of an existing bridge primarily depends on; geometric configuration, detailing of the member and level of seismic excitation, which can be defined functional evaluation earthquake (FEE) and safety evaluation earthquake (SEE). Evaluation approach includes analysis of the bridge using various analysis methods to observe earthquake demands on the structure. It is important to choose accurate analysis method based on the geometric configuration and importance of the bridge to quantify performance of the bridge in terms of local and global indices. As a result of the analysis under earthquake loads determined in accordance with seismicity of the region, demands on the structural components are compared with their capacities to determine performance level.

Adopted provisions for required performances in seismic design code, which bridges should meet are more severe as compared to the old design and evaluation philosophy. For instance, critical structures are expected to respond elastically to incident ground motion. Most other structures are allowed to show inelastic behavior and structural damage is permitted to some extent in design phase. In this context, bridge structures generally are categorized as important or ordinary (i.e. Caltrans and A.A.S.H.T.O.) depending on the desired performance level. Important bridges are distinguished from ordinary bridges, as those would be expected to carry normal traffic and should not need repair or have minimal damage following an earthquake. In other words, structural response is elastic during major earthquake. In seismic performance assessment of Sadabat V3 viaduct, the viaduct was evaluated as an important bridge.

The design of the transportation structures to perform satisfactorily under expected seismic conditions requires that realistic earthquake loadings during their life times be specified and that the structural component be proportioned to resist these loadings within desired performance limits. As mentioned above, two levels of earthquake loadings, FEE and SEE are defined to adopt two level-design strategies for bridges. Functional evaluation earthquake is defined as the event, which has a high probability of occurrence during the lifetime of a structure. The structure should be proportioned to resist the intensity produced by this event without significant damage. Safety evaluation earthquake is defined as the most severe event, which can be expected to occur at the site. Because the earthquake has a very low probability of occurrence during the life of a structure, significant structural damage is permitted. However, important bridge located on major traveled route, where no convenient alternative routes exist, like Sadabat V3 viaduct, is expected to remain functional immediately following an SEE event. They must be proportioned to resist the intensity of this event without experiencing significant damage. In evaluation of Sadabat V3 viaduct, expected performance is the same as the required performance adopted for important bridges mentioned above, and accordingly, level of seismic excitation was described as SEE event and represented by smoothed elastic response spectrum defined in the section 6.3.

6.2. Selection of Analysis Methods

The aim of the analysis is to estimate dynamic characteristics and structural response under representative earthquake loading. It is possible to choose various analysis methods resulting from the combination of the options: linear/nonlinear, static/dynamic. The appropriate choice in codes depends on the seismic hazard, importance of the bridge, and structural regularity. According to seismic design codes for bridges (A.A.S.H.T.O., Eurocode 8), Regularity of a bridge is a function of mass and stiffness distribution and number of spans. Therefore, time history analysis is reasonable and inevitable analysis method for irregular long viaducts where particularly, isolation devices are used, like Sadabat V3 viaduct. Linear analysis method has been also used as a preliminary approach in performance evaluation of the Sadabat viaduct to estimate demands on the structure. As a nonlinear analysis tool, nonlinear time history and collapse mechanism analyses have been used to define performance of the bridge exactly.

Linear analysis methods are suitable for the structures expected to respond linearly. For assessment purpose, linear analysis can be used for preliminary analysis to determine that the bridge needs retrofit measures. As a linear analysis tool, response spectrum analysis was used for Sadabat V3. Analysis model used for response spectrum analysis is linear elastic model based on cracked or effective stiffness of the members. After performing linear analysis, more sophisticated analysis techniques such as nonlinear time history may be used to determine required retrofit measures exactly. Capacity /demand ratio approach associated with elastic analysis is widely used to evaluate demand in preliminary phase. Force and deformation demands resulting from the elastic analysis are compared with the capacities of the components. When the ratio of demand and capacity is greater than one, inelastic response is expected. Where ductile behavior is assured, ratio, greater than one, may be accepted. Linear elastic analyses are also used for structures intended to respond nonlinearly. Structural displacement of inelastic system can be estimated using equal displacement or equal energy rules. Based on these rules, required strength of inelastic system can be defined to reduce the strength corresponding to the elastic system having the same initial period by means of reduction factor.

Particularly for assessment of existing bridges, nonlinear analysis methods are more appropriate with respect to linear elastic analyses in order to observe the inelastic deformation demands on the components and to compare with their capacities. By this way, it is possible to monitor the available capacity and seismic demand simultaneously. Nonlinear static procedure (pushover analysis) is one of the nonlinear analysis methods. In this method, lateral force proportioned to mass and first mode shape is applied to the structure incrementally, upgrading the stiffness of the system at every step. It is possible to observe inelastic deformations and displacements of the components, until the target displacement demanded by the earthquake is reached. Although pushover analysis is one of the most useful analyses for assessment of existing bridges, it has some restrictions in application for irregular long viaducts. Due to the consideration of single mode contribution, the designer should be aware of higher mode effects being neglected. Another nonlinear analysis method is inelastic time history analysis that contains the demand and the capacity side of the evaluation. The demand side includes a number of earthquake ground motions in accordance with the expected ground motion at the site of the bridge, whereas the capacity side contains cyclic force-deformation characteristics of the members, such as the widely known moment-rotation relation of plastic hinge region of columns or force-deformation relation of friction slider bearings. In addition to the hysteretic member characterization, Interaction between bridge components, such as abutment or expansion joints in spans, can be characterized by using gap and tension only elements. Nearly realistic response of the structure can be achieved by using inelastic time history analysis.

6.3. Response Spectrum Analysis

6.3.1. Definition of Earthquake Ground motion

In a response spectrum analysis, earthquake demand is characterized by ground motion response spectrum for specified hazard level. Expected ground motion can be determined on either probabilistic or deterministic basis. For the analysis of the Sadabat V3 viaduct, acceleration response spectrum representing expected ground motion at the site has been determined from probabilistic seismic hazard map of Turkey prepared by KOERI, Department of Earthquake Engineering. According to the requirement for important bridges in A.A.S.H.T.O and Caltrans, acceleration response spectrum with probability of exceedance 2% in 50 years corresponding to 2475 return period has been used to define earthquake hazard level. 5% damped response spectrum with appropriate site class was constructed by using Fema 356 general response spectrum format as shown in Figure.6.1.

Due to lack of detailed information about the site geology, appropriate site class in accordance with Fema 273 was assumed as D, on the basis of calculation report of Sadabat V3.

6.3.2. Assumptions

For structure responding elastically during earthquake, modal maximum responses do not occur at the same time. Therefore, it is required to use combination methods to account for modal contributions to the total response. After determining amplitudes of the modal contribution from elastic acceleration response spectrum, the contributions are superimposed using statistics rules such as CQC or SRSS. In the response spectrum analysis of Sadabat V3 viaduct, CQC (complete quadratic combination) was used to superimpose modal effects. The number of modes included in response analysis in a given direction is important to estimate structural response accurately. Significant mode numbers in the response analysis should be considered to capture at least 90% mass participation in each of the bridge's principal horizontal direction. Natural vibration periods and participating mass ratios for modes included in the response analysis were summarized in Table 6.1. Equivalent viscous damping ratio for all modes was assumed 5%. Analysis model used in the response analysis is linear elastic model based on cracked or effective stiffness properties of the members, except for superstructures. Effective stiffness properties have been used for the piers derived from bilinear representations of force-deformation relation (pushover analysis) of the piers as a subsystem.

In many seismic design codes, elastic acceleration response spectrum constitutes the fundamental basis of the required performance that should be provided by a structure, but it has some well-known and widely accepted limitations [Priestly, M.J.N., *Myths and Fallacies in Earthquake Engineering]*. For instance, structures are designed according to peak response under earthquake ground motion without considering duration effect. Especially for structures having short period, cumulative damage due to a great number of response cycles during earthquake should be taken into consideration. Another limitation is that relative responses between adjacent components vibrating independently cannot be determined exactly because of the modal contributions with the same algebraic sign. Besides, distribution of force demands is determined based on elastic member properties, but member stiffness changes as inelastic response develops, so the force distribution will not be proportioned to the elastic distribution.

6.3.3. Response Spectrum Analysis Results

When displacement demands on the elastomeric bearings determined from the analysis were compared with their capacities, elastomeric bearings have sufficient capacity to perform elastically under longitudinal seismic effect. As shown in Table 6.2, relative displacement demands are below the calculated displacement capacities determined based on the assumption that maximum shear failures resisted by elastomeric pad prior to failure is estimated at %150. Like the elastomeric bearings, the longitudinal seismic displacements at the top of the piers do not exceed the lateral displacements capacities of the piers as shown in Table 6.3.

However, in transverse response, seismic forces acting at the top of the piers exceed their lateral force capacities. As shown in Table 6.3, lateral strength of the piers5 to 8, pier11 and pier12 were inadequate to respond elastically. Estimated ductility demands for the piers are shown in Figure 6.2 to Figure 6.11 assuming equal displacement rule. In addition, elastomeric bearings located at the top of these piers are probable to fail as shown in Table 6.2.

As a result of the preliminary evaluation, response of the bridge in the longitudinal seismic effect is likely elastic, whereas in the transverse direction, the behavior of the bridge is critical.

6.4. Nonlinear Time History Analysis

6.4.1. Selection of Ground Motion Inputs

In time history analysis, demand side of the analysis is composed of numerous time history acceleration records in accordance with the specified hazard level. Ground motion is significantly affected by source mechanism, travel path geology and local soil condition, so it is almost impossible to find recorded earthquakes matching site seismicity of the bridge and structural dynamic characteristics exactly. Particularly, for structures with long period like Sadabat V3 viaduct, nonuniform responses should be expected for different ground motions because the earthquake energy is distributed in short period ranges. In addition, due to the development of strong ground motion instrumentation in early decades, number of strong ground motion records is still limited especially for earthquake having large return period. Because of the uncertainties mentioned above, a number of acceleration time history input n should be used to observe dynamic structural response well and reduce the uncertainties in the selection of ground motions.

Six acceleration time history records have been used for the time history analysis. Three of them are recorded earthquakes as shown in Table 6.4 and Figure 6.12. These earthquake records have been selected to have a magnitude, distance from source to site, and site condition that are similar to the magnitude, source to site distance, and site condition of the expected ground motion. Then, the selected records have been scaled in time domain so that the average value of the spectra of all scaled records matches the target response spectrum over the fundamental period range of the bridge for both orthogonal directions.

In addition to the recorded ground motions, artificially generated ground motions shown in Figure 6.13 have been used. Three accelerograms were generated using the program SIMQKE, matching the target response spectrum and assuming a total duration of the seismic event of 30 seconds for two of them and 35 seconds for the other. Scaled response spectrums of the six records are shown in the Figure 6.14 with the target response spectrum.

Table 6.4. Record Information

ID	Earthquake	Date	Station	PGA,(g)
IMP	Imperial Valley	10/15/79	Brawley Airport	0.22
LOMAP	Loma Prieta	10/18/89	Hollister Diff Array	0.269
SUPERS	Superstition Hills	11/24/87	Wildlife Liquefaction Array	0.207

6.4.2. Assumptions

As a result of the response spectrum analysis in the preliminary phase of the evaluation, comparisons of demand and capacity of the components individually provides an indication of where inelastic deformation may occur. Assessing the performance of an irregular bridge under safety evaluation earthquake condition should focus primarily on evaluating global displacement and deformations in those individual components, which experience yielding. A response spectrum modal analysis should not be used at this stage of the evaluation process Rather, nonlinear finite element modeling of the overall system should be established for use in carrying out nonlinear time history analysis having the objective of determining maximum values of component deformations, which can be compared with their corresponding deformation capacities.

In carrying out nonlinear time history analysis, acceleration records mentioned above have been applied to nonlinear analysis model of the bridge in both horizontal directions independently. All input motions were assumed to be synchronous at all piers.

Several time history analysis procedures are available in response analyses of structures. Analysis procedure adopted by the program is superposition of normalized modal time histories in time domain. Load dependent Ritz vectors rather than standard eigenvectors analysis was employed to obtain modal displacements. For all modes, structural viscous damping ratio was assumed to be 5%.

Accuracy of the nonlinear analysis depends on the ability to model nonlinear cyclic member characteristics. Many different hysteresis rules in the form of force-deformation relationships have been developed to represent nonlinear behavior of the components. Analysis program (sap 2000) used for the time history includes force/displacement and force/velocity dependent hysteretic elements. The types of nonlinear behavior that can be modeled with this element include; bilinear force-deformation representation used for piers, gap (compression only) and hook (tension only) used to model boundary condition between the abutment and deck, and rigid-plastic behavior used to model friction sliding devices at the top of the pier 9 to pier13 in the modeling of the Sadabat V3 viaduct.

As compared to other analysis methods, nonlinear time history analysis is widely used and reliable for assessment purposes, but more complex. Because of the complexity, there are some limitations in modeling. For instance, any mathematical model including nonlinear shear behavior and effect of shear deformation to inelastic flexural action is not available. In addition, inadequate lap splices and anchorage zone affect the deformability of the reinforced concrete members. However, such inadequacy in reinforced concrete mechanism cannot be modeled to reflect this nonlinear deformation and effect to flexure of the reinforced concrete members.

6.4.3. Analysis Results

Example hysteretic behaviors of the piers in the transverse direction are shown in Figure 6.15 to Figure 6.17. Other piers, of which hysteresis behaviors are not shown, performed elastically. Maximum top displacement demands and displacement ductility demands in the transverse direction are summarized in Table 6.5 and compared with their ductility capacities. Figure 6.19 and Figure 6.22 shows example transverse top displacement time history at pier 6, pier 7, pier11 and pier 12.

In the longitudinal direction, Pier 1 and pier13 exceed their lateral force capacities. Hysteretic behavior of pier1 and pier13 are shown in Figure 6.18. Maximum pier displacement demands and displacement ductility demands in the longitudinal direction are summarized in Table 6.5 and compared with their ductility capacities.

Elastomeric bearing relative displacements are summarized in Table 6.6 according to the transverse and longitudinal direction. Example hysteretic loops of the PTFE elastomeric bearings located at the top of pier9 to pier13 are shown in Figure 6.23 and Figure 6.24 due to SUPERS motion. Maximum displacement of the sliding bearings determined from the analysis are compared with steel plate limit, assumed to be 170cm according to the construction drawings.

Superstructure moment demands obtained from the time history analyses are summarized in Table 6.7 and compared with the flexural capacity of the section.

Example hysteretic response due to SIMQ3 of the tie-back device in longitudinal direction are shown in Figure 6.25. Maximum displacements determined from the analysis were divided by the length of the cables to obtain strain demand. Strains determined from this calculation are summarized in Table 6.8 and compared with ultimate strain.

6.5. Nonlinear Static (Pushover) Analysis

6.5.1. Assumptions

For elastic systems, modal analysis is the most practical method to evaluate structural response. However, for inelastic system it is not feasible because of the inability of elastic analysis to capture response modification caused by inelastic member behavior. The alternative method to inelastic time history analysis adopted recently is nonlinear static analysis, in other words, pushover analysis. Nonlinear static analysis is widely used and accepted analysis tool in engineering practice especially for existing structures to evaluate structural capacity and to estimate deformation demands.

Nonlinear static analysis is based on the lateral force-displacement representation (Pushover curve) of the multidegree-of-freedom (MDOF) system under monotonically increasing lateral load pattern in proportion to mass per unit length times the corresponding generalized single-degree-of freedom (SDOF) system. At the same time, it is assumed that pushover curve represents the envelope of the peak response of generalized SDOF system under earthquake ground motion. Therefore, pushover analysis of Sadabat V3 viaduct is composed of two stages. Lateral force-displacement representation of the MDOF (global) system is the first stage, and the second is determination of an equivalent SDOF system with bilinear force-displacement relationship based on the computed pushover curve of the MDOF system and evaluation of seismic demands in terms of global and local damage indices.

Pushover analysis of the bridge was performed only in transverse direction by hand calculation. At initial stage, before carrying out lateral force-displacement relation of the global system, pushover analysis of the individual piers were performed independently to reduce number of degree-of-freedom contributing to the first mode response of the system and to obtain simple model and meaningful pushover analysis. Detailed pushover analyses of the individual piers have been explained in section 5.2.2. Effective stiffness of each pier based on the pushover curve of the piers is represented by spring element, and masses of the piers contributing to the first mode are assigned to these springs. After modeling the overall system, lateral load was applied to the deck level and load shape was assumed to be constant throughout the analysis. Unit load, Δq_i, applied to the each degree of freedom was calculated based on the following equation 6.1 In equation, m_i and ϕ_i denote the tributary mass and modal shape vector for each degree of freedom in transverse direction (global Y direction), respectively.

$$\Delta q_{yi} = m_i * \Psi_{yi} / \sum_{i=1}^{n} m_i * \Psi_{yi} \tag{6.1}$$

Push analysis was carried out incrementally, modifying the pier stiffness. As the lateral load increases, deformation and corresponding forces of the piers were controlled at each increment to find which pier experience yielding. At each load increment, the displacement is monitored at the point where experiences the largest displacement at the deck level. As a result of the analysis, pushover curve is plotted in Figure 6.26.

The capacity spectrum curve for the bridge was obtained by transforming the pushover curve from lateral force versus lateral displacement coordinates to spectral acceleration versus spectral displacement coordinate using the modal shape vector, participation factors and modal mass or effective mass. The capacity spectrum was constructed to represent equivalent nonlinear SDOF. Incremental spectral displacement is expressed as:

$$\Delta S_{dy} = \Delta\delta_{yc} / \gamma_{yc} \tag{6.2}$$

In equation 6.2, $\Delta\delta_{yc}$ represents control node displacement at each increment of the pushover curve. γ_{yc} is participation factor for the first mode associated with control node and defined by following equation 6.3 and equation 6.4.

$$\gamma_{yc} = \Psi_{yc} * \Gamma_{y1} \tag{6.3}$$

$$\Gamma_{y1} = \frac{\sum_{i=1}^{n} m_i * \Psi_i}{\sum_{i=1}^{n} m_i * \Psi_i^2} \tag{6.4}$$

Incremental spectral acceleration is obtained by using equation 6.5 ΔV denotes lateral force increment applied to overall system at each increment of the pushover curve. Meff is the participating effective mass for the first mode and defined by equation 6.6.

$$\Delta S_{ay} = \Delta V / M_{eff} \tag{6.5}$$

$$M_{eff} = \frac{\left[\sum_{i=1}^{n} m_i * \Psi_i\right]^2}{\left[\sum_{i=1}^{n} m_i * \Psi_i^2\right]} \tag{6.6}$$

By this way, capacity spectrum can be obtained by summing incremental spectral displacement on the horizontal axis and spectral acceleration on the vertical axes as shown in Figure 6.27.

6.5.2. Demand Estimation

Capacity spectrum is assumed to be backbone curve of the hysteresis model adopted in SDOF seismic demand analysis. Bilinear representation of the capacity curve is required to determine yield displacement and corresponding yield strength, thus global demand parameters, such as displacement ductility demand can be obtained. Bilinear idealization of the capacity spectrum is plotted in Figure 6.27. Seismic demand of the SDOF system in terms of displacement was obtained by performing nonlinear time history analysis. Six acceleration records used in the inelastic time history analysis of the global bridge were also used for the demand estimation. Then, The local seismic demand was determined by pushing the MDOF system to the maximum displacement determined in the previous step. Finally, damage indices for the piers corresponding to the maximum global displacement were obtained.

Despite widely used and practical way to determine deformation capacity of the existing bridges, pushover analysis approach has some limitations. Firstly, This approach provides reasonably more accurate demand predictions where the response can be captured by a predominant mode of vibration, but becomes increasingly more inaccurate as higher modes become more important [H. Krawinkler, *Research Issues in Performance Based Seismic engineering]*. Second, in the pushover analysis, relative displacement between any two degrees of freedom is related to the first mode shape. Therefore, relative displacement between adjacent components vibrating independently due to the large stiffness variation cannot be estimated accurately. Such cases can be encountered in case of bridges isolated by means of elastomeric bearings. Relative displacement between the flexible superstructure and the short pier is playing important role in estimation of displacement demand for the isolation devices. Third, as mentioned previously in inelastic time history analysis, inelastic action considered in the analysis is solely flexure. Brittle modes, such as reinforcement slippage or shear failure before the section at pier base reaches its flexural capacity cannot be included in the modeling of the bridge

6.5.3. Analysis Results

As a result of the pushover analysis, global and local displacement demands and corresponding ductility factors as a measure of the performance have been determined. Maximum top displacement demands of the piers experiencing yielding are summarized in Table6.9 and compared with the ultimate displacements. Corresponding displacement ductility demand and ductility capacities of the piers are summarized in the same table.

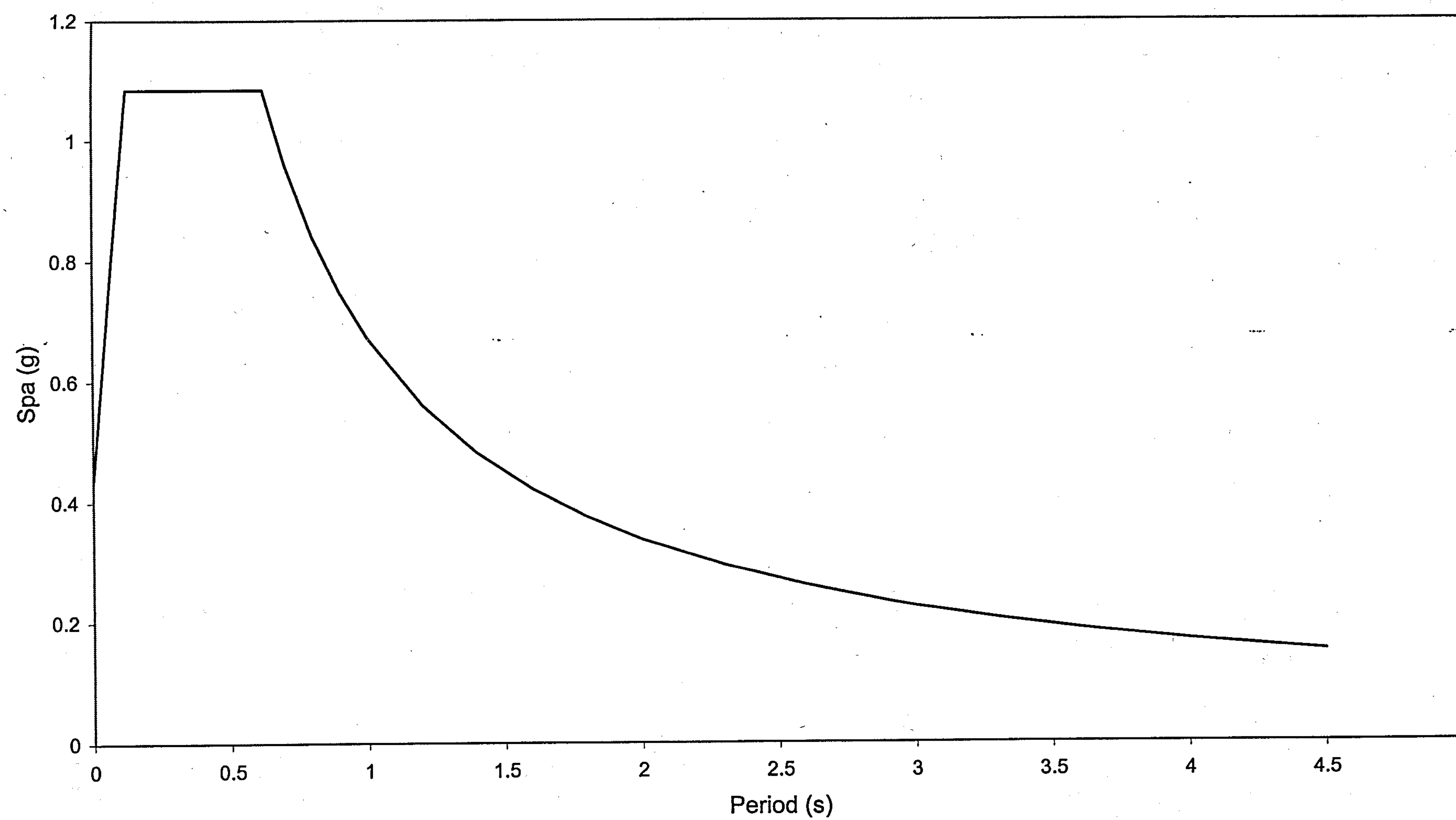

Figure 6.1 Fema 356 acceleration response spectrum with 5% damping ratio.

Table 6.1. Natural vibration periods and participating mass ratios for the first 20 modes.

Mode	Period(s)	Modal participating Mass Ratios			
		Individual Mode (percent)		Cumulative Sum (percent)	
		Longitudinal	Transverse	Longitudinal	Transverse
1	3.56	0.00	66.91	0.00	66.91
2	2.86	0.00	0.08	0.00	66.99
3	2.22	0.00	17.13	0.00	84.12
4	1.71	0.00	0.39	0.00	84.51
5	1.64	0.76	0.00	0.76	84.51
6	1.43	0.74	0.00	1.51	84.51
7	1.33	0.00	6.88	1.51	91.39
8	1.26	89.78	0.00	91.29	91.39
9	1.03	0.59	0.00	91.88	91.39
10	1.03	0.00	0.01	91.88	91.40
11	0.81	0.00	2.28	91.88	93.68
12	0.65	0.00	0.01	91.88	93.69
13	0.55	0.00	0.84	91.88	94.54
14	0.51	0.94	0.00	92.82	94.54
15	0.51	0.00	0.00	92.82	94.54
16	0.50	0.07	0.00	92.90	94.54
17	0.50	0.00	0.00	92.90	94.54
18	0.50	0.44	0.00	93.34	94.54
19	0.49	0.01	0.00	93.35	94.54
20	0.49	0.01	0.00	93.36	94.54

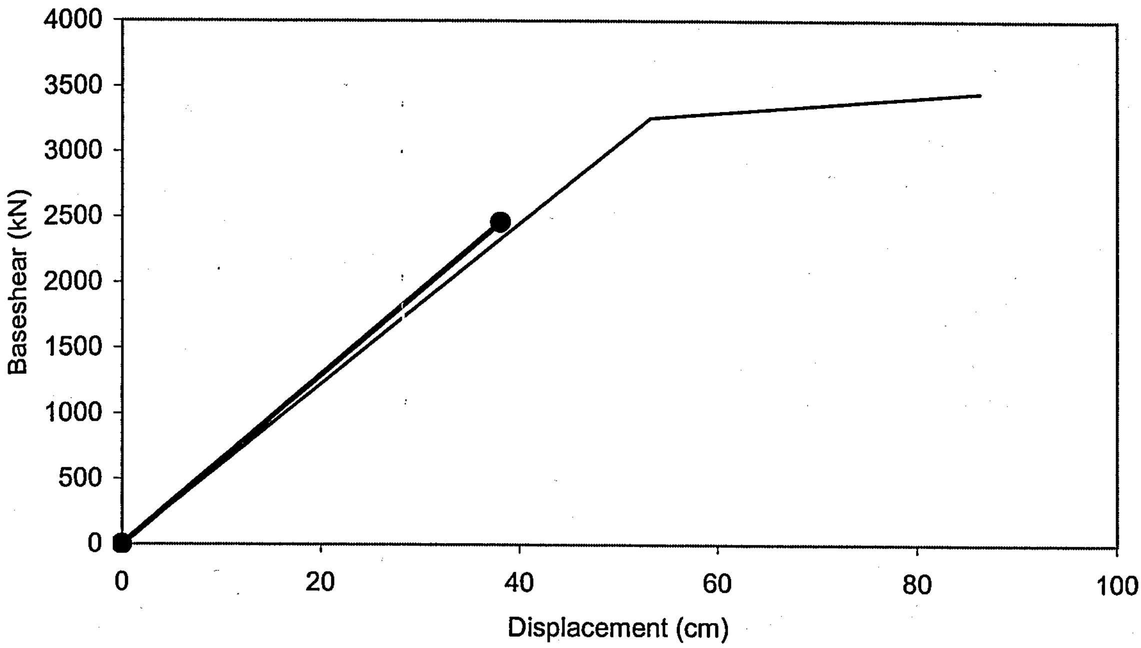

Figure 6.2. Displacement demand for Pier 3

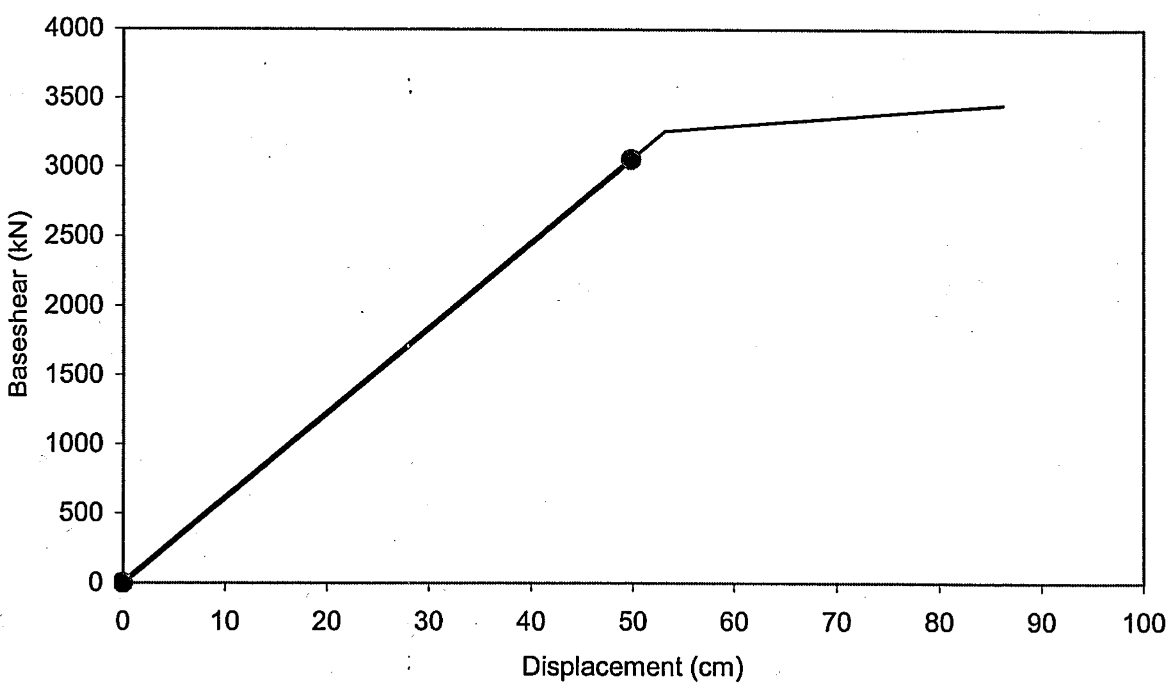

Figure 6.3. Displacement demand for Pier 4

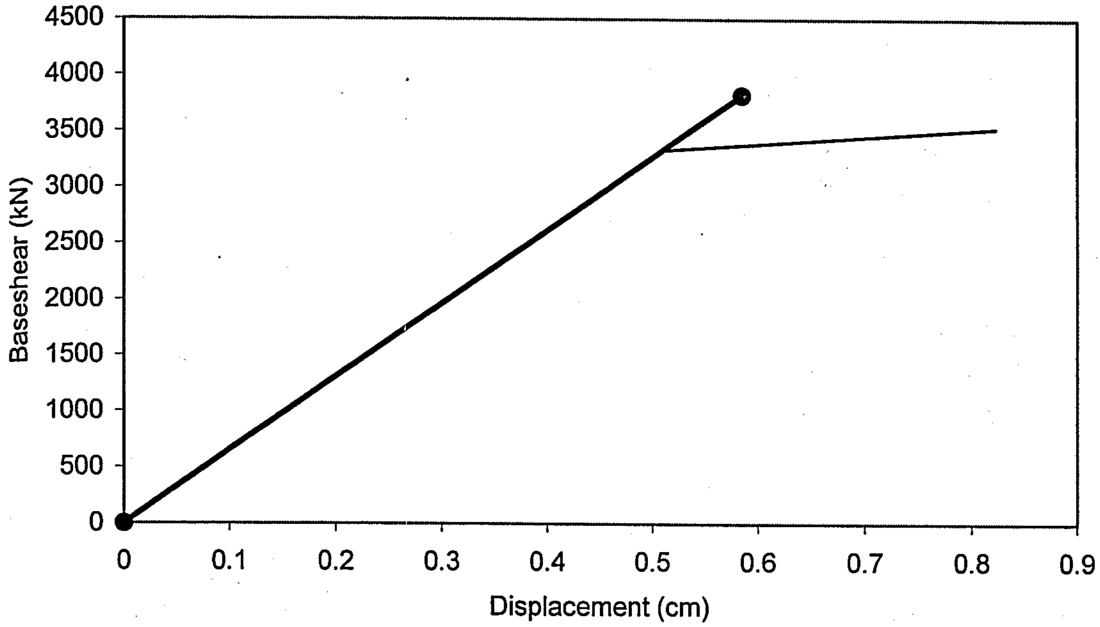

Figure 6.4. Displacement demand for Pier 5

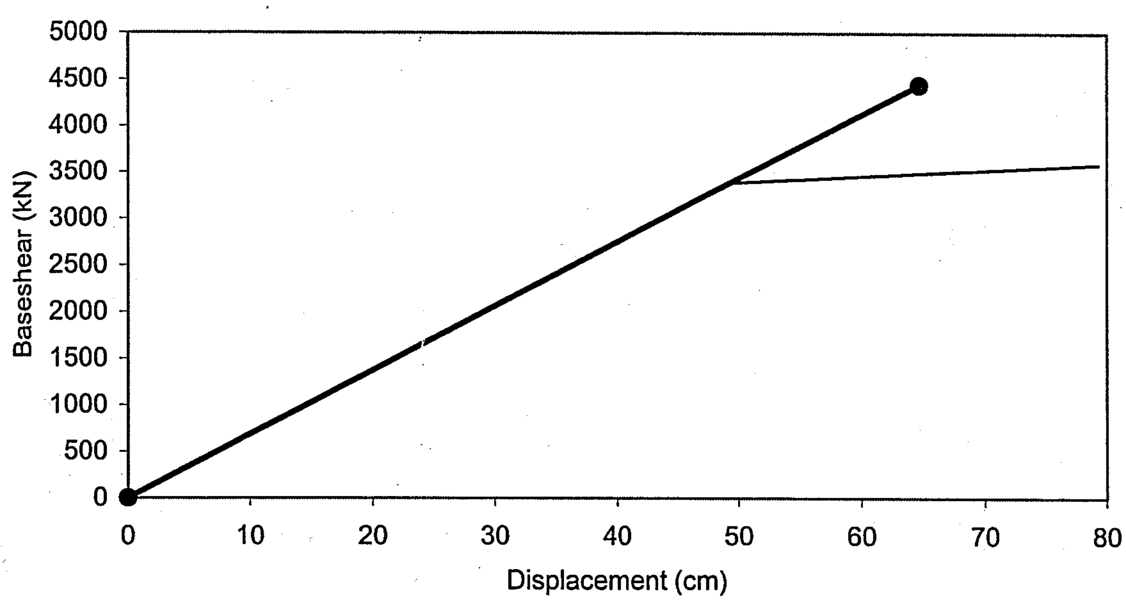

Figure 6.5. Displacement demand for Pier 6

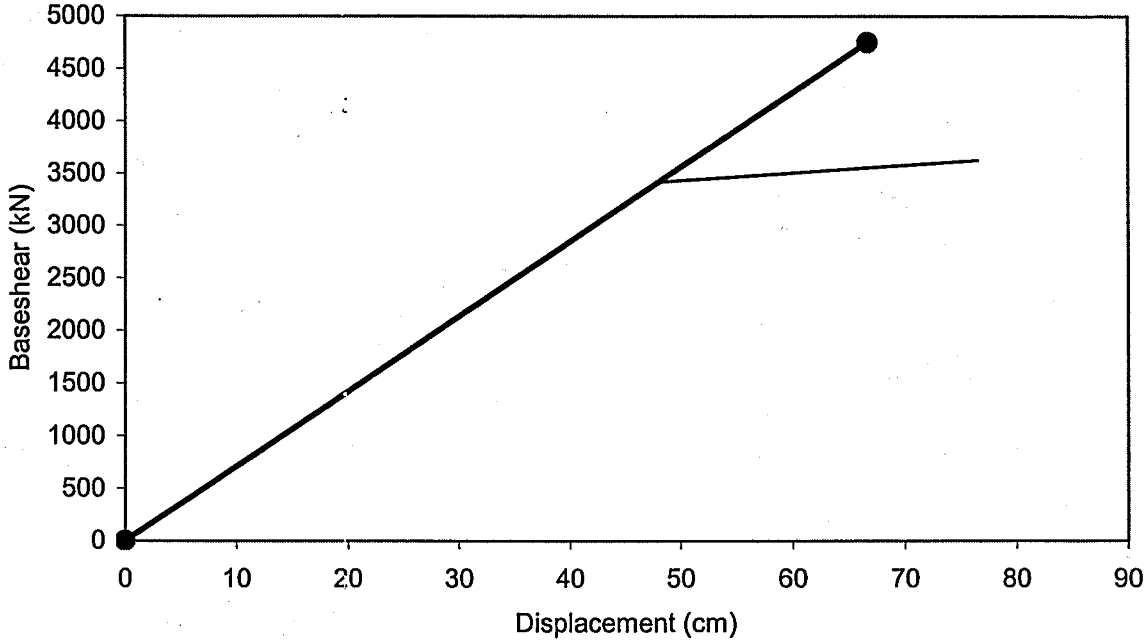

Figure 6.6. Displacement demand for Pier 3 and Pier 7

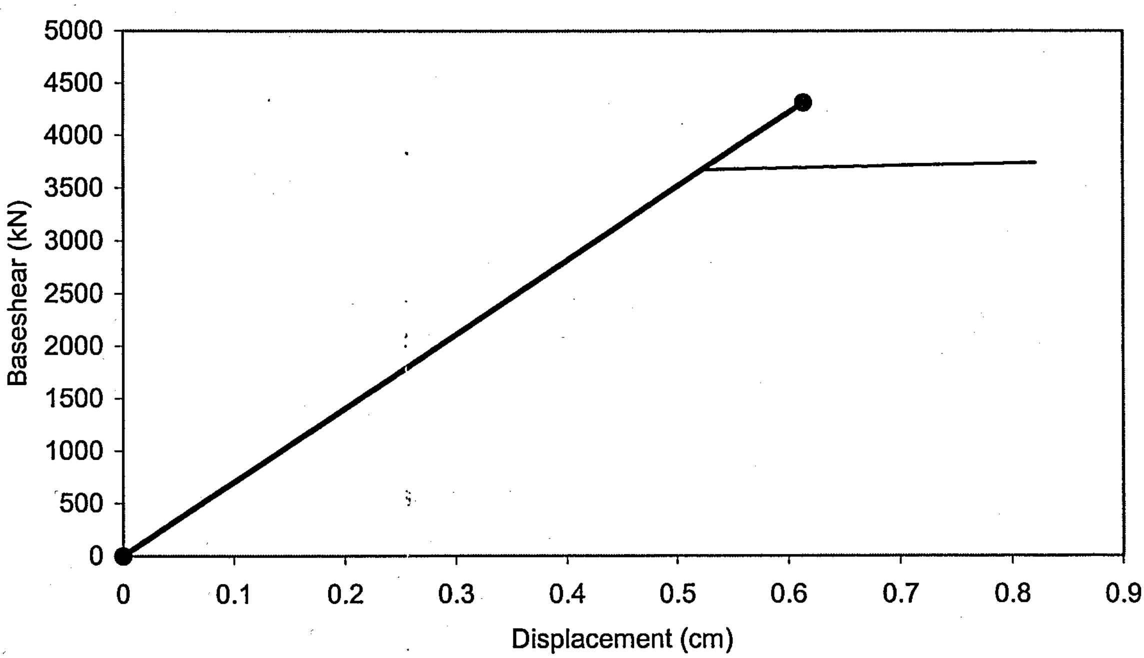

Figure 6.7. Displacement demand for Pier 8

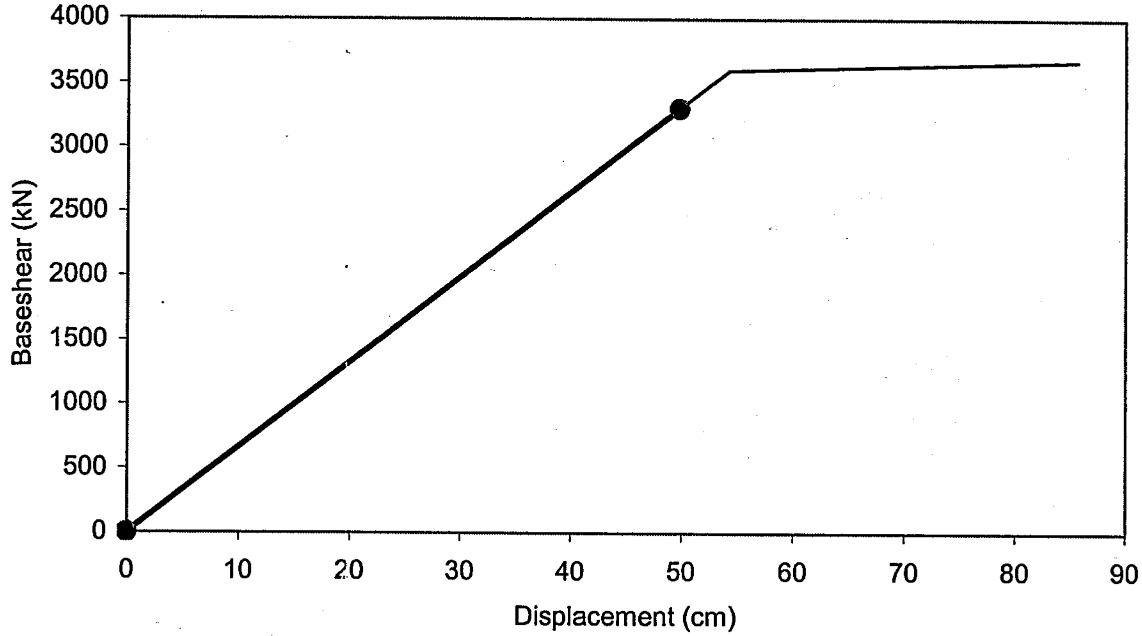

Figure 6.8. Displacement demand for Pier 9

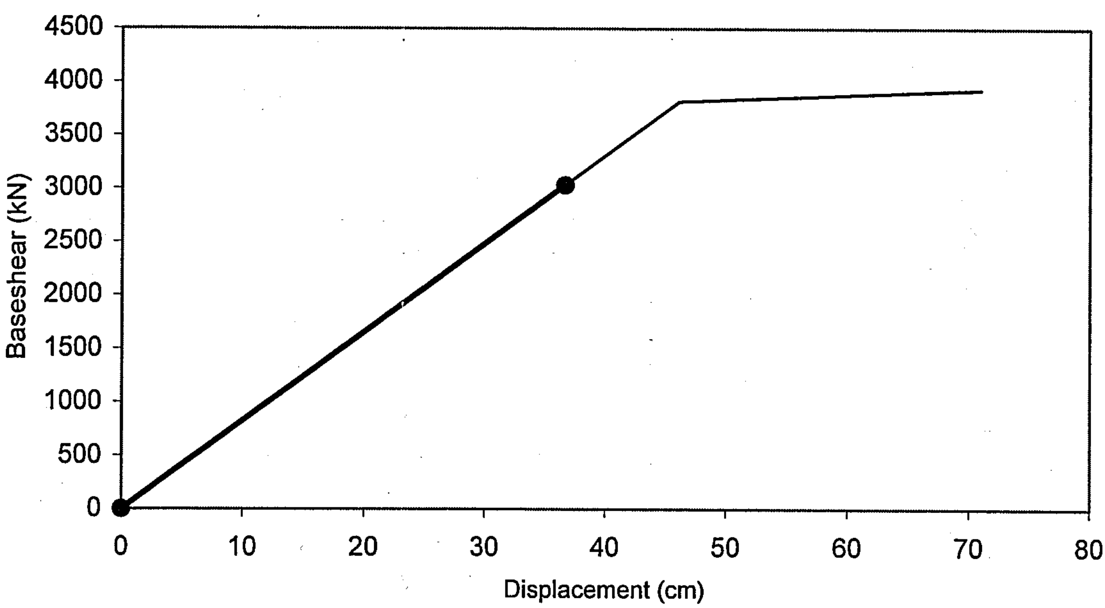

Figure 6.9. Displacement demand for Pier 10

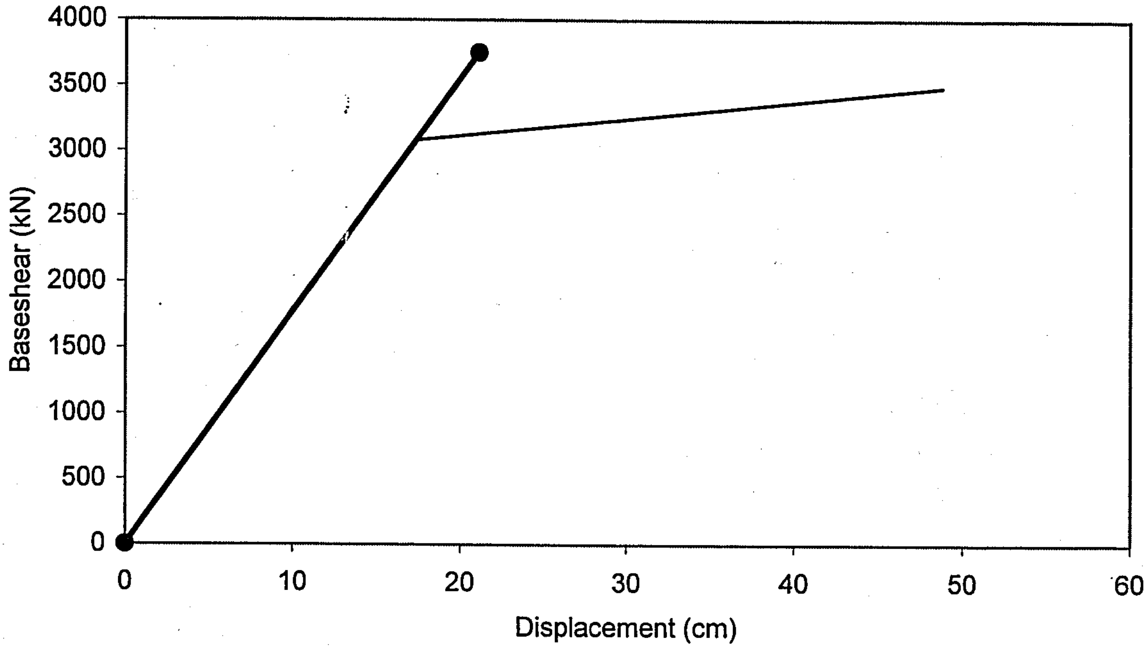

Figure 6.10. Displacement demand for Pier 11

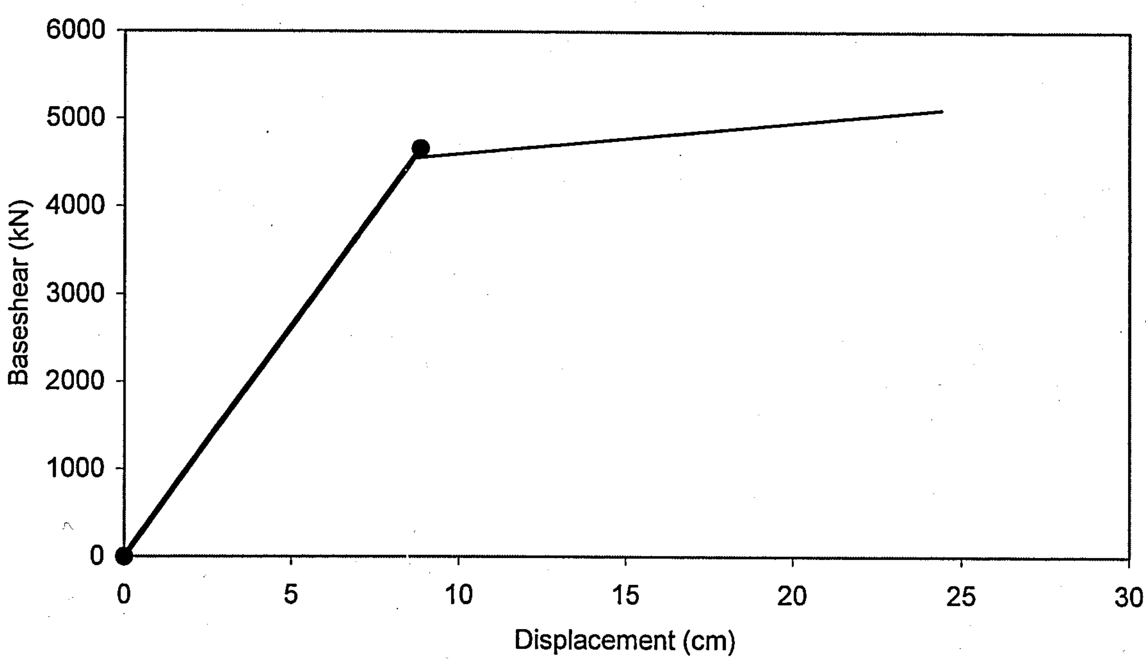

Figure 6.11. Displacement demand for Pier 12

Table 6.2. Relative displacement demands at bearings (from response spectrum analysis results)

Pier No	Dimension (cm)	Displacement Capacity (cm)	Longitudinal Displacement Demand (cm)	Transverse Displacement Demand (cm)
Pier 1	80/80/8	12	8.80	11.42
Pier 2	80/65/8	12	5.95	7.85
Pier 3	80/65/8	12	5.31	7.53
Pier 4	80/65/8	12	4.59	8.83
Pier 5	80/65/8	12	3.62	11.00
Pier 6	80/65/8	12	2.62	12.99
Pier 7	80/65/8	12	1.89	13.75
Pier 8	80/65/8	12	1.61	12.62
Pier 9	70/65/8	12	0.03	11.03
Pier 10	70/65/8	12	0.03	10.01
Pier 11	70/65/8	12	0.03	13.07
Pier 12	80/65/8	12	0.03	14.55
Pier 13	80/65/8	12	0.03	9.66

Table 6.3. Displacement demands at pier tops (from response spectrum analysis results)

	In Transverse Earthquake Direction				
	Δ_{yield}(m)	$\Delta_{ultimate}$(m)	$\mu_{Capacity}=\Delta_{ultimate}/\Delta_{yield}$	$\Delta_{pier-top}$(m)	$\mu_{Demand}=\Delta_{pier-top}/\Delta_{yield}$
Pier 1	0.011	0.042	3.82	0.004	0.40
Pier 2	0.28	0.601	2.15	0.209	0.75
Pier 3	0.513	0.823	1.60	0.381	0.74
Pier 4	0.532	0.862	1.62	0.498	0.94
Pier 5	0.51	0.823	1.61	0.585	1.15
Pier 6	0.493	0.793	1.61	0.647	1.31
Pier 7	0.48	0.765	1.59	0.667	1.39
Pier 8	0.522	0.821	1.57	0.614	1.18
Pier 9	0.543	0.857	1.58	0.498	0.92
Pier 10	0.461	0.71	1.54	0.366	0.79
Pier 11	0.172	0.488	2.84	0.211	1.23
Pier 12	0.086	0.244	2.84	0.089	1.03
Pier 13	0.053	0.157	2.96	0.028	0.53

	In Longitudinal Earthquake Direction				
	Δ_{yield}(m)	$\Delta_{ultimate}$(m)	$\mu_{Capacity}=\Delta_{ultimate}/\Delta_{yield}$	$\Delta_{pier-top}$(m)	$\mu_{Demand}=\Delta_{pier-top}/\Delta_{yield}$
Pier 1	0.018	0.063	3.47	0.01	0.46
Pier 2	0.399	1.219	3.05	0.13	0.32
Pier 3	0.725	1.891	2.61	0.16	0.22
Pier 4	0.752	1.973	2.62	0.18	0.24
Pier 5	0.720	1.877	2.61	0.20	0.27
Pier 6	0.696	1.808	2.60	0.21	0.30
Pier 7	0.738	1.763	2.39	0.23	0.31
Pier 8	0.768	2.065	2.69	0.24	0.31
Pier 9	0.800	2.201	2.75	0.28	0.35
Pier 10	0.662	1.592	2.40	0.24	0.37
Pier 11	0.344	1.061	3.08	0.17	0.50
Pier 12	0.155	0.495	3.20	0.07	0.43
Pier 13	0.091	0.321	3.53	0.03	0.28

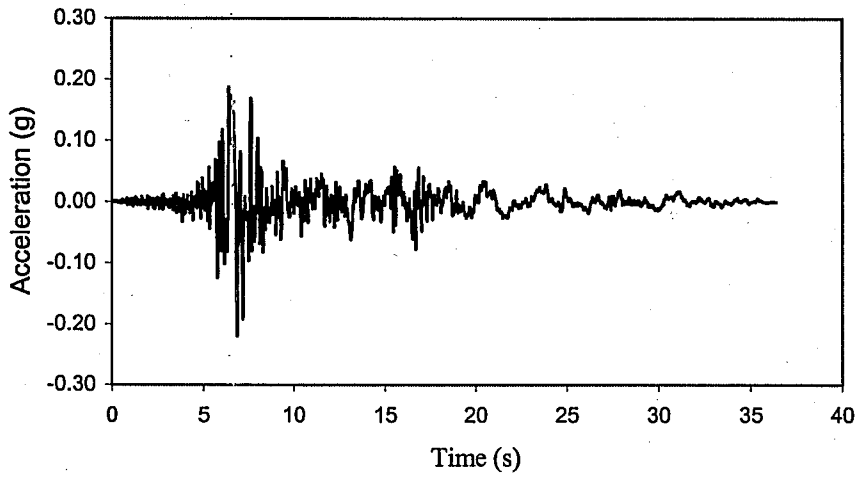

(a)

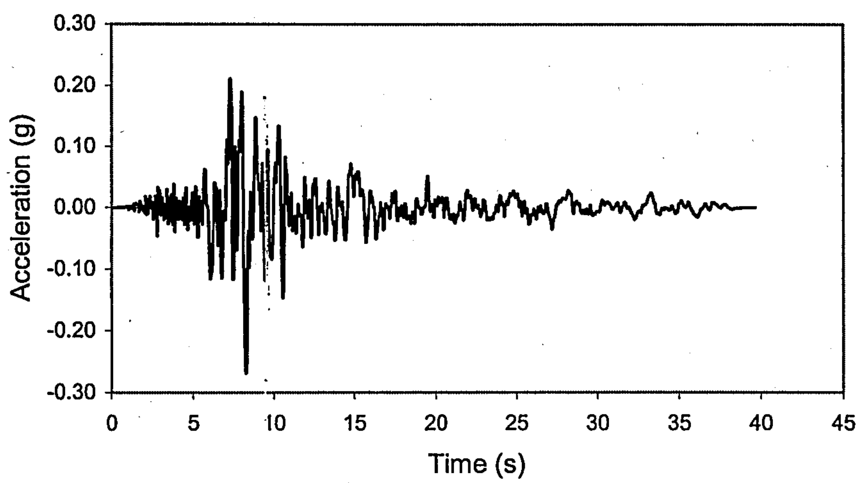

(b)

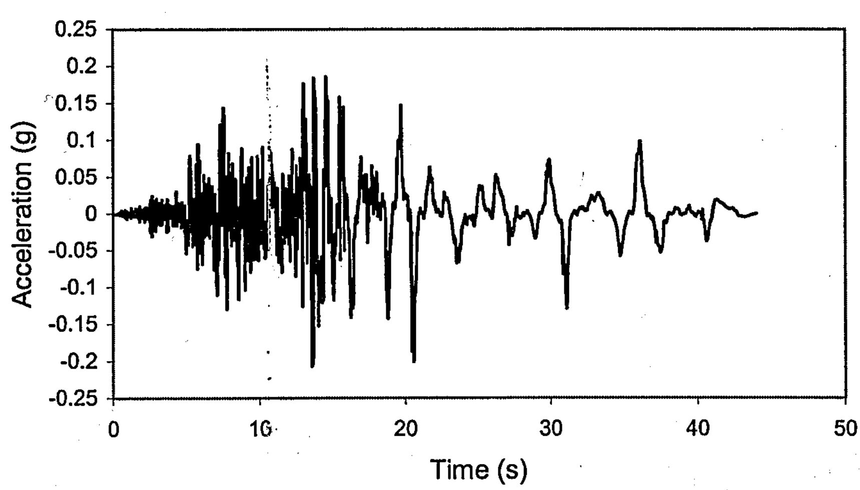

(c)

Figure 6.12. (a) Imperial Valley, (b) Loma Prieta, (c),Superstition Hills accelerograms

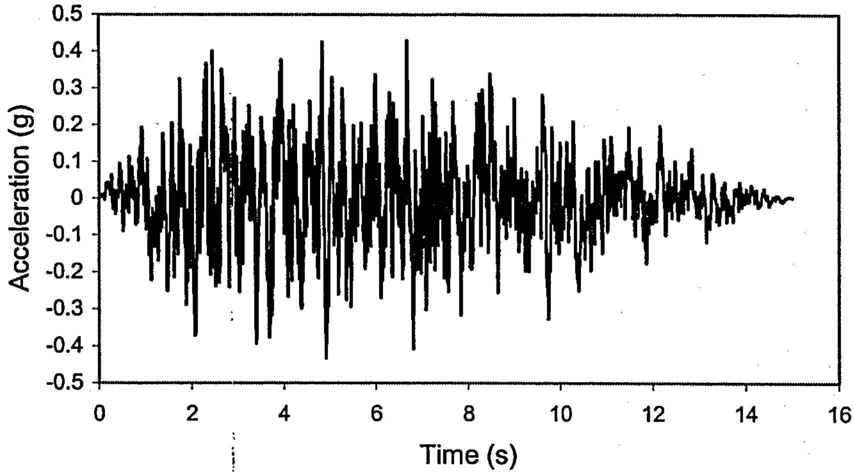

(a)

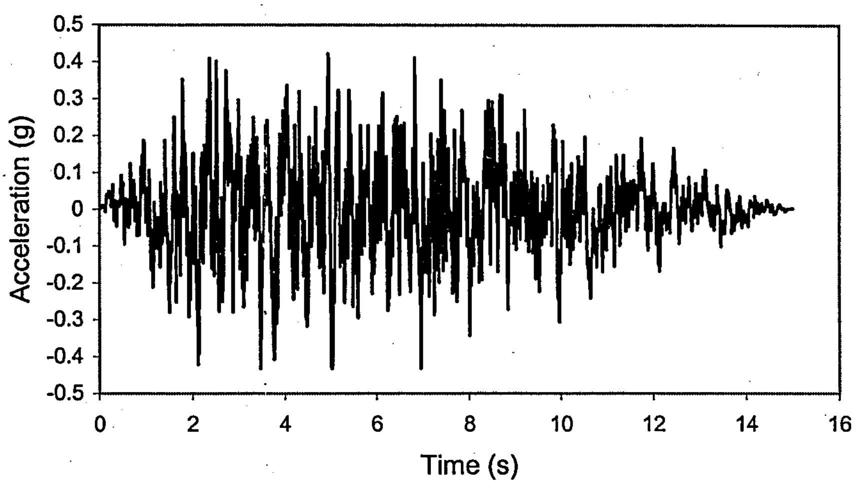

(b)

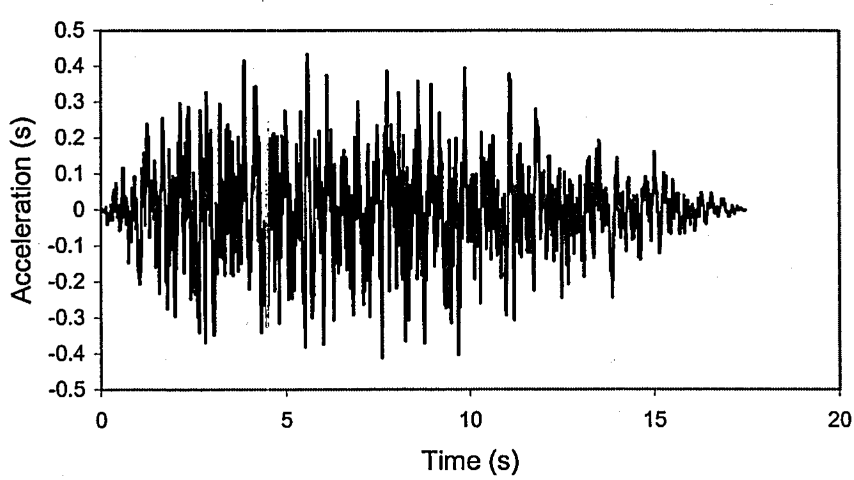

(c)

Figure 6.13. (a) Simq1, (b) Simq2, (c),Simq3 accelerograms

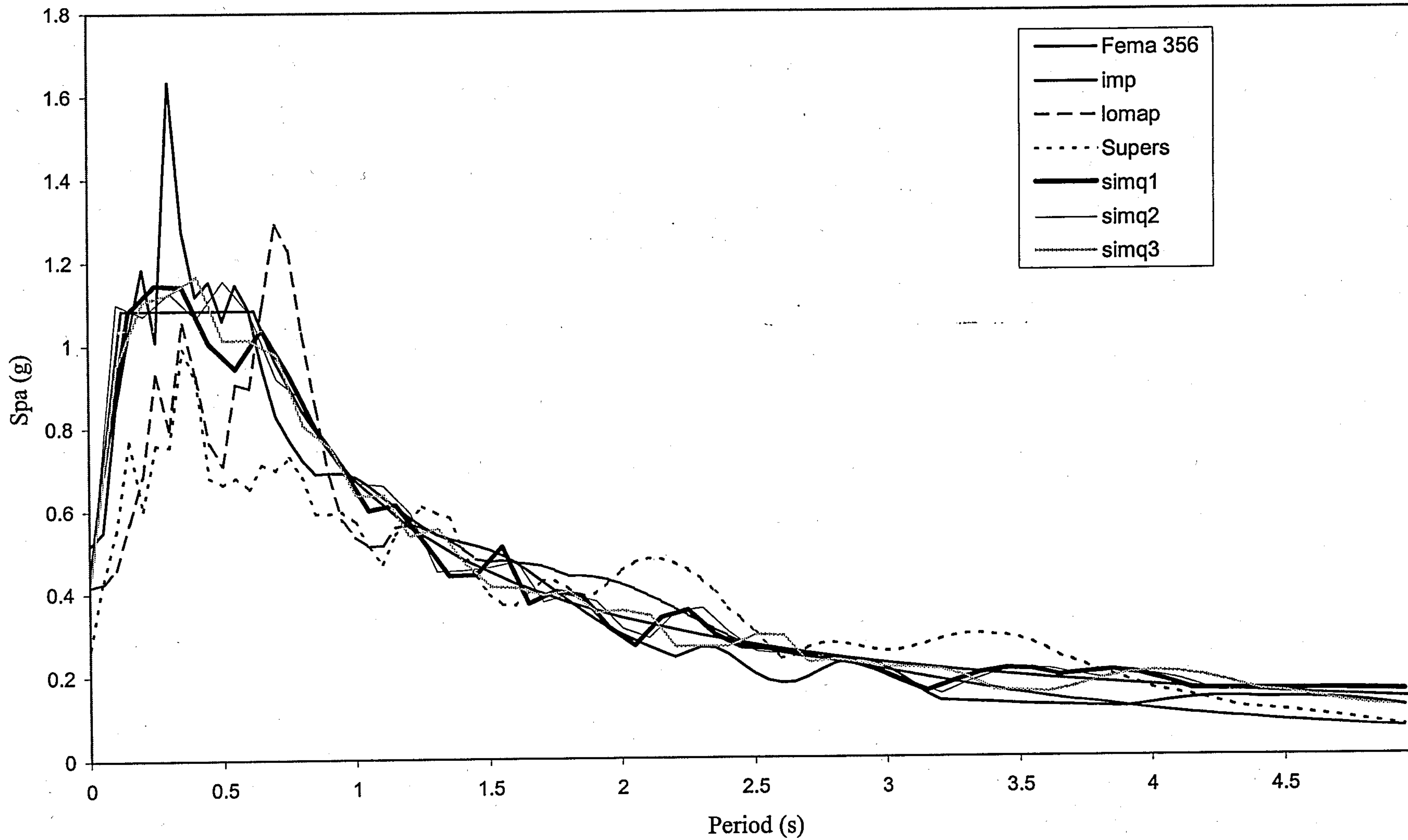

Figure 6.14. %5 Damped response spectrum representation of the records used in the analysis.

Table 6.5.(a) Top displacement and ductility demand of the piers determined from the time history analyses.

Pier1 (transverse)	$\Delta_{pier\text{-}top}$	$\mu_{Demand}=\Delta_{pier\text{-}top}/\Delta_{yield}$
SIMQ1	0.005	0.49
SIMQ2	0.005	0.49
SIMQ3	0.004	0.39
IMP	0.005	0.45
LOMAP	0.005	0.48
SUPERS	0.005	0.42

Pier1(longitudinal)	$\Delta_{pier\text{-}top}$	$\mu_{Demand}=\Delta_{pier\text{-}top}/\Delta_{yield}$
SIMQ1	0.065	3.57
SIMQ2	0.057	3.15
SIMQ3	0.077	4.22
IMP	0.121	6.67
LOMPR	0.050	2.73
SUPERS	0.065	3.56

Pier2 (transverse)	$\Delta_{pier\text{-}top}$	$\mu_{Demand}=\Delta_{pier\text{-}top}/\Delta_{yield}$
SIMQ1	0.254	0.91
SIMQ2	0.234	0.84
SIMQ3	0.194	0.69
IMP	0.238	0.85
LOMAP	0.250	0.89
SUPERS	0.215	0.77

Pier2(longitudinal)	$\Delta_{pier\text{-}top}$	$\mu_{Demand}=\Delta_{pier\text{-}top}/\Delta_{yield}$
SIMQ1	0.158	0.40
SIMQ2	0.143	0.36
SIMQ3	0.151	0.38
IMP	0.228	0.57
LOMPR	0.105	0.26
SUPERS	0.146	0.37

Pier3 (transverse)	$\Delta_{pier\text{-}top}$	$\mu_{Demand}=\Delta_{pier\text{-}top}/\Delta_{yield}$
SIMQ1	0.393	0.77
SIMQ2	0.370	0.72
SIMQ3	0.351	0.68
IMP	0.412	0.80
LOMAP	0.423	0.82
SUPERS	0.408	0.79

Pier3(longitudinal)	$\Delta_{pier\text{-}top}$	$\mu_{Demand}=\Delta_{pier\text{-}top}/\Delta_{yield}$
SIMQ1	0.169	0.23
SIMQ2	0.158	0.22
SIMQ3	0.156	0.22
IMP	0.280	0.39
LOMPR	0.108	0.15
SUPERS	0.139	0.19

Table 6.5.(b) Top displacement and ductility demand of the piers determined from the time history analyses.

Pier4 (transverse)	$\Delta_{pier\text{-}top}$	$\mu_{Demand}=\Delta_{pier\text{-}top}/\Delta_{yield}$
SIMQ1	0.527	0.99
SIMQ2	0.536	1.01
SIMQ3	0.410	0.77
IMP	0.457	0.86
LOMAP	0.509	0.96
SUPERS	0.551	1.04

Pier4(longitudinal)	$\Delta_{pier\text{-}top}$	$\mu_{Demand}=\Delta_{pier\text{-}top}/\Delta_{yield}$
SIMQ1	0.187	0.25
SIMQ2	0.175	0.23
SIMQ3	0.183	0.24
IMP	0.330	0.44
LOMPR	0.127	0.17
SUPERS	0.162	0.22

Pier5 (transverse)	$\Delta_{pier\text{-}top}$	$\mu_{Demand}=\Delta_{pier\text{-}top}/\Delta_{yield}$
SIMQ1	0.655	1.29
SIMQ2	0.668	1.31
SIMQ3	0.534	1.05
IMP	0.452	0.89
LOMAP	0.556	1.09
SUPERS	0.639	1.25

Pier5(longitudinal)	$\Delta_{pier\text{-}top}$	$\mu_{Demand}=\Delta_{pier\text{-}top}/\Delta_{yield}$
SIMQ1	0.177	0.25
SIMQ2	0.165	0.23
SIMQ3	0.170	0.24
IMP	0.296	0.41
LOMPR	0.118	0.16
SUPERS	0.159	0.22

Pier6 (transverse)	$\Delta_{pier\text{-}top}$	$\mu_{Demand}=\Delta_{pier\text{-}top}/\Delta_{yield}$
SIMQ1	0.697	1.41
SIMQ2	0.712	1.44
SIMQ3	0.531	1.08
IMP	0.595	1.21
LOMAP	0.560	1.14
SUPERS	0.681	1.38

Pier6(longitudinal)	$\Delta_{pier\text{-}top}$	$\mu_{Demand}=\Delta_{pier\text{-}top}/\Delta_{yield}$
SIMQ1	0.174	0.25
SIMQ2	0.161	0.23
SIMQ3	0.170	0.24
IMP	0.282	0.41
LOMPR	0.116	0.17
SUPERS	0.162	0.23

Table 6.5.(c) Top displacement and ductility demand of the piers determined from the time history analyses.

Pier7 (transverse)	$\Delta_{pier\text{-}top}$	$\mu_{Demand}=\Delta_{pier\text{-}top}/\Delta_{yield}$
SIMQ1	0.687	1.43
SIMQ2	0.667	1.39
SIMQ3	0.528	1.10
IMP	0.661	1.38
LOMAP	0.637	1.33
SUPERS	0.685	1.43

Pier7(longitudinal)	$\Delta_{pier\text{-}top}$	$\mu_{Demand}=\Delta_{pier\text{-}top}/\Delta_{yield}$
SIMQ1	0.176	0.24
SIMQ2	0.163	0.22
SIMQ3	0.180	0.24
IMP	0.287	0.39
LOMPR	0.123	0.17
SUPERS	0.171	0.23

Pier8 (transverse)	$\Delta_{pier\text{-}top}$	$\mu_{Demand}=\Delta_{pier\text{-}top}/\Delta_{yield}$
SIMQ1	0.635	1.22
SIMQ2	0.641	1.23
SIMQ3	0.500	0.96
IMP	0.593	1.14
LOMAP	0.536	1.03
SUPERS	0.645	1.24

Pier8(longitudinal)	$\Delta_{pier\text{-}top}$	$\mu_{Demand}=\Delta_{pier\text{-}top}/\Delta_{yield}$
SIMQ1	0.181	0.24
SIMQ2	0.168	0.22
SIMQ3	0.194	0.25
IMP	0.301	0.39
LOMPR	0.135	0.18
SUPERS	0.181	0.24

Pier9 (transverse)	$\Delta_{pier\text{-}top}$	$\mu_{Demand}=\Delta_{pier\text{-}top}/\Delta_{yield}$
SIMQ1	0.552	1.02
SIMQ2	0.568	1.05
SIMQ3	0.472	0.87
IMP	0.418	0.77
LOMAP	0.551	1.01
SUPERS	0.575	1.06

Pier9(longitudinal)	$\Delta_{pier\text{-}top}$	$\mu_{Demand}=\Delta_{pier\text{-}top}/\Delta_{yield}$
SIMQ1	0.184	0.23
SIMQ2	0.170	0.21
SIMQ3	0.197	0.25
IMP	0.315	0.39
LOMPR	0.135	0.17
SUPERS	0.181	0.23

Table 6.5.(d) Top displacement and ductility demand of the piers determined from the time history analyses.

Pier10 (transverse)	$\Delta_{pier\text{-}top}$	$\mu_{Demand}=\Delta_{pier\text{-}top}/\Delta_{yield}$
SIMQ1	0.375	0.81
SIMQ2	0.380	0.82
SIMQ3	0.316	0.69
IMP	0.393	0.85
LOMAP	0.469	1.02
SUPERS	0.407	0.88

Pier10(longitudinal)	$\Delta_{pier\text{-}top}$	$\mu_{Demand}=\Delta_{pier\text{-}top}/\Delta_{yield}$
SIMQ1	0.185	0.28
SIMQ2	0.172	0.26
SIMQ3	0.198	0.30
IMP	0.317	0.48
LOMPR	0.135	0.20
SUPERS	0.183	0.28

Pier11 (transverse)	$\Delta_{pier\text{-}top}$	$\mu_{Demand}=\Delta_{pier\text{-}top}/\Delta_{yield}$
SIMQ1	0.272	1.58
SIMQ2	0.246	1.43
SIMQ3	0.178	1.04
IMP	0.271	1.57
LOMAP	0.267	1.55
SUPERS	0.267	1.55

Pier11(longitudinal)	$\Delta_{pier\text{-}top}$	$\mu_{Demand}=\Delta_{pier\text{-}top}/\Delta_{yield}$
SIMQ1	0.184	0.53
SIMQ2	0.171	0.50
SIMQ3	0.194	0.56
IMP	0.313	0.91
LOMPR	0.132	0.38
SUPERS	0.181	0.53

Pier12 (transverse)	$\Delta_{pier\text{-}top}$	$\mu_{Demand}=\Delta_{pier\text{-}top}/\Delta_{yield}$
SIMQ1	0.119	1.38
SIMQ2	0.117	1.36
SIMQ3	0.097	1.13
IMP	0.112	1.30
LOMAP	0.101	1.17
SUPERS	0.118	1.37

Pier12(longitudinal)	$\Delta_{pier\text{-}top}$	$\mu_{Demand}=\Delta_{pier\text{-}top}/\Delta_{yield}$
SIMQ1	0.095	0.61
SIMQ2	0.085	0.55
SIMQ3	0.099	0.64
IMP	0.121	0.78
LOMPR	0.076	0.49
SUPERS	0.081	0.53

Table 6.5.(e) Top displacement and ductility demand of the piers determined from the time history analyses.

Pier13 (transverse)	$\Delta_{pier\text{-}top}$	$\mu_{Demand}=\Delta_{pier\text{-}top}/\Delta_{yield}$
SIMQ1	0.034	0.65
SIMQ2	0.036	0.69
SIMQ3	0.035	0.66
IMP	0.035	0.66
LOMAP	0.031	0.59
SUPERS	0.038	0.72

Pier13(longitudinal)	$\Delta_{pier\text{-}top}$	$\mu_{Demand}=\Delta_{pier\text{-}top}/\Delta_{yield}$
SIMQ1	0.071	0.78
SIMQ2	0.064	0.70
SIMQ3	0.070	0.77
IMP	0.105	1.16
LOMPR	0.050	0.55
SUPERS	0.060	0.66

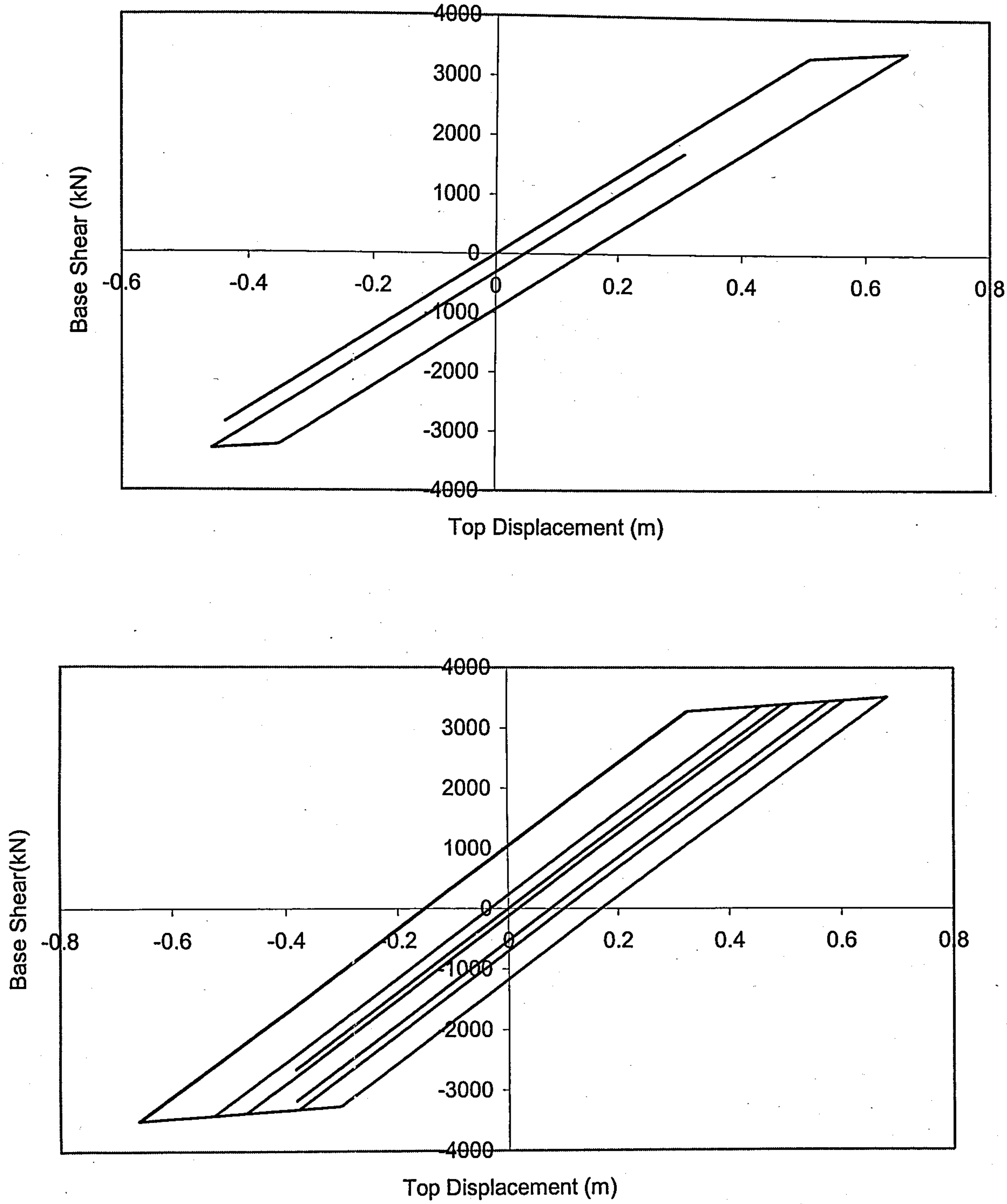

Figure 6.15 Pier5 and pier6 response to SIMQ2.

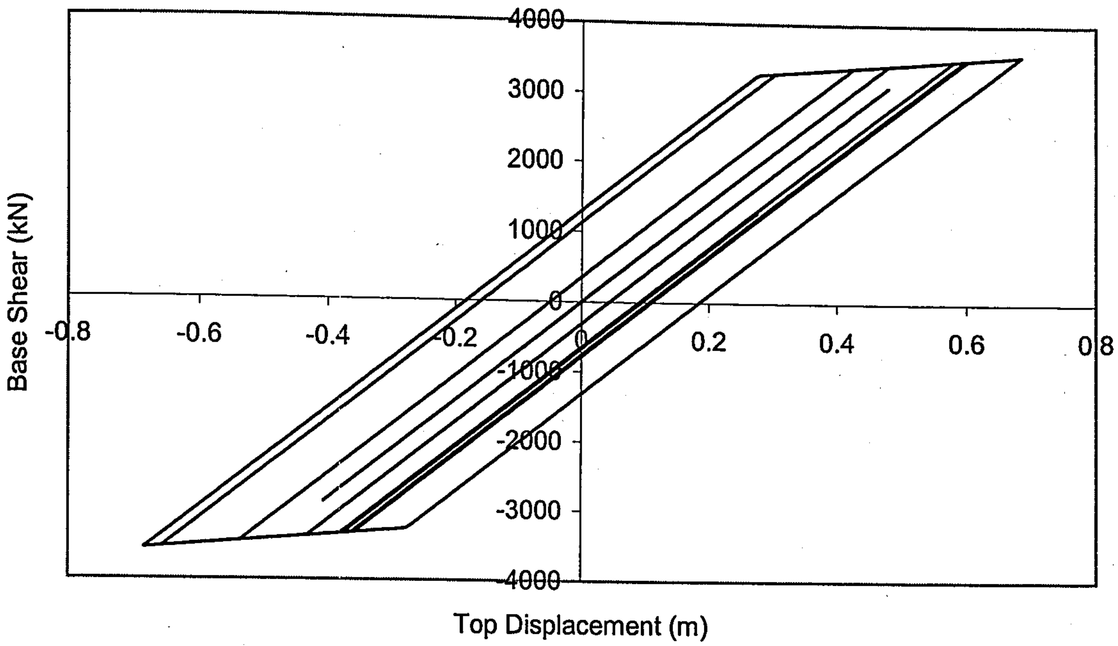

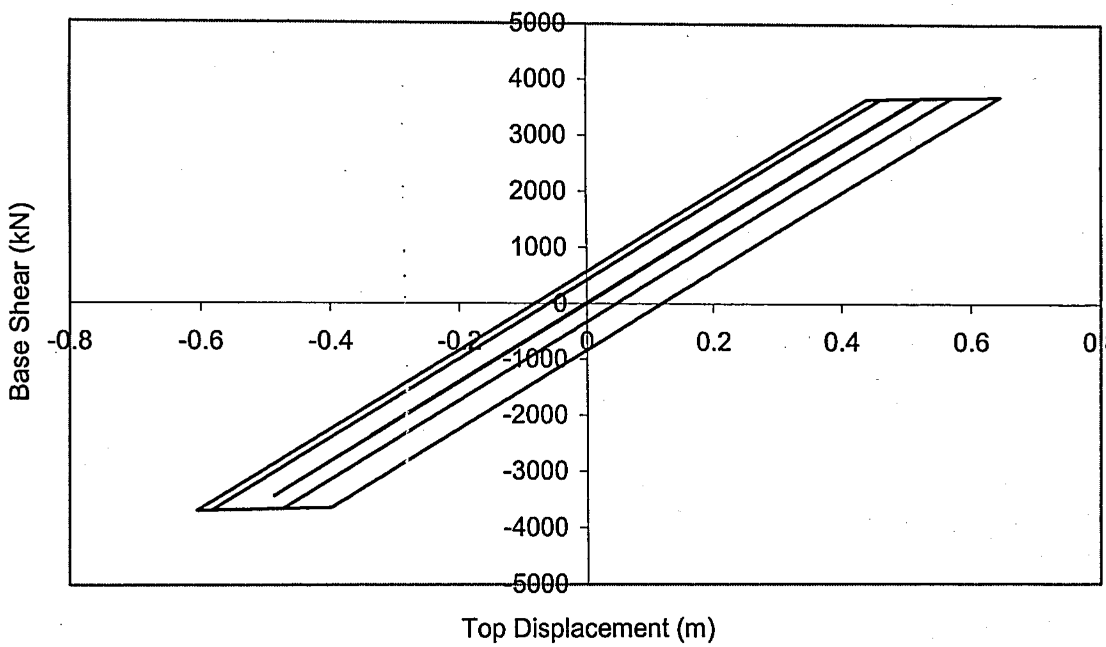

Figure 6.16 Pier7 and pier8 response to SUPERS.

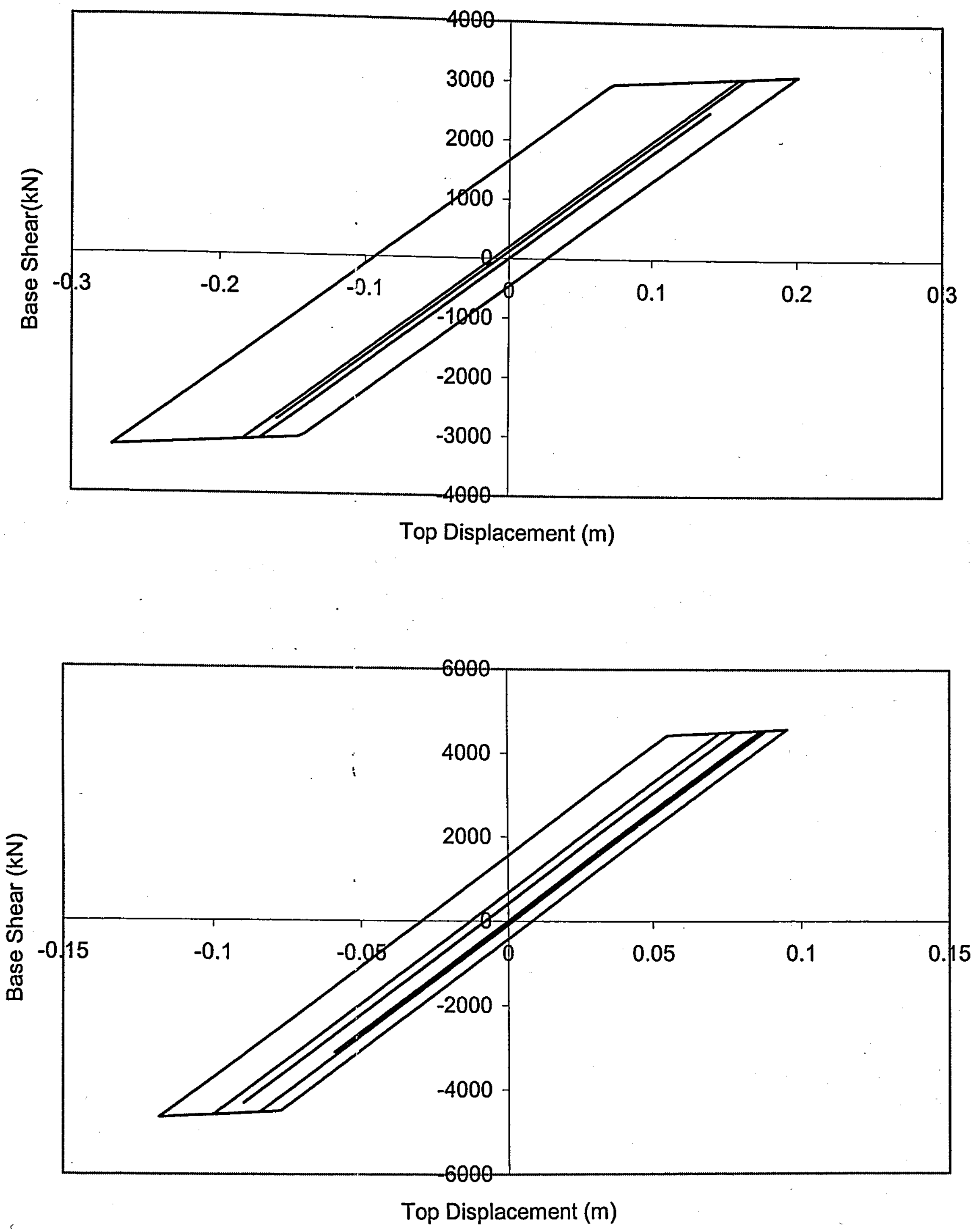

Figure 6.17 Pier11 and pier12 response to SUPERS.

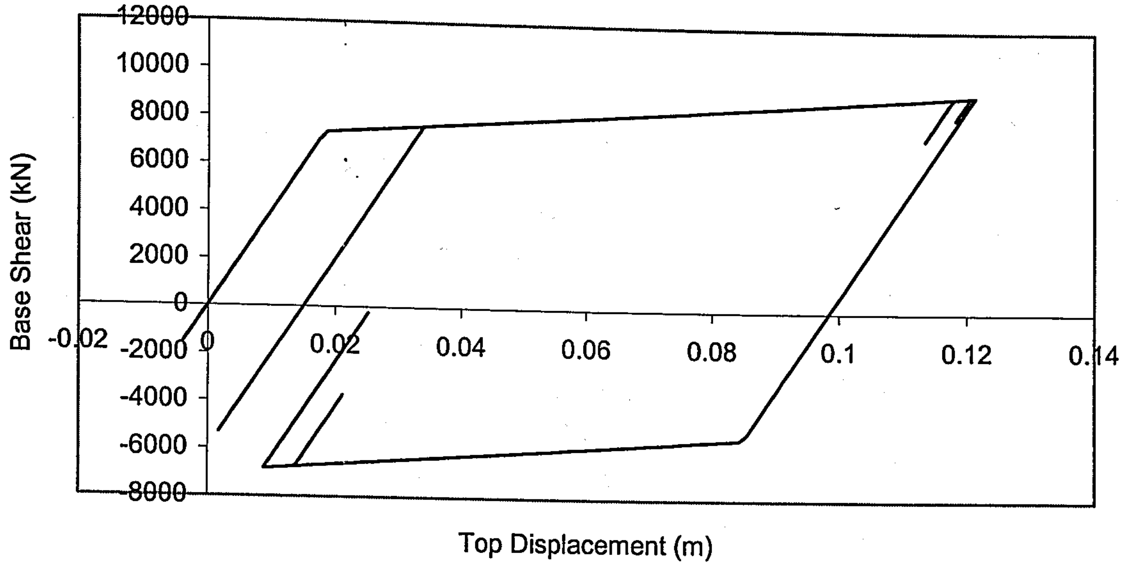

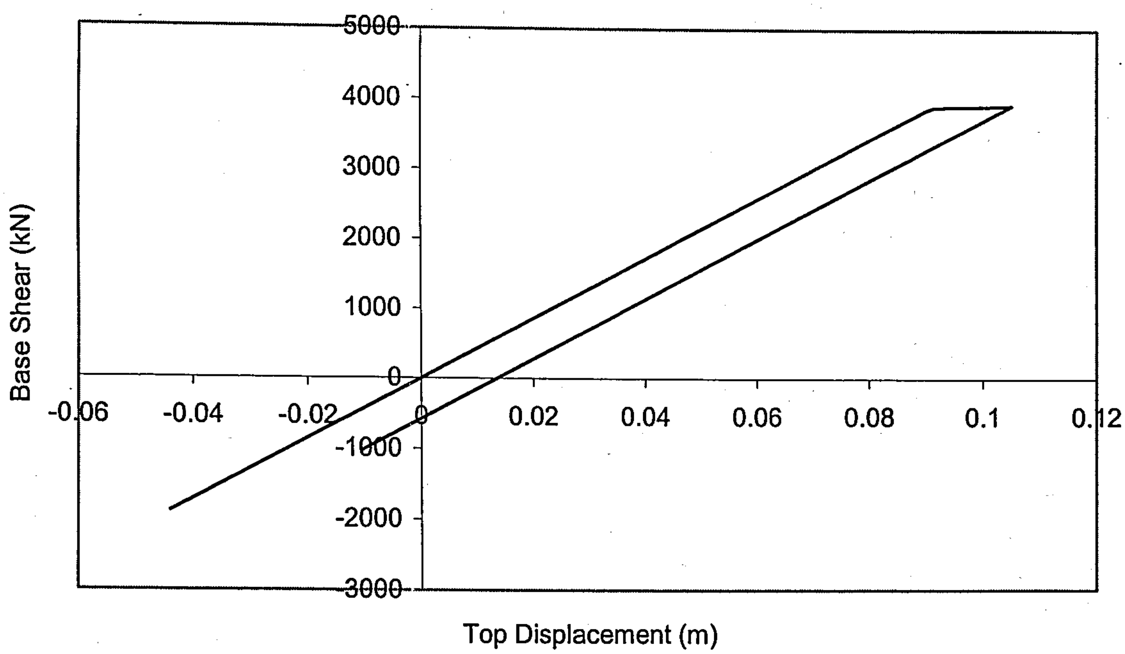

Figure 6.18 Pier1 and pier13 response to IMP.

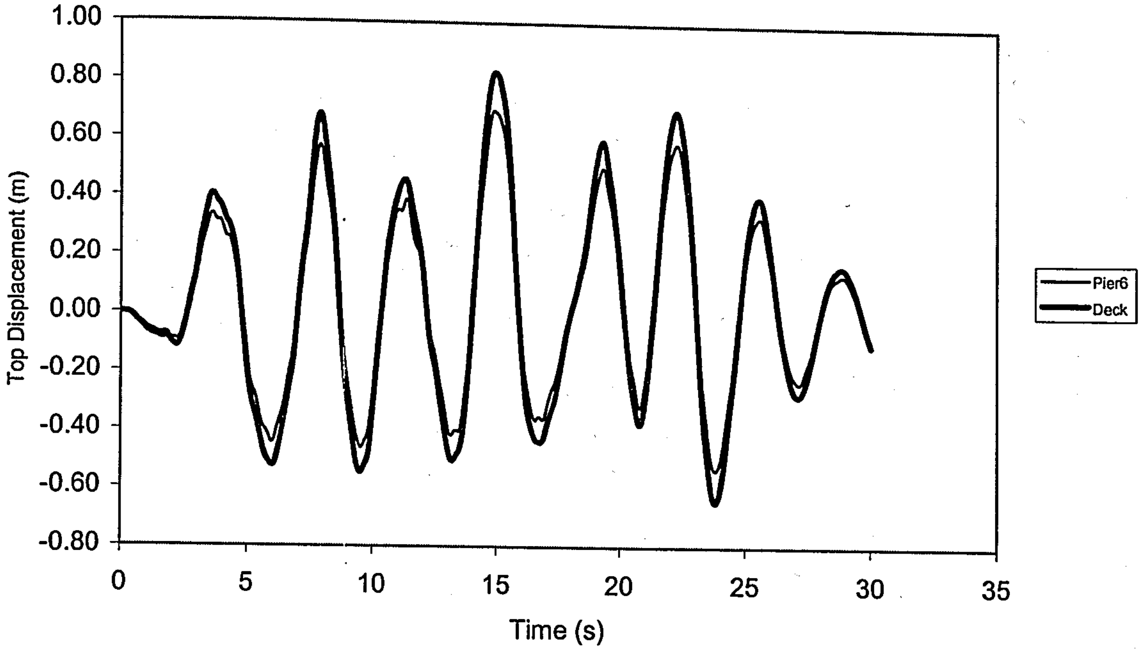

Figure 6.19 Displacement time history of Pier6 and deck for SIMQ1 motion.

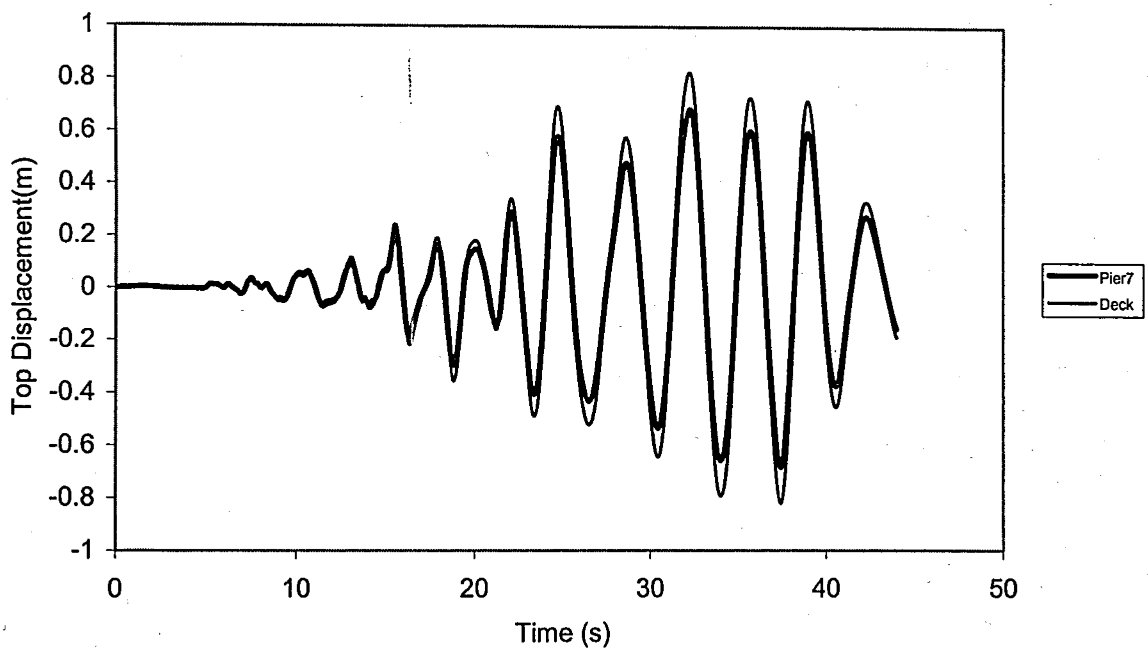

Figure 6.20 Displacement time history of Pier7 and deck for SUPERS motion.

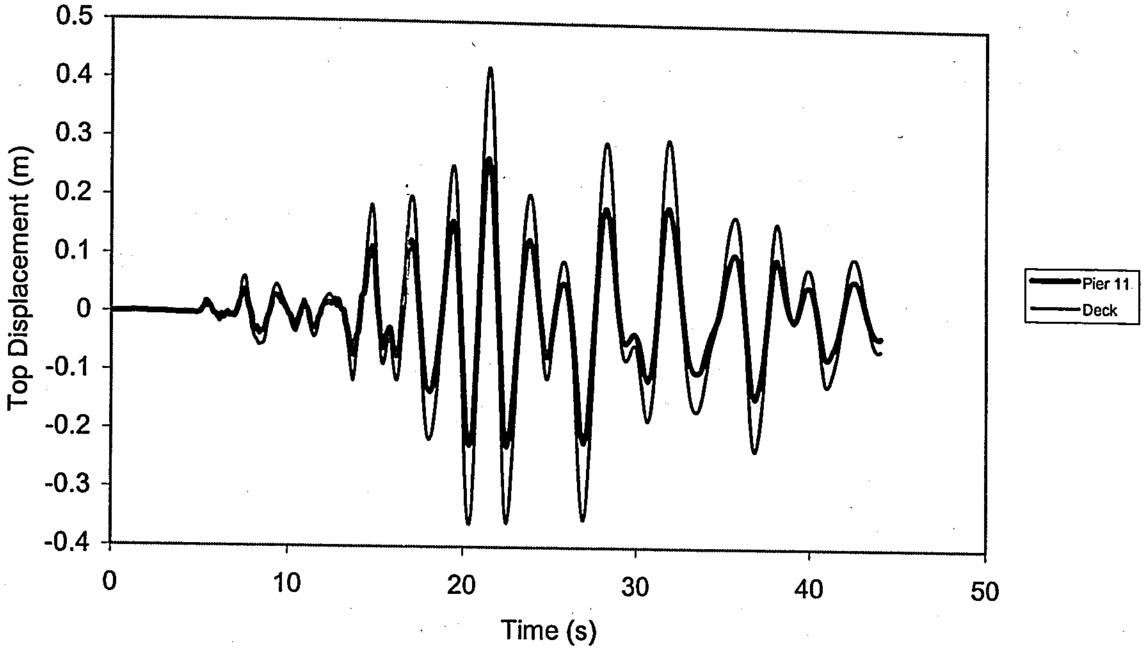

Figure 6.21 Displacement time history of Pier11 and deck for SUPERS motion.

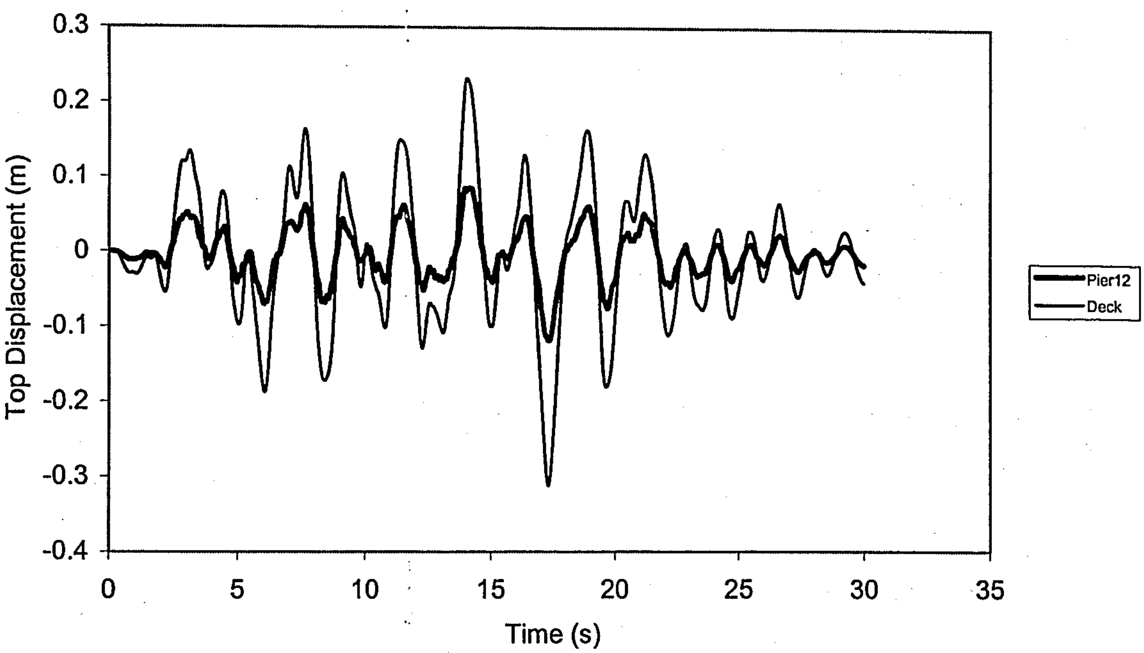

Figure 6.22 Displacement time history of Pier12 and deck for SIMQ1 motion.

Table 6.6 Maximum displacement at elastomeric bearings for both direction

	Displacement in Transverse Direction (m)												
	Pier 1	Pier 2	Pier 3	Pier 4	Pier 5	Pier 6	Pier 7	Pier 8	Pier 9	Pier 10	Pier 11	Pier 12	Pier 13
Elastomer Dim.(cm)	80/80	80/65	80/65	80/65	80/65	80/65	80/65	80/65	70/65	70/65	70/65	80/65	80/65
SIMQ1	0.139	0.092	0.078	0.100	0.115	0.136	0.146	0.133	0.110	0.107	0.168	0.194	0.115
SIMQ2	0.135	0.085	0.078	0.100	0.117	0.135	0.149	0.133	0.119	0.104	0.154	0.193	0.119
SIMQ3	0.113	0.075	0.070	0.070	0.090	0.110	0.118	0.110	0.095	0.082	0.110	0.160	0.118
IMP	0.140	0.084	0.088	0.089	0.088	0.123	0.131	0.117	0.101	0.103	0.151	0.189	0.125
LOMPR	0.139	0.100	0.084	0.107	0.097	0.110	0.123	0.112	0.109	0.136	0.177	0.173	0.109
SUPERS	0.123	0.075	0.074	0.099	0.114	0.130	0.143	0.130	0.116	0.110	0.156	0.187	0.125

	Displacement in Longitudinal Direction (m)							
	Abutment 0	Pier 1	Pier 2	Pier 3	Pier 4	Pier 5	Pier 6	Pier 7
Elastomer Dim.(cm)	80/65	80/80	80/65	80/65	80/65	80/65	80/65	80/65
SIMQ1	0.120	0.078	0.046	0.048	0.048	0.030	0.021	0.016
SIMQ2	0.107	0.070	0.043	0.047	0.049	0.030	0.022	0.017
SIMQ3	0.136	0.080	0.040	0.049	0.036	0.032	0.020	0.013
IMP	0.205	0.117	0.066	0.084	0.075	0.054	0.032	0.017
LOMPR	0.091	0.055	0.038	0.047	0.038	0.032	0.022	0.015
SUPERS	0.119	0.076	0.038	0.045	0.032	0.030	0.022	0.013

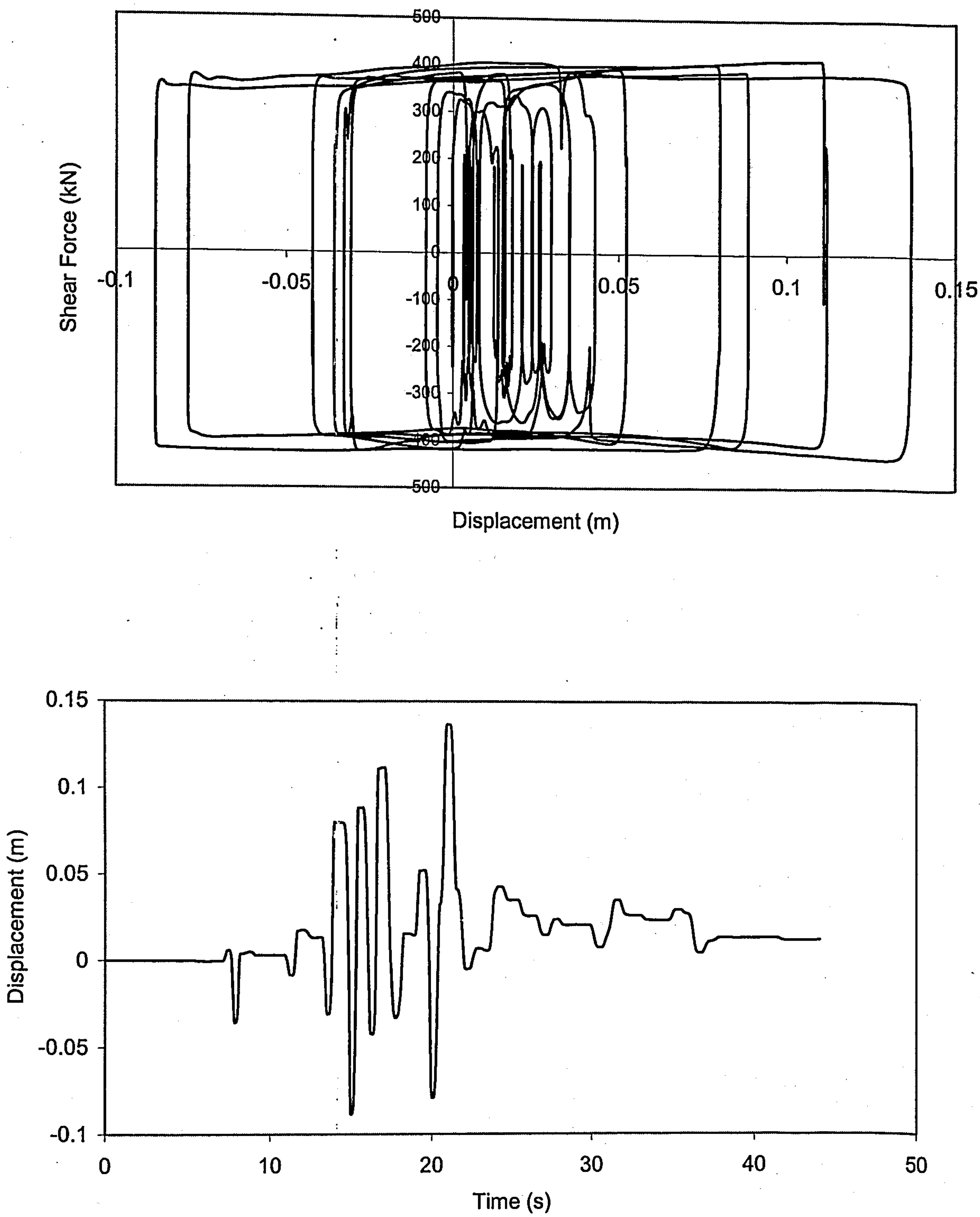

Figure 6.23 Hysteretic response and displacement time history of PTFE sliding bearing at Pier12 due to SUPERS motion.

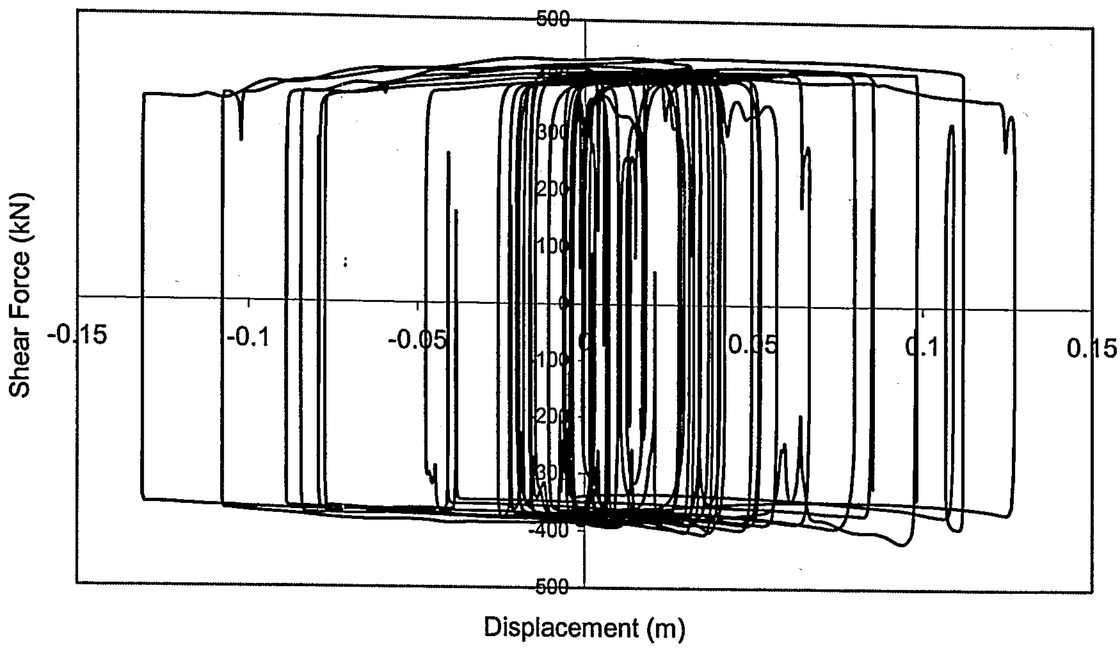

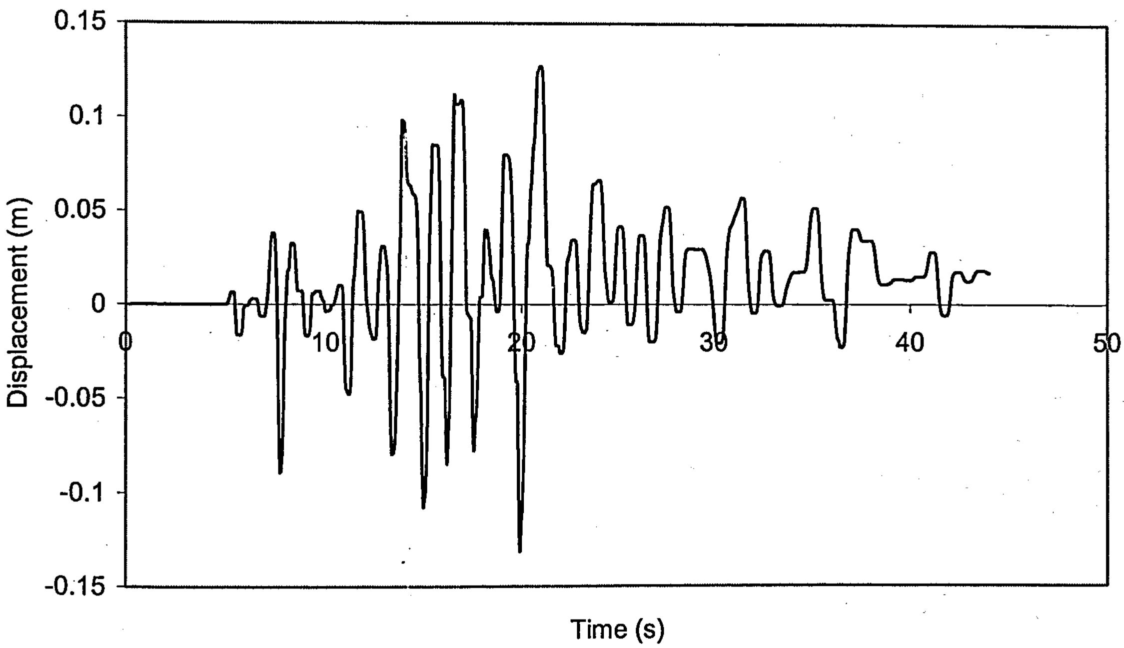

Figure 6.24 Hysteretic response and displacement time history of PTFE sliding bearing at Pier13 due to SUPERS motion.

Table 6.7 Maximum superstructure force demand.

	Bending Moment at Mid Span (kNm)	Bending Moment at the Support (kNm)
SIMQ1	176225	173782
SIMQ2	159981	168792
SIMQ3	204884	204904
IMP	227534	200183
LOMAP	236835	231666
SUPERS	245621	233394

Table 6.8 Extension in cables of the tie back device due to the longitudinal behavior of the tie back device

	$\Delta_{Tie\text{-}back}$ (m)	$\varepsilon=\Delta_{Tie\text{-}back/L}$	ε_{su}
SIMQ1	0.122	0.020	0.12
SIMQ2	0.109	0.018	0.12
SIMQ3	0.136	0.023	0.12
IMP	0.206	0.034	0.12
LOMAP	0.091	0.015	0.12
SUPERS	0.121	0.020	0.12

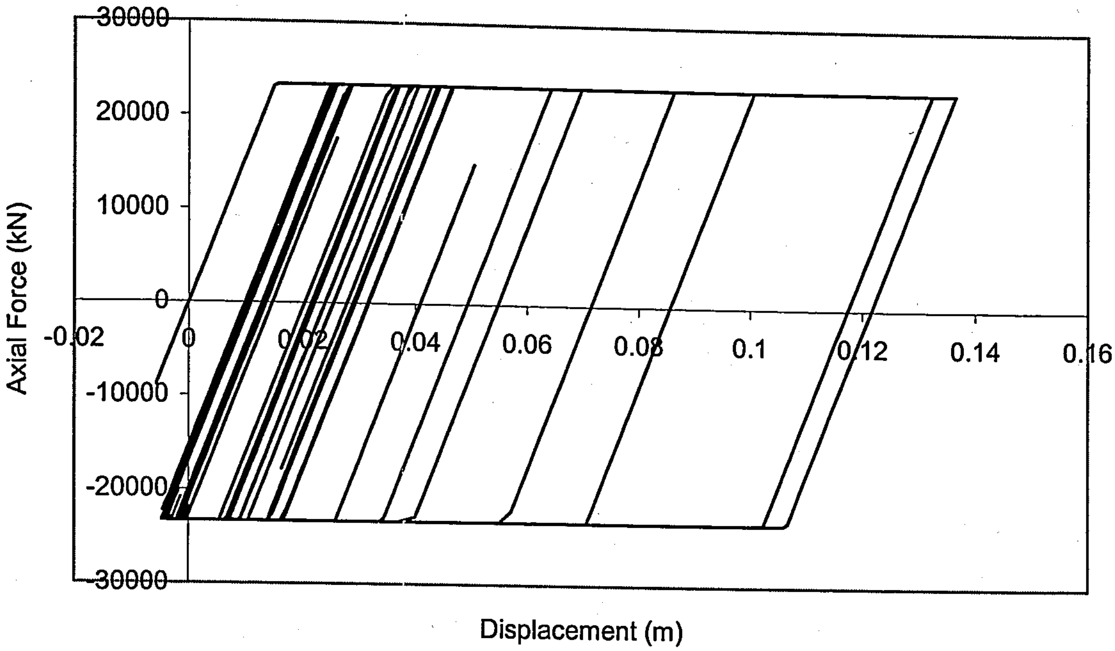

Figure 6.25 Tie back device response in longitudinal direction due to SIMQ3

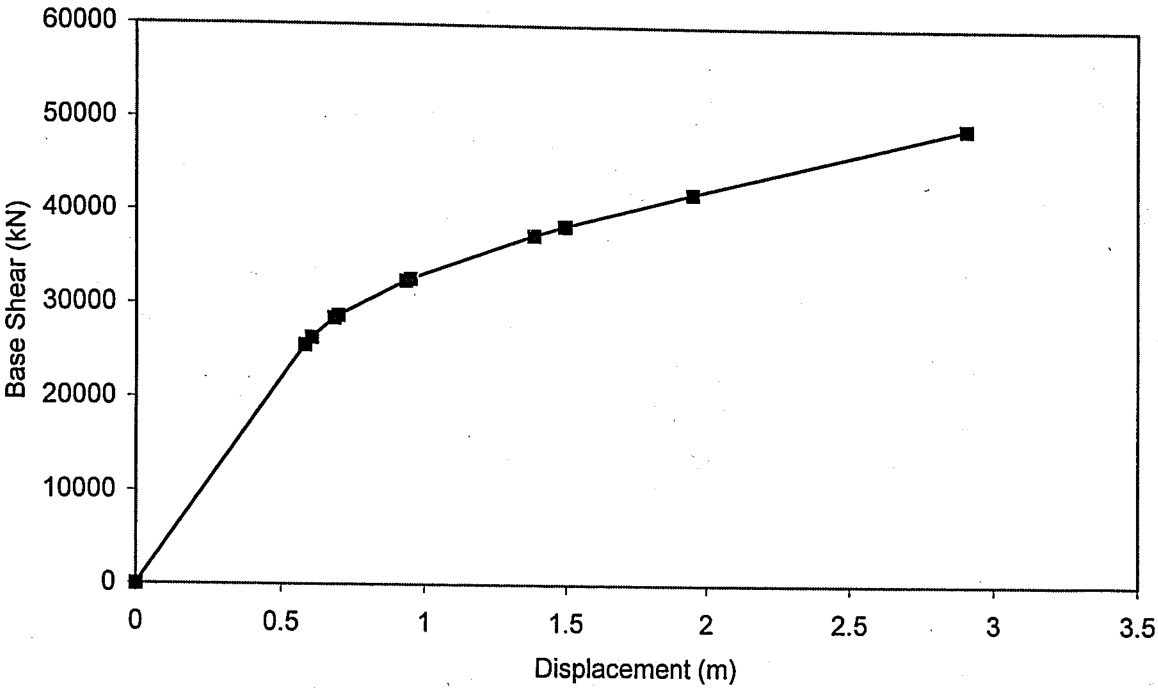

Figure 6.26 Pushover Curve of the global system in the transverse direction

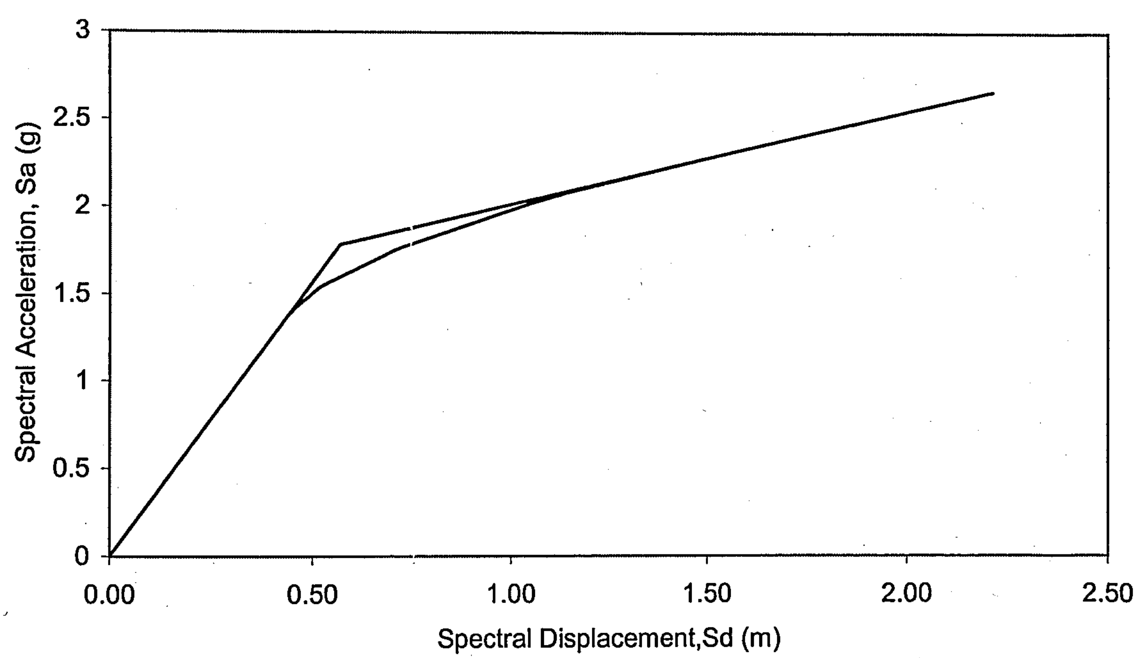

Figure 6.27 Capacity spectrum and bilinear representation.

Table 6.9. For piers experiencing yielding, comparison of the ductility and the capcity

	Displacement Demand (cm)			
	pier7	pier6	pier8	pier5
simq1	76.11	74.31	68.38	63.77
simq2	77.42	75.58	69.55	64.83
simq3	Elastic	Elastic	Elastic	Elastic
Imp	Elastic	Elastic	Elastic	Elastic
Lomap	Elastic	Elastic	Elastic	Elastic
Super	83.42	81.42	75.11	70.36

Ultimate Displacement(cm)			
pier7	pier6	pier8	pier5
76.50	79.30	82.12	82.30

	Ductilty demand			
	pier7	pier6	pier8	pier5
simq1	1.59	1.51	1.31	1.25
simq2	1.61	1.53	1.33	1.27
simq3	Elastic	Elastic	Elastic	Elastic
Imp	Elastic	Elastic	Elastic	Elastic
Lomap	Elastic	Elastic	Elastic	Elastic
Super	1.74	1.65	1.44	1.38

Ductiltiy Capacity			
pier7	pier6	pier8	pier5
1.59	1.61	1.57	1.61

7. Conclusion On The Seismic Performance

Sadabat V3 viaduct was designed in end 80's according to seismic design provisions of A.S.S.H.T.O. (1983). It was noted that old seismic design philosophy has been adopted in the design phase of the bridge. For instance, the single mode spectral method, which is widely accepted method for the design of bridges in the past, was used in seismic analysis and inadequate confinement detailing at the pier section was observed.

Time history analysis indicates that elastomeric bearings located on the flexible piers (pier6 to pier8, pie10 to pier13) and short piers are susceptible to failure in transverse direction. Displacement demands on these bearings exceed their capacity. As a general configuration, the bridge has a continuous superstructure and piers of different height, so severe shear force demand is expected on the stiff piers. The insertion of the isolating system regularizes the response, imposing nearly equal stiffness to the piers. Therefore, it can be concluded that because of the adoption of single mode response in designing of the viaduct, relative displacement demand on the elastomeric bearing were not estimated accurately. However, elastomeric bearings have sufficient capacity to remain elastic in longitudinal response.

Pushover analysis of the piers for both transverse and longitudinal directions independently show that the flexible intermediate piers have inadequate ductility capacity ranging from 1.5 to 2.5 because of the low flexural ductility in plastic hinge region. The crossties in plastic hinge region are widely spaced so that core concrete is poorly confined. As a result of the time history analysis, Pier 5 to 8 and pier11 and 12 are the most critical piers under transverse seismic effect. The pier columns are unlikely to tolerate cyclic displacement much exceeding yield.

Short piers, particularly pier1 and pier13, attract severe base shear due to their large stiffness when compared with the flexible intermediate piers. Therefore, it is required to verify whether the short piers have adequate shear strength to ensure that inelastic flexural response. Based on shear strength estimation for short piers in section?, it can be concluded that piers have sufficient shear strength to provide capacity protected action and deformation capacity to fail in flexure.

Capacity of the PTFE elastomeric bearings in longitudinal direction depends on the limits of the sole plate installed above bearing to provide sliding surface. Hysteresis behavior of the bearings located on the pier9 to pier13 and abutment indicates that maximum displacement is within the limits of sole plate.

It should be noted that the deflection in horizontal plane of the superstructure under transverse seismic effect is similar to that of a simple beam pinned at the supports. For that reason, moments acting at the mid spans are considerably large. Comparison of flexural capacity and demands shows that superstructure has a sufficient bending stiffness in transverse direction to remain elastic. This result validates the assumption that behavior of the superstructure in the analysis is represented by linear elastic elements.

Tie back device has adequate strength and ductility to prevent excessive force demand transferring from the superstructure to the abutment. Tie back device also provides a ductile response in the longitudinal direction. In the event that the deck moves towards abutment because of the earthquake induced forces, bumper system composed of six elastomeric bearings located between deck and abutments were installed to prevent pounding. Analysis results indicate that bumper system is stiff enough to prevent pounding.

According to analysis results stated above, the behavior of the bridge in transverse direction is considered critical. As to longitudinal response, it can be concluded that the bridge response is essentially elastic.